THE BEHAVIOR OF LNG VAPOR CLOUDS: Wind-Tunnel Tests on the Modeling of Heavy Plume Dispersion

FINAL REPORT

(July 1979 - September 1981)

Prepared by

D. E. Neff and R. N. Meroney

Fluid Mechanics and Wind Engineering Program
Department of Civil Engineering
Colorado State University
Fort Collins, Colorado 80523

CER81-82DEN-RNM25

For

GAS RESEARCH INSTITUTE

Contract No. 5014-352-0203

GRI Project Manager

Steve J. Wiersma

Environment and Safety Department

March 1982

GRI DISCLAIMER

LEGAL NOTICE This report was prepared by Colorado State University as an account of work sponsored by the Gas Research Institute (GRI). Neither GRI, members of GRI, not any person acting on behalf of either:

a. Makes any warranty or representation, expressed or implied with respect to the accuracy, completeness, or usefulness of the information contained in this report, or that the use of any information, apparatus, method or process disclosed in this report may not infringe privately owned rights; or

b. Assumes any liability with respect to the use of, or for damages resulting from the use of, any information, apparatus, method, or process disclosed in this report.

50272-101

REPORT DOCUMENTATION PAGE	1. REPORT NO. GRI 80/0145	2.	3. Recipient's Accession No.

4. Title and Subtitle
THE BEHAVIOR OF LNG VAPOR CLOUDS: Wind-Tunnel Tests on the Modeling of Heavy Plume Dispersion

5. Report Date
March 1982

6.

7. Author(s)
D. E. Neff and R. N. Meroney

8. Performing Organization Rept. No.
CER81-82DEN-RNM25

9. Performing Organization Name and Address

Civil Engineering Department
Colorado State University
Fort Collins, Colorado 80523

10. Project/Task/Work Unit No.

11. Contract(C) or Grant(G) No.
(C) 5014-352-0203
(G)

12. Sponsoring Organization Name and Address
Gas Research Institute
8600 West Bryn Mawr Avenue
Chicago Illinois 60631

13. Type of Report & Period Covered
Final (July 1979 - September 1981)

14.

15. Supplementary Notes

16. Abstract (Limit: 200 words)

Visual and concentration measurements were made for a large number of continuous ground-level releases of heavy gases into a wind-tunnel boundary layer. These different plumes were not affected by any topographic or building wake influences. The experiments provided a broad coverage of the variable range of source gas specific gravity, source gas flow rate, and approach flow wind speed. From an investigation of the physical similarity between plumes, the permissible modeling distortion in source density, volume flux ratio, and length scale ratio was quantified. The concentration scaling theory which was previously limited to far-field behavior was extended to cover the entire range of plume concentrations. Generalized behavior models were constructed from the laboratory tests. These models were scaled up to atmospheric conditions. The range of atmospheric scenarios to which these laboratory data are applicable is summarized. Measurements on the behavior of transient dense plumes were also obtained.

17. Document Analysis a. Descriptors

Liquefied Natural Gas, wind tunnel, dispersion of heavy plumes, vapor cloud dispersion

b. Identifiers/Open-Ended Terms

c. COSATI Field/Group

18. Availability Statement	19. Security Class (This Report)	21. No. of Pages
Distribution Unlimited	Unclassified	120
	20. Security Class (This Page) Unclassified	22. Price

(See ANSI-Z39.18) See Instructions on Reverse

OPTIONAL FORM 272 (4-77)
(Formerly NTIS-35)
Department of Commerce

RESEARCH SUMMARY

Title	The Behavior of LNG Vapor Clouds: Wind-Tunnel Tests on the Modeling of Heavy Plume Dispersion
Contractor	Civil Engineering Department Colorado State University Fort Collins, Colorado 80523 GRI Contract Number: 5014-352-0203
Principal Investigators	D. E. Neff and R. N. Meroney
Report Period	July 1979 - September 1981 Final Report
Objective	The objective of this task was to simulate in a wind tunnel idealized LNG spills to improve knowledge of physical modeling similarity and provide empirical descriptions of plume behavior that are applicable to a large range of atmospheric plume scenarios.
Technical Perspective	When liquefied natural gas (LNG) spills from a storage vessel or transportation container. The LNG vaporizes and a potentially flammable cloud is formed. Techniques to predict the extent of the flammable zone are needed to assist in developing siting criteria and plant layout design.
Results	An extensive data base on the structure of different laboratory heavy plumes was obtained. These experiments included a large range of conditions for source gas specific gravity, gas flow rate, gas time duration, and wind speed. The deviations in plume similarity as a result of different modeling approximations were examined. A useful empirical description of all the continuous plume tests was developed, and its applicability to field conditions discussed.
Technical Approach	An LNG vapor plume at boiloff conditions is heavier than air. Although the plume will eventually become positively buoyant due to heat absorbed from the surroundings, much of the dispersion will occur while the plume density is greater than the that of air. The dispersion during the heavier-than-air phase may be approximated in a wind tunnel by means of isothermal-model plumes produced by high-molecular-weight gases. In laboratory tests, heavy gases were introduced into the wind tunnel via an area source of constant diameter mounted flush on the wind-tunnel floor. The floor was level and smooth for all tests. Concentration sensors downwind of this source were used to measure the structure of the different model plumes tested.

Project Implications

This work has produced a useful empirical description of wind tunnel modeling of continuous-spill LNG plume dispersion. However, several factors concerning the scaling of turbulent motion are not yet sufficiently understood to clarify the range of applicability of wind tunnel plume data to field conditions. Additional tests will be carried out in a future project. Colorado State University is currently investigating the surface heat transfer effects on the dispersion of LNG plumes. Results from this task will also be used to identify future research that is necessary to clarify the applicability of wind tunnel tests to large scale releases of LNG.

GRI Project Manager
Steve J. Wiersma
Manager, Safety Research

TABLE OF CONTENTS

LIST OF TABLES

LIST OF FIGURES

LIST OF SYMBOLS

Dimensions are given in terms of mass (m), length (L), time (t), moles (n), and temperature (T).

Symbol	Definition	
A	Area	$[L^2]$
@	at	
C_p	Specific heat capacity at constant pressure	$[L^2t^{-2}T^{-1}]$
C_p^*	Molar specific heat capacity at constant pressure	$[L^2mt^{-2}T^{-1}n^{-1}]$
D	Source diameter	$[L]$
g	Gravitational acceleration	$[Lt^{-2}]$
g'	$(= g(\rho_s-\rho_a)/\rho_a)$ gravitational parameter	$[Lt^{-2}]$
k	Thermal conductivity	$[mLT^{-1}t^{-3}]$
ℓ_b	Buoyancy length scale	$[L]$
L	Length	$[L]$
L_{u_x}	Longitudinal integral length scale	$[L]$
M	Molecular weight	$[mn^{-1}]$
$\bar{M}$	Equivalent molecular weight	$[mn^{-1}]$
n	Mole or frequency	$[n]$, $[t^{-1}]$
P	Pressure	$[mL^{-1}t^{-2}]$
p	Velocity power law exponent	-
Q	Volumetric rate of gas flow	$[L^3t^{-1}]$
$\bar{R}$	Universal gas constant	$[nm^{-1}L^2t^{-1}T^{-1}]$
$S_u(n)$	Spectral power density	$[L^2t^{-1}]$
T	Temperature	$[T]$
ΔT	Temperature difference across some reference layer	$[T]$
t	Time	$[t]$
u_*	Friction velocity	$[Lt^{-1}]$
u_e	Entrainment velocity	$[Lt^{-1}]$

U,u	Mean velocity	$[Lt^{-1}]$
$\forall$	Volume	$[L^3]$
W,w	Plume vertical velocity	$[Lt^{-1}]$
x	General downwind coordinate	$[L]$
y	General lateral coordinate	$[L]$
z	General vertical coordinate	$[L]$
z_o	Surface roughness parameter	$[L]$
α	Temperature ratio or proportional to	-
∇	Gradient of quantity	$[L^{-1}]$
γ	Heat capacity ratio	-
δ	Boundary layer thickness	$[L]$
η	General vertical position	$[L]$
λ_p	Peak wavelength	$[L]$
ν	Kinematic viscosity	$[L^2t^{-1}]$
ξ	General lateral position	$[L]$
ρ	Density	$[mL^{-3}]$
σ	Standard deviation or plume surface area	- , $[L^2]$
χ	Mole fraction of gas component	-
Ω	Angular velocity of earth = 0.726×10^{-4} (radians/sec)	$[t^{-1}]$

Subscripts

a	Air
bg	Background
cal	Calibration value
g	Gas
H	Evaluated at height H
H_o	Lateral to the source
H_x	Lateral to position x

iso	Isothermal
℄	On centerline
LNG	Liquefied Natural Gas
m	Model
mea	Measured
p	Prototype, peak
r	Reference conditions
s	Source gas
th	Thermal
u	Upwind

Superscripts

$\overline{()}$	Mean of a quantity
()'	Fluctuating part of a quantity
$(\dot{})$	Quantity per unit time
()"	Quantity per unit area

Dimensionless Parameters

Re	Reynolds number
Ri	Bulk Richardson number
Ro	Rossby number
Pr	Prandtl number
Ec	Eckert number
Ma	Mach number
M	Mass flux ratio
F	Momentum flux ratio
Fr	Densimetric Froude number
Fr_s	Densimetric Froude number relative to inertia of the plume
$\dot{F}r$	Flux Froude number

V	Volume flux ratio
SG	Specific gravity
K	Dimensionless concentration
f	Dimensionless plume parameter
ϕ_ε	Dimensionless dissipation rate for turbulent energy

1.0 INTRODUCTION

Natural gas is a highly desirable form of energy for consumption in the United States. A sophisticated distribution network already services a major part of the country. Recent efforts to expand this nation's natural gas supply include the transport of natural gas in a liquid state from distant gas fields and the temporary storage of surplus capacity in peak shaving facilities. To transport and store liquefied natural gas (LNG) it is cooled to a temperature of -162°C. At this temperature if a storage tank on a ship or land were to rupture and the contents spill out onto the earth's surface, rapid boiling of the LNG would ensue and the liberation of a flammable vapor would result [1,2]. Past studies [3,4] have demonstrated that the cold LNG vapor plume will remain negatively buoyant for a majority of its flammable lifetime. This hazard will extend downwind until the atmosphere has diluted the LNG vapor below the lower flammability limit (a local concentration for methane below 5 percent by volume).

It is important that accurate predictive models for LNG vapor cloud physics be developed, so that the associated hazards of transportation and storage may be evaluated. Various industrial and governmental agencies have sponsored a combination of analytical, empirical, and physical modeling studies to analyze problems associated with the transportation and storage of LNG. Since these models require assumptions to permit tractable solution procedure one must perform atmospheric scale tests to verify their accuracy.

A multitask research program has been designed by a combined Gas Research Institute (GRI)/Department of Energy (DOE) effort to address the problem of preditive methods in LNG hazard analysis. One aspect of

this program, the physical simulation of LNG vapor dispersion in a meteorological wind tunnel is the subject of this report. GRI research contract number 5014-352-0203 consists of four tasks.

Task 1: Laboratory Support Tests for the Forty Cubic Meter LNG Spill Series at China Lake, California.

Task 2: Physical Simulation in Laboratory Wind Tunnels of the 1981 LNG Spill Tests performed at China Lake, California.

Task 3: Wind-Tunnel Tests on the Modeling of Heavy Plume Dispersion.

Task 4: Laboratory Tests Defining LNG Plume Interaction with Surface Obstacles.

Task one results were presented in the July 1980 annual report. Results of tasks two and four were presented in the final reports [5] and [6]. Task three, wind-tunnel tests on the modeling of heavy plume dispersion is the subject of this report.

Certain constraints on a physical models ability to predict large scale atmosphere plume behavior exist. The most confining of these constraints is the difference in Reynolds number between the model and the field. Fortunately the portion of the spectrum that has the greatest affect on plume dispersion remains invariant over a large range of Reynolds numbers. The Reynolds number influences the turbulent production and dissipation dynamics in a shear layer, and thus the energy spectrum of turbulent velocities is dependent on its magnitude. Nonetheless, many situations of interest in the atmosphere if scaled rigorously result in model Reynolds numbers on and below the lower bound of this invariant range. To circumvent this modeling restriction less rigorous scaling methodologies which increase the model Reynolds number

are commonly used. One purpose of this report is to explain the effect on plume similarity of these less rigorous scaling methodologies. With this knowledge the limits of physical modeling for dense plumes may now be stipulated, i.e., minimal wind speeds and maximum plume release rates.

This report also develops a generalized continuous plume model. This simple empirical formulation is based upon measured plume behavior. The generalized plume model predicts heavy plume dispersion in the absence of topographic or building wake effects.

Techniques which correlated laboratory plumes may be applied to relate different atmospheric scale plumes. Such techniques permit one to predict the behavior of a large class of plumes from the behavior of a single reference plume.

Scaling methods employed during physical modeling of atmospheric and plume motion are discussed in Chapter 2. The details of the experimental measurements are described in Chapter 3. Chapter 4 discusses the laboratory tests and the data obtained. Chapter 5 analyzes the continuous plume data presented in Chapter 4 with respect to the scaling laws that govern heavy plume behavior. Chapter 6 develops an empirical description for all of the continuous plume data and discusses its range of applicability at atmospheric scales. Chapter 7 summarizes the conclusions obtained from this study. Chapter 8 gives recommendations for future work.

2.0 MODELING OF PLUME DISPERSION

To obtain a predictive model for a specific plume dispersion problem one must quantify the pertinent physical variables and parameters into a logical expression that determines their interrelationships. This task is achieved implicitly for processes occurring in the atmospheric boundary layer by formulating the conservation equations for mass, momentum, and energy. These equations together with site and source conditions and associated constituitive relations describe the actual physical interrelationship between the various independent (space and time) and dependent (velocity, temperature, pressure, density, concentration, etc.) variables.

These generalized conservation statements are too complex to be solved by present analytical or numerical techniques. It is also impossible to create a physical model at a reduced geometric scale for which exact similarity exists for all the dependent variables over all the scales of motion present in the atmosphere. Thus, one must resort to various degrees of approximation to obtain a predictive model. At present purely analytical or numerical solutions of plume dispersion are unavailable because of the classical problem of turbulent closure [7]. Alternative techniques rely heavily upon empirical input from observed or physically modeled data. The empirical-analytical-numerical solutions have been combined into several different predictive approaches [8,9,10]. The estimates of dispersion by these approaches are often crude; hence, they should only be used when the approach and site terrain are uniform and without obstacles. Boundary layer wind tunnels are capable of accurately modeling plume processes in the atmosphere under certain restrictions. These restrictions are discussed in the next few sections.

2.1 PHYSICAL MODELING OF THE ATMOSPHERIC BOUNDARY LAYER

The atmospheric boundary layer is that portion of the atmosphere extending from ground level to a height of approximately 1000 meters within which the major exchanges of mass, momentum, and heat occur. This region of the atmosphere is described mathematically by statements of conservation of mass, momentum, and energy [11]. The mathematical requirements for rigid laboratory-atmospheric-flow similarity may be obtained by fractional analysis of these governing equations [12]. This methodology is accomplished by scaling the pertinent dependent and independent variables and then casting the equations into dimensionless form by dividing by one of the coefficients (the inertial terms in this case). Performing these operations on such dimensional equations yields dimensionless parameters commonly known as:

Reynolds number	$Re = (UL/\nu)_r$	$= \frac{\text{Inertial Force}}{\text{Viscous Force}}$
Bulk Richardson number	$Ri = [(\Delta T)/T)(L/U^2)g]_r$	$= \frac{\text{Gravitational Force}}{\text{Inertial Force}}$
Rossby number	$Ro = (U/L\Omega)_r$	$= \frac{\text{Inertial Force}}{\text{Coriolis Force}}$
Prandtl number	$Pr = [\nu/(k/\rho C_p)]_r$	$= \frac{\text{Viscous Diffusivity}}{\text{Thermal Diffusivity}}$
Eckert number	$Ec = [U^2/C_p(\Delta T)]_r$	

For exact similarity between different flows which are described by the same set of equations, each of these dimensionless parameters must be equal for both flow systems. In addition to this requirement, there must be similarity between the surface-boundary conditions and the approach flow wind field.

Surface-boundary condition similarity requires equivalence of the following features:

a. surface-roughness distributions,

b. topographic relief, and

c. surface-temperature distribution.

If all the foregoing requirements are met simultaneously, all atmospheric scales of motion ranging from micro- to mesoscale could be simulated within the same flow field [13]. However, all of the requirements cannot be satisfied simultaneously by existing laboratory facilities; thus, a partial or approximate simulation must be used. This limitation requires that atmospheric simulation for a particular wind-engineering application be designed to simulate most accurately those scales of motion which are of greatest significance for the given application.

2.1.1 Partial Simulation of the Atmospheric Boundary Layer

For the specific case of the interactions between a heavy plume released at ground level and the atmospheric boundary layer several of the aforementioned parameters are unnecessarily restrictive and may be relaxed without causing a significant effect on the resultant concentration field. The Rossby number magnitude controls the extent to which the mean wind direction changes with height. The effect of coriolis force driven lateral wind shear on plume dispersion is only significant when the plume height is of the same order of magnitude as the boundary layer height. Ground level dense plume heights are usually two orders of magnitude smaller than the atmospheric boundary layer height. The Eckert number (in air $Ec = 0.4\ Ma^2\ (T_r/\Delta T_r)$, where Ma is the Mach number [7]) is the ratio of energy dissipation to the convection of energy. In both the atmosphere and the laboratory flow the wind velocities and temperature differences are such that the Eckert number

is very small; hence, it is neglected. Prandtl number equality guarantees equivalent rates of momentum and heat transport. Since air is the working fluid in both the atmosphere and the laboratory Prandtl number equality is always maintained.

The Richardson number (Ri) and Reynolds number (Re) determine the kinematic and dynamic structure of turbulent flow within a boundary layer [7]. This influence is apparent in the variations that occur in the spectral distribution of turbulent kinetic energies[1] with changing Ri (Figure 1) and changing Re (Figure 2).

Richardson numbers characteristic of non-neutrally stable conditions can be obtained in wind tunnel facilities that control air and floor temperatures. Figure 1 displays the influence of stratification on the turbulent structure in the atmospheric boundary layer [14]. Unstable conditions cause the energy of large scale fluctuations to increase and stable conditions cause the energy of large scale fluctuations to decrease.

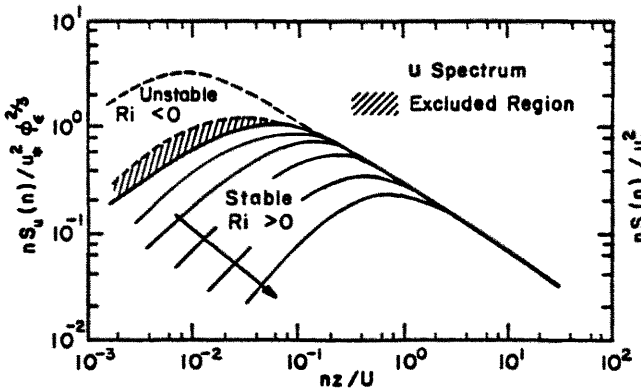

Figure 1. Variation of Turbulent Velocity Power Spectrum with Richardson Number [14]

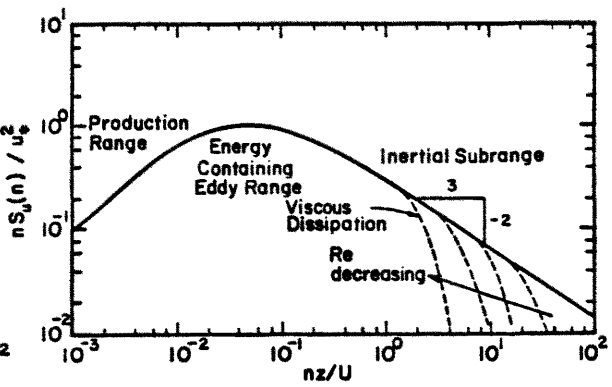

Figure 2. Variation of Turbulent Velocity Power Spectrum with Reynolds Number

[1]For a discussion of this type of description see Section 4.4.3.

Re equality implies $u_m = (L_p/L_m)u_p$, Re equality at a significantly reduced length scale would cause the models flow velocity to be above sonic; hence, its equality must be distorted. Figure 2 shows that a reduced Re changes only the higher frequency portion of an Eulerian type description of the spectral energy distribution. Unfortunately there is no precise definition as to which portion of an Eulerian Spectrum is dominant in a given dispersion application.

Most investigators use a minimum Re requirement, i.e. $Re = u_* z_0/\nu < 2.5$, where u_*, the friction velocity, and z_0, the roughness length, are derived from a log-linear fit to the measured mean velocity profile. The value 2.5 is an empirically determined constant. At Re below 2.5 it is observed that the mean velocity profiles in turbulent pipe flow lose similarity in shape and deviate from the universal curve of a rough wall turbulent boundary layer [15]. For Re above 2.5 it is observed that the surface drag coefficient (and thus the normalized mean velocity profile) is invariant with respect to increasing Re. For Re between 0.11 and 2.5 the velocity profiles are characteristic of smooth wall turbulent boundary layers, and for values below 0.11 the growth of a laminar sublayer on the wall is observed to increase with decreasing Re.

Extrapolation of these results from pipe flow measurements to flat plate boundary layers may cause a shift in the magnitude of the minimum Re requirement, but it is generally felt that this shift is small [7,15]. Precise similarity in the universal form of mean wind shear may be necessary for invariance with respect to the surface drag coefficient, but this does not necessitate that precise similarity must exist for the invariance of passive dispersion. It is the distribution of

turbulent velocities which has the greatest effect on dispersion. It is the mean wind shear, however, which generates the turbulent velocities. It is possible that the specification of a minimum Re of 2.5 is overly conservative. The criteria, $Re > 2.5$ is not applicable for flow over complex terrain or building clusters.

To define the lower limit of Re for which turbulent dispersion is invariant in a particular model setting, the investigator should perform several passive plume releases at decreasing wind speeds (decreasing Re). The source strength corrected concentration fields (see section 2.2.2) of the Re invariant plumes will all display a similar structure. The minimum acceptable Re is the lower limit of this class of similar plumes. At Re below this value the proper portion of the spectral energy distribution is not simulated.

Halitsky [16] reported such tests performed for dispersion in the vicinity of a cube placed in a near uniform flow field. He found that for Re invariance of the concentration distributions over the cube surface and downwind the Re magnitude (based on H, the height of the cube and u_H, the velocity at H) must exceed 11,000.

The presence of a non-passive plume could significantly change the Re range over which dispersion invariance exists. Velocities within a heavy plume released at ground level have been observed to be significantly less than those in the approach flow [17]. The laminarization of the velocity field within the dense plume under these situations is highly possible; hence, the effect of Re magnitude on plume similarity can only be evaluated by direct comparison to field results.

2.2 PHYSICAL MODEL OF PLUME MOTION

In addition to modeling the turbulent structure of the atmosphere in the vicinity of a test site it is necessary to properly scale the

plume source conditions. One approach would be to follow the methodology used in section 2.1, i.e., writing the conservation statements for the combined flow system followed by fractional analysis to find the governing parameters. An alternative approach, the one which will be used here, is that of similitude [12]. The method of similitude obtains scaling parameters by reasoning that the mass ratios, force ratios, energy ratios, and property ratios should be equal for both model and prototype. When one considers the dynamics of gaseous plume behavior the following nondimensional parameters of importance are identified [16,17,18,19,20].[1]

$$\text{Mass Flux Ratio } (M) = \frac{\text{mass flow of plume}}{\text{effective mass flow of air}} = \frac{\rho_g W_g A_g}{\rho_a U_a A_a} = \left[\frac{\rho_s Q}{\rho_a U_a L^2}\right]_{\substack{@\\ \text{source}}}$$

$$\text{Momentum Flux Ratio } (F) = \frac{\text{inertia of plume}}{\text{effective inertia of air}} = \frac{\rho_g W_g^2 A_g}{\rho_a U_a^2 A_a} = \left[\frac{\rho_s Q^2}{\rho_a U_a^2 L^4}\right]_{\substack{@\\ \text{source}}}$$

$$\text{Densimetric Froude No. relative to the inertia of air } (Fr) = \frac{\text{effective inertia of air}}{\text{buoyancy of plume}} = \frac{\rho_a U_a^2 A_a}{g(\rho_g - \rho_a)\forall_g} = \left[\frac{U_a^2}{g\left(\frac{\rho_s - \rho_a}{\rho_a}\right) L}\right]_{\substack{@\\ \text{source}}}$$

$$\text{Densimetric Froude No. relative to inertia of the plume } (Fr_s) = \frac{\text{inertia of plume}}{\text{buoyancy of plume}} = \frac{\rho_g W_g^2 A_g}{g(\rho_g - \rho_a)\forall_g} = \left[\frac{Q^2}{g\left(\frac{\rho_s - \rho_a}{\rho_s}\right) L^5}\right]_{\substack{@\\ \text{source}}}$$

$$\text{Flux Froude No. } (\dot{F}r) = \frac{\text{momentum flux of air}}{\text{buoyancy momentum flux of plume}} = \frac{\rho_a U_a^2 A_a}{Qg(\rho_g - \rho_a)(L/U_a)} = \left[\frac{U_a^3 L}{Qg\left(\frac{\rho_s - \rho_a}{\rho_a}\right)}\right]_{\substack{@\\ \text{source}}}$$

$$\text{Volume Flux Ratio } (V) = \frac{\text{volume flow of plume}}{\text{effective volume flow of air}} = \frac{W_g A_g}{U_a A_a} = \left[\frac{Q}{U_a L^2}\right]_{\substack{@\\ \text{source}}}$$

[1]The scaling of plume Reynolds number is also a significant parameter. Its effects are invariant over a large range. This makes it possible to accurately model its influence by maintaining model tests above a minimum plume Reynolds number requirement. For the spread of a dense plume in a calm environment Simpson and Britter [21] demonstrate that to obtain invariance for the entrainment rate and gravity head shape the Reynolds number, $Re = UH/\nu$ must exceed 500, where U is the head velocity and H is the height of the intrusion just behind the gravity head.

It is necessary to maintain equality of the plumes specific gravity, ρ_g/ρ_a, over the plumes entire lifetime to obtain simultaneous simulation of all of these parameters. Unfortunately a requirement for equality of the plume gas specific gravity leads to several complications in practice. These are:

1) Equality of the source gas specific gravity between a model and its atmospheric equivalent leads to a wind speed scaling of $u_m = (L_m/L_p)^{\frac{1}{2}}u_p$. For a significant range of atmospheric wind speeds this relationship leads to wind tunnel speeds at which there is a possible loss of the Reynolds number invariance in the approach flow. To avoid this problem one could build a larger wind tunnel than those commonly in use today; thus permiting scaling of the atmospheric flow at a larger length scale or use an enhanced scaling scheme which relaxes equality of some of the previously mentioned plume parameters. A discussion of the implications of several different enhanced scaling schemes is presented in sections 2.2.1.1, 2.2.1.2, and 2.2.1.3.

2) A thermal plume in the atmosphere is frequently simulated in the laboratory by an isothermal plume formed from a gas of appropriate molecular weight. Under certain situations this practice will lead to a variation of the equality of plume density as the plume mixes with air. A discussion of this behavior is presented in section 2.2.1.4.

It is important to examine each modeling situation and decide if an approximation to complete plume behavior may be employed without a significant loss in the similarity of the modeled plume structure. Section 2.2.1 discusses several different approximation methodologies which help formulate a physical model, and it addresses the errors incurred by such approximations.

2.2.1 Partial Simulation of Plume Motion

The different modeling techniques proposed to overcome the restriction of plume source density equality are critically reviewed in section 2.1.1.1. Section 2.2.1.2 discusses an enhanced[1] scaling

[1]The word "enhanced" in plume modeling terminology usually refers to a technique whereby the model reference wind speed is increased.

technique in which the plume source density equality may be maintained for plumes that have small initial source momentum. Section 2.2.1.3 discusses the potential of velocity field length scale distortion as a technique for Re enhancement. Section 2.2.1.4 reviews and estimates the errors incurred through use of isothermal gases to simulate thermal plumes.

2.2.1.1 The Relaxation of Source Density Equality

The relaxation of source density equality during the modeling of plume dispersion has been proposed by several investigators [17,19,22,23,24]. This practice is employed to avoid low wind speeds that are operationally difficult to maintain in most wind-tunnel facilities. Low wind speeds also introduce questions concerning the Reynolds number invariance of the approach flow. All enhanced scaling schemes which use the relaxation of source density equality increase the velocities used in the model. The scheme dependent velocity increase can be calculated from the equations in Appendix A. The relaxation of source density equality prohibits simulataneous equality of the remaining plume parameters. One must now choose which of these parameters are dominant for the plume being studied.

For the elevated release of a positively buoyant plume into a modeled shear flow several different combinations of plume parameters have been described as being dominant in the plume physics [22]. Skinner and Ludwig [19] argue that the Flux Froude No. (Fr) and the Momentum Flux Ratio (F) are dominant and all other parameters are relaxed.[1] Isyumov, Jandali, and Davenport [24] suggest that the Densimetric Froude No. relative to the air (Fr) and the Momentum Flux

[1]When using an approach where the Volume Flow Ratio is relaxed then it is important that the measured concentration field be scaled appropriately (see section 2.2.2).

Ratio (F) are dominate. This technique also maintains equality of the Densimetric Froude No. relative to the plume (Fr_s), but all other parameter equalities are relaxed. Cermak [13] argues that the Densimetric Froude No. relative to the air (Fr) and the Volume Flux ratio (V) are dominate. This technique also maintains equality of the Flux Froude No. ($\dot{F}r$), but all other parameters are relaxed.

Isyumov and Tanaka [22] performed an evaluation of these three different plume approximation schemes. They reported that for an isolated stack all three approximate techniques resulted in a significant overprediction of far field plume rise from that of a reference wind-tunnel plume (anywhere from 15-44% dependent on the test conditions). The two schemes in which F equality was maintained were very similar and resulted in larger deviation from the actual plume rise than that maintaining equality of V and Fr. It is perplexing, however, that V and Fr equality resulted in an overprediction of plume rise. Physical reasoning suggests the initial plume momentum would be underestimated in such a scheme. The magnitudes of plume centerline concentrations were generally within 30 percent with V and Fr equality modeling showing the largest deviations. When aerodynamic downwash was significant results from the two schemes in which F equality was maintained were very similar; nonetheless, they underpredicted concentrations downwind of the release complex by as much as 150 percent. Equality of V and Fr resulted in overprediction of concentrations by as much as 15 percent.

During the ground level release of a dense plume in which the release momentum is small it has been consistently argued that the dominate parameters are the Densimetric Froude No. with respect to the air (Fr) and the Volume Flux ratio (V) [5,17,25]. Since plume momentum

is negligible and equality of the Flux Froude No. ($\dot{F}r$) exists the only neglected parameter of significance is the Mass Flux Ratio (M). Hall [17] found good agreement between two tests in which the source gas specific gravities were 2.37 and 4.74. Recent tests conducted by TNO [25], however, found significant differences between plumes which had source specific gravities of 1.38 and 4.18. Tests conducted at Colorado State University (CSU) reported in section 5.1 demonstrate that the relaxation of source specific gravity will lead to significant errors when the source specific gravity is below a value of 2.0. All of the CSU tests reported above are for continuous releases in which there were no topographic or building wake effects. For a further discussion of these findings see section 5.1.

2.2.1.2 Similarity between Plumes which have Negligible Initial Momentum

When a plume has very small initial momentum then an enhanced scaling technique is possible without the distortion of the source density. In this technique it is assumed that the Flux Froude No. ($\dot{F}r$) is the only dominant parameter, but the Volume Flux Ratio must not be grossly distorted.[1] Figures 3 and 4 demonstrate the potential for using this technique to enhance model scale wind speeds for the specific case of liquefied natural gas (LNG) spills.

Figure 3 converts the variables associated with a field reference plume (u_p, Q_p, SG_p) to those used in a physical model as constrained by the equality of the Densimetric Froude No., Fr and the Volume Flux Ratio, V (and thus equality of $\dot{F}r$). The intersection of the dark line with the dashed line representative of wind-tunnel to field length scale

[1]Whenever the Volume Flux Ratio is distorted between model and field plumes, then the model concentration field must be scaled to that which would be seen in the field (see section 2.2.2 for details).

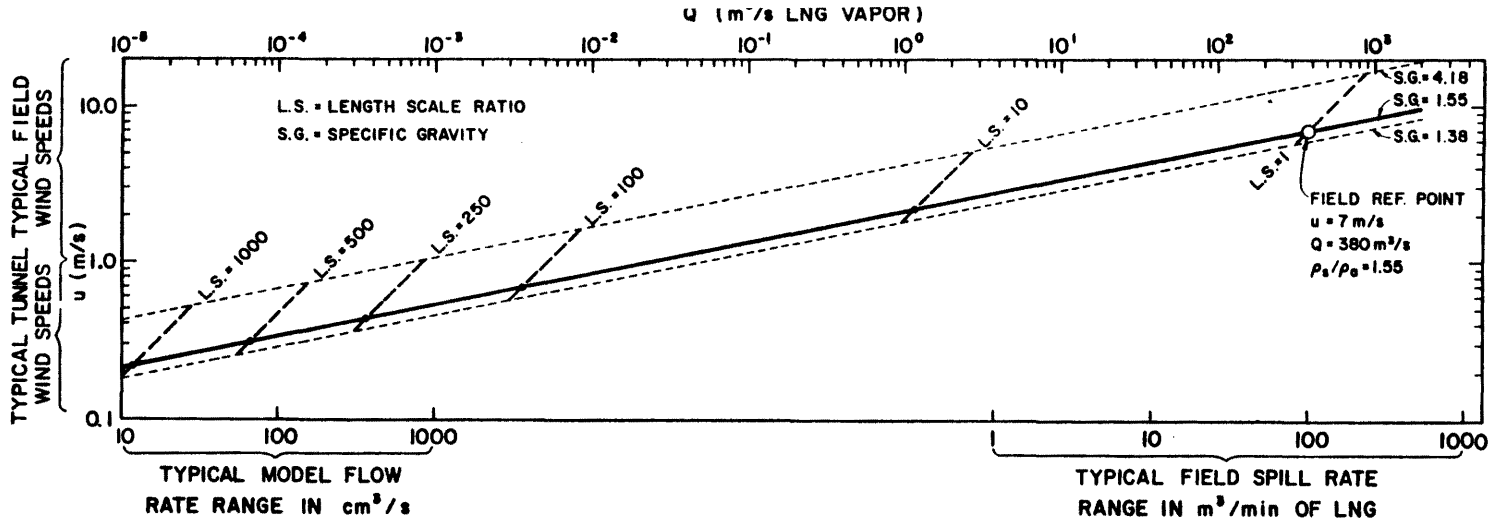

Figure 3. Field to Model Conversion Diagram for Densimetric Froude Number and Volume Flux Ratio Equality

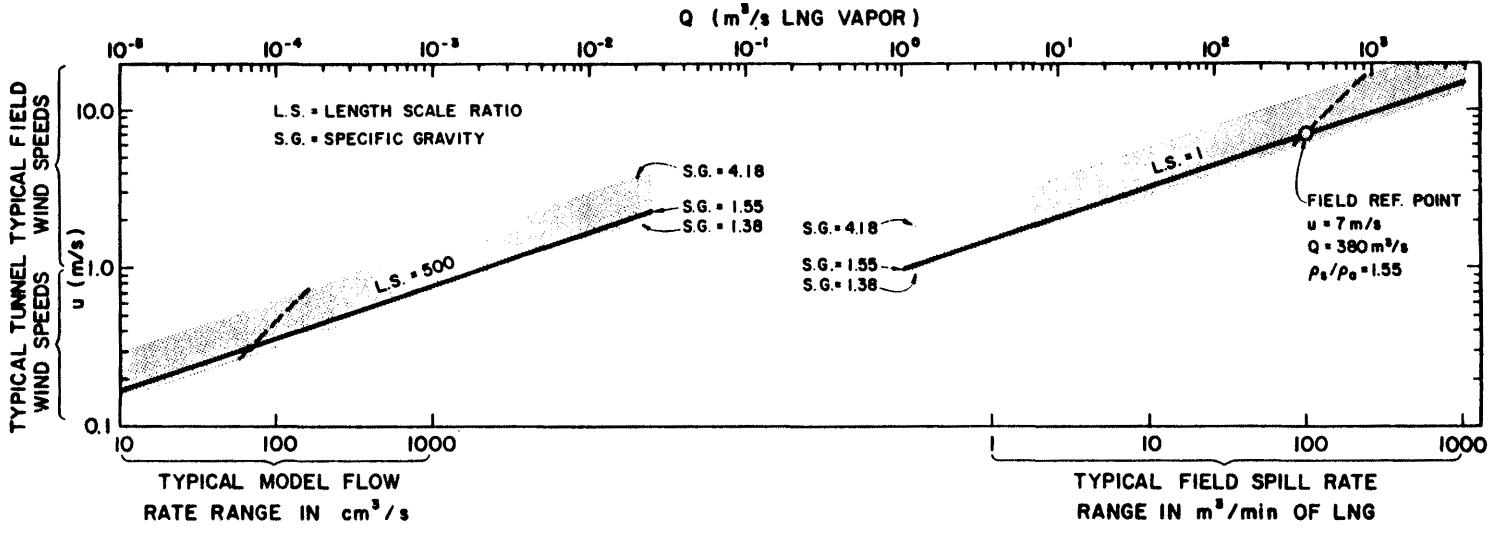

Figure 4. Field to Model Conversion Diagram for Flux Froude Number Equality

ratio yields the unique point for rigid similarity. If distortion in source density is allowed the simulation variables may be any point along a dashed line characteristic of the chosen length scale.

Figure 4 describes an alternative enhanced situation where only equality of the Flux Froude No. ($\dot{F}r$) is specified. Instead of a unique similarity point at a given length scale there is now a locus of points expressed by Q is proportional to u^3. If a distortion of plume source density is permissible then there is a broad band over which similar wind tunnel conditions may be chosen.

Section 5.2 of this report describes the results from a dense plume test series during which only a $\dot{F}r$ criteria was used. It was found that the plumes were similar within experimental error for volume ratio distortions up to 1.5. All of the plumes studied were negatively-buoyant, ground-level releases with no topographic or building wake effects.

2.2.1.3 Plume Similarity when the Velocity Field Length Scale has been Distorted

The choice of a length scale which is characteristic of a model boundary layer is a subject of some debate. Several different length scaling criteria have been cited. Some of these proposed scaling lengths are the roughness length, z_o, the boundary layer thickness, δ, the longitudinal integral scale of turbulence, and the peak wave number of the energy spectra of turbulent velocity fluctuations. Each of these scaling lengths has large variations associated with its calculation. For example, the parameter z_o can vary over a factor of two in describing the same velocity profile. This wide latitude in geometric scale partially explains why model length scale ratios for similar atmospheric situations often vary by a factor of ten in the literature.

Some variation in model length scale ratio is permissible because plume dispersion will be dominated by only a small portion of the scales of motion presented in a turbulent flow.

In light of the above arguments one way to enhance a model's wind speed would be to model the flow at a larger length scale. This type of model enhancement is particularly viable if the plume being modeled only occupies a small portion of the boundary layer. Figure 5 displays the distortion in the mean shear flow for a length scale exaggeration of two. The deviation is quite small when one considers errors of this magnitude could be made in the estimation of the velocity profile in either boundary layer.

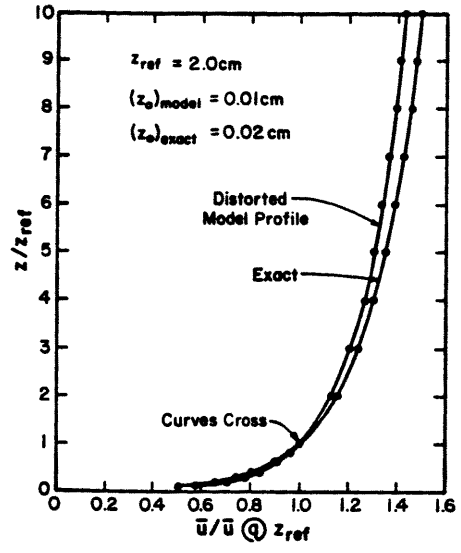

Figure 5. Mean Wind Shear Variation for a Two-fold Model Length Scale Distortion

Section 5.3 of this report utilizes this technique to compare different plumes released into the same velocity field. The results indicate that the technique works quite well for the case of near-field dispersion of ground based heavy plumes in the absence of topographic or wake effects. This same technique can be used to extend the measured

results from a single plume released into the atmosphere to predict the behavior of many other atmospheric plumes over a limited scale distortion range.

2.2.1.4 Plume Modeling when Buoyancy is not Conserved

Often during physical modeling experiments the proper source density is obtained isothermally through the use of a light or heavy gas. There is no attempt to try to compensate for nonconservative thermal effects on the plumes buoyancy. Unfortunately, there are several thermal effects that can change the density history of a plume as it disperses. These are:

1. Heat transfer by conduction, convection or radiation across plume boundaries,

2. Release of latent heat during the entrainment of humid air, and

3. Thermal expansion or contraction of the plume due to differences in the molar specific heat capacity of the plume source gas and air (i.e. $C^*_{p_a} \neq C^*_{p_g}$).

Heat transfer across plume boundaries is often small [5] even in the case of an LNG vapor plume and, when small, will not significantly affect the plume buoyancy.

The release of latent heat through the entrainment of humid air can have a very significant effect on the density history of a thermal plume. Figure 6 displays the variation of plume density versus mole fraction of cold methane vapors when adiabatically mixed with atmospheres of different humidities. During an isothermal physical simulation of humid air/cold gas mixing large deviations in plume similarity would occur.

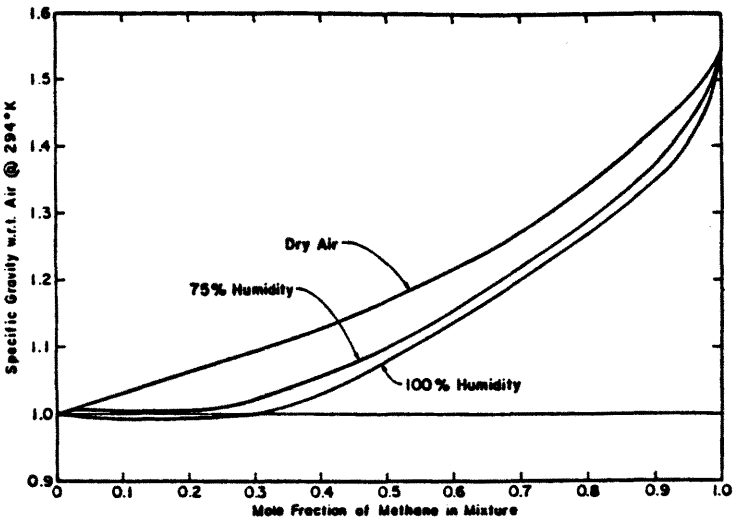

Figure 6. Specific Gravity of LNG Vapor-Humid Atmosphere Mixtures

The effect of molar specific heat capacity differences between the air and the plume is portrayed by considering the adiabatic mixing of two volumes of gas, one being the source gas, $\forall_s$, the other being ambient air, $\forall_a$. Consideration of the conservation of mass and energy for this system yields [19][1]:

$$\frac{\rho_g}{\rho_a} = \frac{\frac{\rho_s}{\rho_a}\forall_s + \forall_a}{\left(\frac{T_a}{T_s}\forall_s + \forall_a\right)\left(\frac{(C_p^*)_s}{(C_p^*)_a}\forall_s + \forall_a\right)\left(\frac{(C_p^*)_s}{(C_p^*)_a}\frac{T_a}{T_s}\forall_s + \forall_a\right)^{-1}}$$

If the temperature of the air, T_a, equals the temperature of the source gas, T_s, or if the molar specific heat capacity, C_p^*, is equal for both source gas and air then the equation reduces to:

$$\frac{\rho_g}{\rho_a} = \frac{\frac{\rho_s}{\rho_a}\forall_s + \forall_a}{\forall_s + \forall_a} \quad .$$

[1]The pertinent assumption in this derivation is that the gases are ideal and properties are constant.

Thus for two prototype cases: 1) an isothermal plume and 2) a thermal plume which is mostly composed of air; it does not matter how one models the density ratio, thermally or isothermally as long as the initial density ratio value is equal for both model and prototype. For the case of a thermal plume whose molar specific heat capacity is different from air, such as an LNG vapor plume, the modeling of the density history variation within the plume can only be approximate. Figure 7 displays the variation in the density history behavior for the isothermal simulation of an LNG vapor plume. Figure 8 displays the variation in the plume cross sectional area as the plume mixes with air for this same situation. Appendix B discusses the mathematical details for the construction of these two figures. Consideration of these two figures suggests that, although an isothermal simulation of an adiabatic LNG vapor cloud as it entrains dry air is not exact, it is a good approximation to actual behavior.

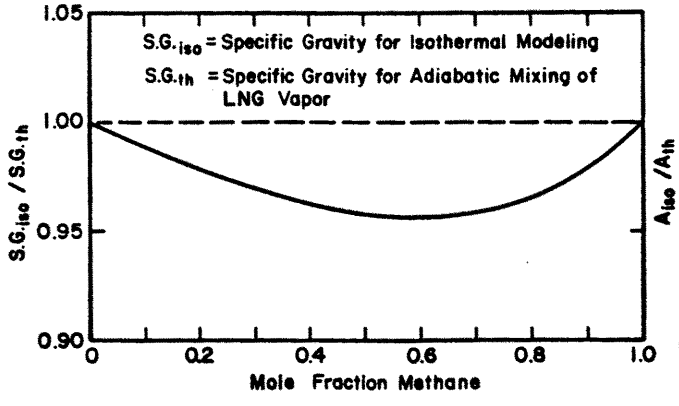

Figure 7. Specific Gravity Deviation in an Isothermal Model of LNG Vapor Dispersion

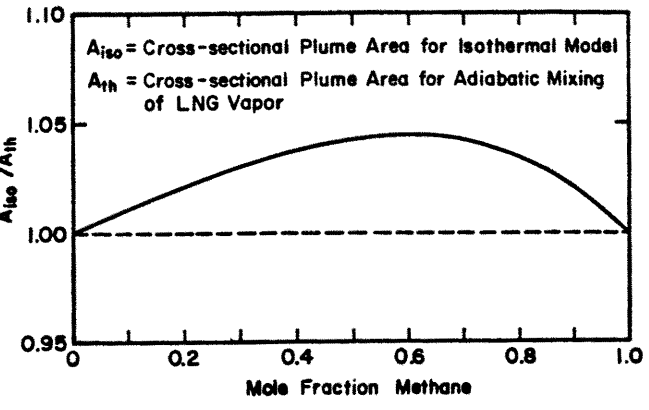

Figure 8. Plume Cross-sectional Area Deviation in an Isothermal Model of LNG Vapor Dispersion

2.2.2 Concentration Scaling Theory

Most plume studies measure the concentration magnitudes at distances far downwind from the source. In the limit as concentrations approached zero, the conventional concentration scaling laws for steady state plumes were developed [8]. The form of this expression is:

$$K(x) = \chi U_H L^2/(\frac{T_a}{T_s})Q \quad ,$$

where T_a and T_s are the temperatures of the ambient air and the source gas respectively. Q in this expression is the total source gas flow rate evaluated at source conditions. When modeling the plume at a reduced scale the function K(x) is determined by experimental measurements usually in an isothermal setting where $T_a = T_s$. Provided that the proper similarity requirements were satisfied then the function K(x) will be equal for field and model plumes. The effects of Volume Flux Ratio distortion and source gas temperature differences between model and prototype are corrected by the expression. This technique is completely satisfactory in the limit as concentration approaches zero. In the case of modeling plume concentration in the near field, such as is the case with flammable plumes, this relationship is not satisfactory. The problems lie in the asymptotic behavior as the concentration, χ, approaches one. $K(0) = U_H L^2/(\frac{T_a}{T_s})Q$ indicates that K is not a function of the downwind position, x, alone. It is a function of both x and $U_H L^2/(\frac{T_a}{T_s})Q$. To alleviate these problems the following generalized concentration scaling methodology was formulated.

Figure 9 will aid in understanding the derivation of this generalized concentration scaling methodology. Continuity of total molar flow rate of source gas at the source (section A-A) and at some downwind cross-sectional area (section B-B) requires that

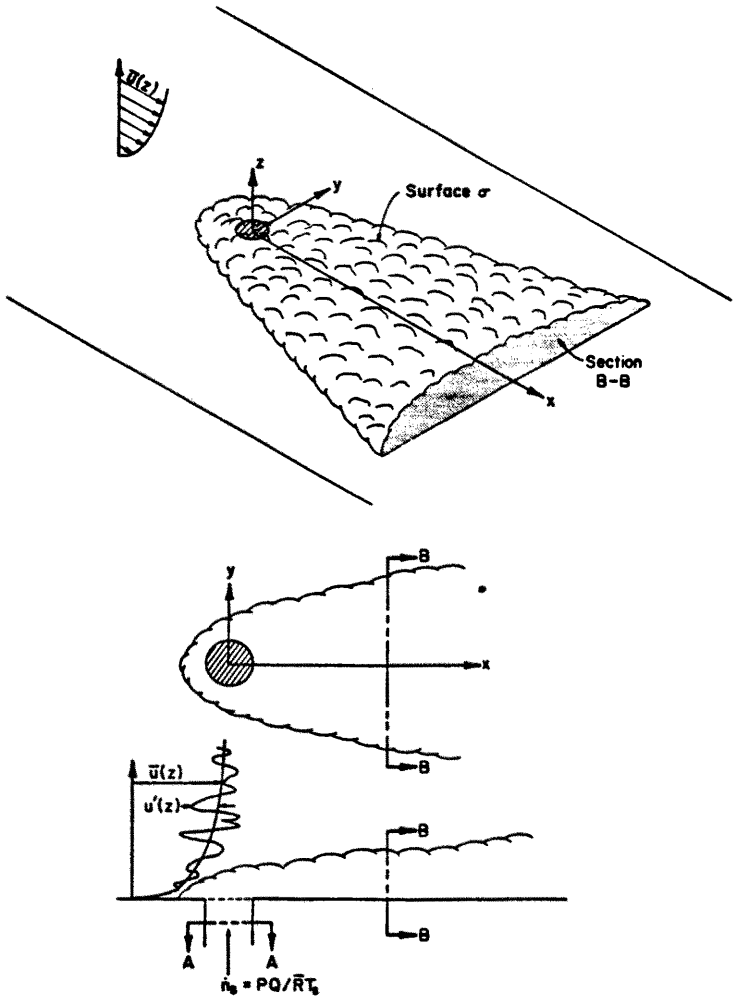

Figure 9. Notation Definition Diagram for Concentration Scaling Theory Derivation

$$\dot{n}_s = \int_{B-B} \dot{n}''_s \, dB \ .$$

where $\dot{n}_s$ is the total molar flow rate of source gas and $\dot{n}''_s$ is the molar flux of source gas through some differential area dB. Definition of concentration χ requires that

$$\chi = \frac{\dot{n}''_s}{\dot{n}''_s + \dot{n}''_a} \ .$$

Rewriting this expression as $\dot{n}''_s = (\frac{\chi}{1-\chi})\dot{n}''_a$ and substituting it into the expression for $\dot{n}_s$ yields

$$\dot{n}_s = \int_{B-B} \left(\frac{\chi}{1-\chi}\right) \dot{n}''_a \, dB \ .$$

The mean value theorem of integral calculus allows one to rewrite the equation as

$$\dot{n}_s = \frac{\chi(\xi,\eta)}{1 - \chi(\xi,\eta)} \int_{B-B} \dot{n}''_a \, dB \ ,$$

where $\chi(\xi,\eta)$ is the value of χ at some point, (ξ,η) on the surface B-B. The total molar flow rate of air across the entire plume boundary up to section B-B (surface σ) and the molar flow rate of air through section B-B are equal; hence,

$$\dot{n}_s = \frac{\chi(\xi,\eta)}{1-\chi(\xi,\eta)} \int_{\sigma} \dot{n}''_a \, d\sigma \ .$$

Let $\dot{n}_s = \frac{PQ}{\bar{R}T_s}$ and $\dot{n}''_a = \frac{Pu_e}{\bar{R}T_a}$ where u_e is the entrainment velocity of air across the boundary σ. Dividing the entire equation by $\frac{\chi}{1-\chi}$, where χ is evaluated at the point of interest on the surface B-B, say χ_{ℓ} and rearranging the equation cancelling constant quantities such as P and $\bar{R}$ yields

$$\left(\frac{T_s}{T_a}\right)\left(\frac{\chi_{\ell}}{1 - \chi_{\ell}}\right) \frac{\int u_e d\sigma}{Q} = \frac{\chi_{\ell}/(1-\chi_{\ell})}{\chi(\xi,\eta)/(1-\chi(\xi,\eta))} \ .$$

The expression on the right side of this equation is a function of the χ profile at the surface B-B; thus, it is a function of downwind position position, x, only. Provided that two plumes satisfy the proper similarity requirements then $\frac{(u_e)_m}{(u_e)_p} = \frac{(u_H)_m}{(u_H)_p}$ (or $u_e \propto u_H$), $\sigma_m/\sigma_p = L_m^2/L_p^2$ (or $\sigma \propto L^2$), and the concentration profiles will have the same form. Utilizing these factors, the final form of a concentration scaling law that relates the concentration distributions in plumes that are physically similar is

$$\left(\frac{T_s}{T_a}\right)\left(\frac{\chi}{1-\chi}\right)\left(\frac{u_H L^2}{Q}\right) = K(x) \ .$$

Some observations on the utility of this expression are summarized below.

- As concentration, χ approaches zero this expression becomes the conventional form presented in the first part of this section.
- Note that the quantity $u_H L^2/Q$ is the inverse of the Volume Flux Ratio; thus this expression corrects the entire concentration field for distortions in the similarity of this parameter as specified in some of the enhanced simulation techniques described in section 2.2.1.
- The quantity T_s/T_a corrects for the fact that concentrations measured at spacially similar points will be different for a thermal plume than for an isothermal plume.
- The function $K(x)$ can be viewed quite simply in the following format

$$K(x) = \frac{\dot{n}_a/\dot{n}_s}{\dot{n}''_a/\dot{n}''_s} \ .$$

Thus it is the ratio of the quantity $\dot{n}_a/\dot{n}_s$ evaluated for the entire plume to that same quantity evaluated at a single point within the plume.

- Given the equality of $K(x)_m = K(x)_p$ then a convenient formula for the conversion from a modeled concentration to a prototype concentration is given by

$$\chi_p = \frac{\chi_m}{\chi_m + (1-\chi_m)\left[\left(\frac{T_a}{T_s}\right)V\right]_m \Big/ \left[\left(\frac{T_a}{T_s}\right)V\right]_p} \ , \text{ where } V = \frac{Q}{u_H L^2}$$

For reciprocal conversion from prototype to model simply exchange the m's and p's.

- If the indeterminant behavior of this formulation of $K(x)$ as $\chi \to 1$ is bothersome note that by the transformation $K'(x) = \frac{K(x)}{K(x)+1}$ this problem is alleviated.

$$K'(x) = \frac{\chi}{\chi + (1-\chi)\left[\left(\frac{T_a}{T_s}\right)Q/u_H L^2\right]}$$

This new funtion $K'(x)$ has the convenient property that as $\chi \to 0$, $K'(x) \to 0$ and as $\chi \to 1$, $K'(x) \to 1$.

It is reemphasized that $K(x)$ is only a universal function for plumes that are similar in both entrainment physics and normalized concentration variation in downwind plume cross-sections. All passive plumes in the absence of wake effects and significant initial momentum meet these conditions; hence, $K(x)$ should be a universal function for passive plume dispersion. Measurements on plumes of this type have universally confirmed such correlations. As the source and near field factors such as initial momentum, building wakes, and buoyancy effects become more dominant than the background flow in determining the entrainment physics and plume profiles, the universal character of $K(x)$ is lost. For the specific case of downwind dispersion from negatively buoyant sources it is easily envisioned that, unless the buoyancy and inertial effects are properly matched, the resultant plume profiles will be drastically different.

3.0 DATA AQUISITION AND ANALYSIS

In this section the laboratory instruments and operational techniques used in the measurement of physically modeled plumes are discussed. Attention has been drawn to the limitations in the techniques in an attempt to prevent misinterpretation or misunderstanding of the test results presented in the next chapter. Some of the methods used are conventional and need little elaboration.

3.1 WIND-TUNNEL FACILITIES

The Environmental Wind Tunnel (EWT) shown in Figure 10 was used for all tests performed. This wind tunnel, especially designed to study atmospheric flow phenomena, incorporates special features such as an adjustable ceiling, rotating turntables, transparent boundary walls, and a long test section to permit reproduction of micrometeorological behavior at much smaller geometric length scales. Mean wind speeds of 0.15 to 12 m/s can be obtained in the EWT. For the present study the mean wind speed at a height of 2.1 cm ranged from 18 cm/s to 100 cm/s. The flexible test section roof on the EWT was adjusted to a constant height of 195 centimeters.

In addition to the flow straightener honeycombs at the tunnel entrance another set of honeycombs was placed after the tunnels entrance contraction as shown in Figure 10. Two different boundary layer conditioning methods were employed. In condition one, no upwind vortex generators or ground level roughness elements were employed. This configuration was used in all the tests during which the plumes visual outline was recorded. During all plume concentration tests the wind field was modified for condition two by eight tunnel-high vortex

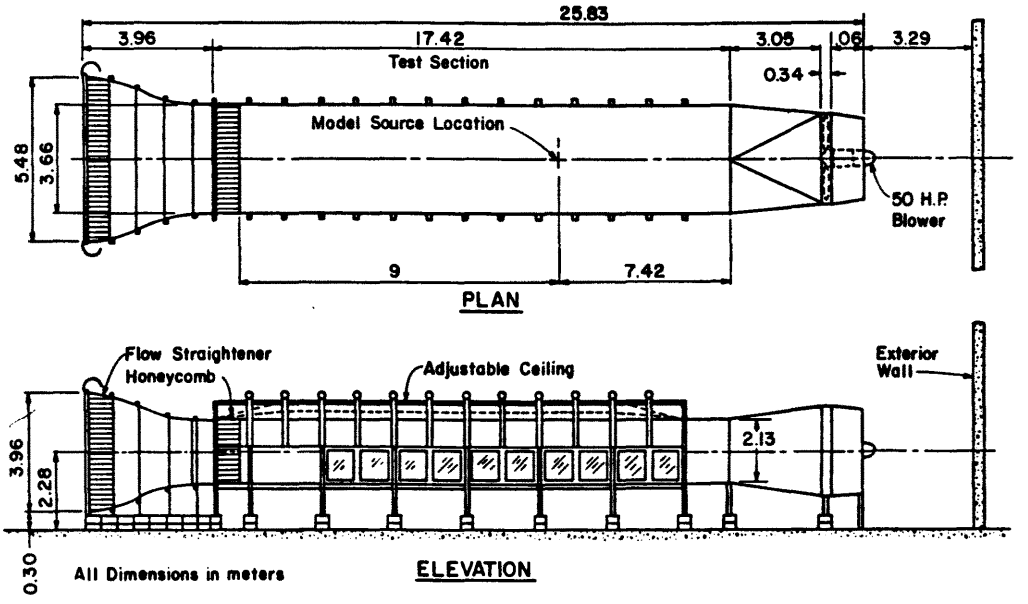

Figure 10. Environmental Wind Tunnel

generators placed near the tunnel entrance [26]. A 20 cm high brick trip was also placed at the base of the vortex generators, and the first six meters of the test section floor was covered with roughness elements whose effective height was approximately three millimeters. A completely smooth tunnel floor in the vicinity of the plume source and at all points downwind was used during all tests.

3.2 THE PLUME AND ITS SOURCE

The plume source was a circular cylinder whose upper surface was covered with a perforated screen of 36% open area. This screen was placed flush with the wind tunnel's false floor. The bottom of the source cylinder was completely sealed except for a fitting through which the source gas could enter. A spreader plate was placed inside the cylinder just above the gas entrance fitting to prevent any jetting effect as the gas passed through the perforated plate into the wind tunnel.

A variety of techniques were employed to introduce a source gas of a specified specific gravity and flow rate into the source cylinder. It is convenient to describe these systems based on the source gas specific gravity chosen.

- Specific Gravity = 1.0

  An analyzed gas mixture of 10 percent ethane, 4.1 percent carbon dioxide and 85.9 percent nitrogen stored in a high pressure cylinder was purchased from Scientific Gas Products. A flowrator was calibrated for use with this gas by one of the three flow rate standards used in the Fluid Dynamic and Diffusion Laboratory (FDDL) at Colorado State University (CSU). These standards are a soap bubble meter, Scientific Gas Products wet test meter, and a Rockwell gas flow meter. The flowrator was calibrated and operated with a back pressure of 15 psig to prevent any flowrate errors due to minor constrictions in the tubing that connected the flowrator to the source cylinder in the wind tunnel.

- Specific Gravity = 1.22

  A gas mixture of 19 percent methane and 81 percent argon was mixed by the method of partial pressures in the FDDL. The 19 percent methane value was analyzed through the use of the FDDL's hydrocarbon sampling system (gas chromotograph with a flame ionization detector) and a Scientific Gas Products analyzed calibration gas. This mixture was introduced into the wind tunnel via a calibrated flowrator operated at a 15 psig backpressure.

- Specific Gravity = 1.365

  A gas mixture of 1.75 percent methane and 98.25 percent argon was mixed by the method of partial pressures in the FDDL. The 1.75 percent methane value was analyzed through the use of the FDDL's hydrocarbon sampling system. This mixture was introduced into the wind tunnel via a calibrated flowrator operated at a 15 psig backpressure.

- Specific Gravity = 1.38

  100 percent argon gas was introduced into the wind tunnel via a calibrated flowrator operated at a 15 psig backpressure.

- Specific Gravity = 1.5

  A gas mixture of 3 percent ethane and 97 percent carbon dioxide was mixed by the method of partial pressures in the FDDL. The 3 percent ethane value was analyzed through the use of the FDDL's hydrocarbon sampling system. This mixture was introduced into the wind tunnel via a calibrated flowrator operated at a 15 psig backpressure.

- Specific Gravity = 1.79

  A Matheson Gas Proportioner with one tube calibrated for use with bottled air at 15 psig and the other tube calibrated for use with Freon-12 at 15 psig was used. From these calibration curves mixture flow rates of 25 percent Freon-12 and 75 percent air were provided.

- Specific Gravity = 2.59

  Mixture flow rates of 50 percent Freon-12 and 50 percent air were provided by the Matheson Gas Proportioner.

- Specific Gravity - 4.18

  100 percent Freon-12 gas was introduced into the wind tunnel via a calibrated flowrator operated at a 15 psig backpressure.

All continuous release plumes were allowed to develop their steady state structure for one to three minutes before any visual or concentration measurements were made. All transient plumes were produced by manual control of a solenoid value over a designated time duration.

3.3 FLOW VISUALIZATION TECHNIQUES

To make the plumes visible the source gas was passed through a container partially filled with titanium tetrachloride before release into the source plenum. A reaction of moisture in the source gas and the titanium tetrachloride produces a fine white suspension of titanium oxide. An example of the plume's appearance is shown in Figure 11. The floor over which the plume would flow was marked with a 15 cm square grid. A record of the visual plume extent was obtained by visual interpolation between the lines of this 15 cm grid by one person situated above the plume looking through a window in the ceiling and another person looking at the plume through the side windows.

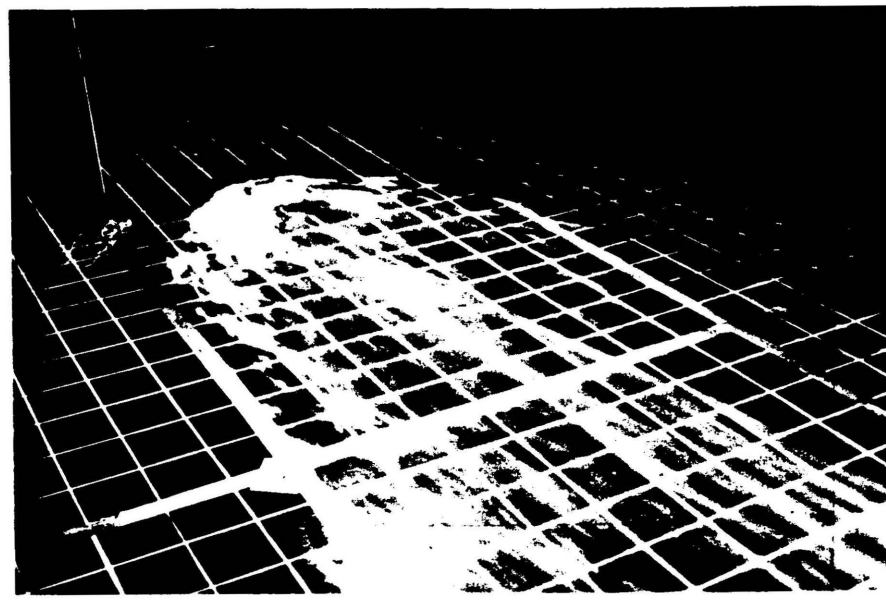

Figure 11. Visual Plume Appearance

3.4 WIND PROFILE AND TURBULENCE MEASUREMENTS

Velocity profile measurements, reference wind speed conditions, and turbulence measurements were obtained with a Thermo-Systems Inc. (TSI) 1050 anemometer and a TSI model 1210 hot-film probe. Since the voltage response of these anemometers is nonlinear with respect to velocity, a multi-point calibration of system response versus velocity was utilized for data reduction.

The velocity standard used in the present study is depicted in Figure 12. This calibration consisted of a Matheson model 8116-0154 mass flowmeter, a Yellowsprings thermistor, and a profile conditioning section designed and calibrated by the FDDL staff at CSU. The mass flowmeter measures mass flow rate independent of temperature and pressure, the thermistor measures the temperature at the exit conditions, and the profile conditioning section forms a flat velocity profile of very low turbulence at the position where the probe is to be located. Incorporating a measurement of the ambient atmospheric

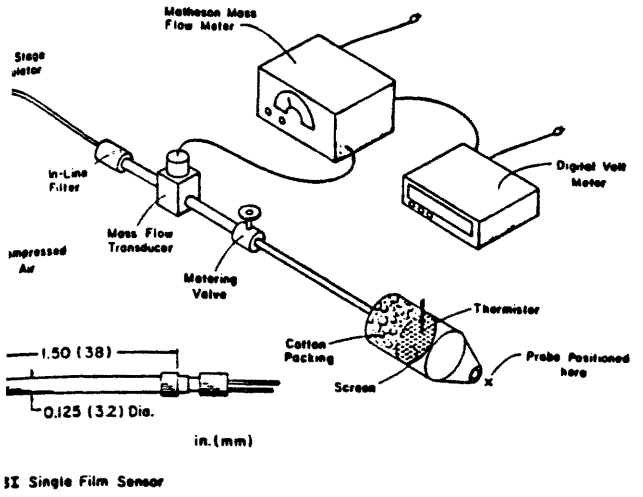

Figure 12. Velocity Probes and Velocity Standard

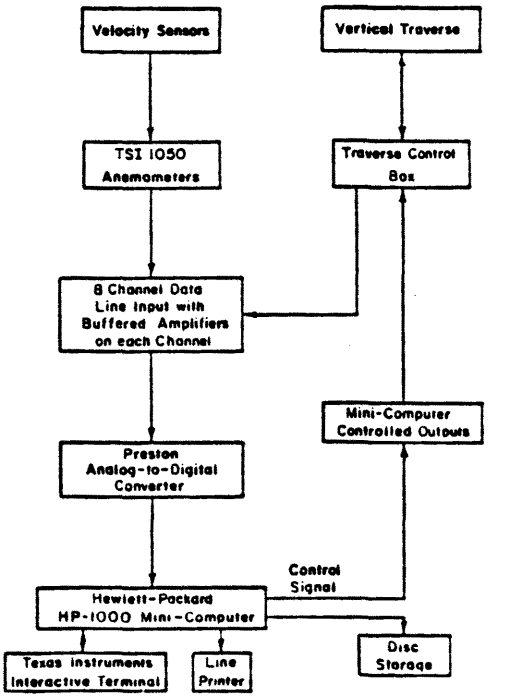

Figure 13. Velocity Data Reduction Flow Chart

pressure and a profile correction factor permits the calibration of velocity at the measurement station from 0.1-2.0 m/s ±20 percent or ±5.0 cm/s. whichever is smaller. During calibration of the single film probe, anemometer voltage response values over the velocity range of interest were fit to a King's law expression [27] with a variable exponent. The accuracy of this technique is approximately ±2 percent of the actual longitudinal velocity.

The velocity sensors were mounted on a vertical traverse and positioned over the measurement location in the wind tunnel. The anemometer's responses were fed to a Preston analog-to-digital converter and then directly to a HP-1000 minicomputer for immediate interpretation. The HP-1000 computer also controlled probe position. A flow chart depicting the control sequence for this process is presented in Figure 13.

3.5 CONCENTRATION MEASUREMENTS

Two different concentration measurement systems were employed in the present study. For source gases which were tagged with a hydrocarbon tracer a gas chromatograph (GC) with a flame ionization detector was used. For source gases which had a large difference between their thermal conductivity and that of air a set of eight aspirating hot-wire probes was employed. Sections 3.5.2 and 3.5.1 describe these two systems respectively. Below is a list of which sampling system was used for the different source gases that were employed in this study.

Source Gas Specific Gravity	Source Gas Composition	GC with flame ionization	hot-wire aspirating probes
1.0	85.9% nitrogen, 10% ethane, 4.1% carbon dioxide	X	
1.22	81% argon, 19% methane	X	
1.365	88.25% argon, 1.75% methane	X	
1.38	100% argon		X
1.5	97% carbon dioxide 3% ethane	X	
1.79	75% air, 25% Freon-12		X
2.59	50% air, 50% Freon-12		X
4.18	100% Freon-12		X

3.5.1 Aspirating Hot-Wire Probes

Hot-wire katharometer probes measure rapid concentration fluctuations. Such probes permit one to specify concentration spectra, concentration standard deviation, peak to mean ratios, etc. at any point. A rack of eight aspirating hot-wire probes was designed to provide simultaneously sampling at multiple points. A layout of this

design is presented in Figure 14. The films on these probes were replaced with 0.005 in. platinum wire to improve signal-to-noise characteristics. These eight instantaneous concentration sensors were connected to an eight-channel TSI hot-wire anemometer system. The output voltages from the TSI unit were conditioned for input to the analog-to-digital converter by a DC-supression circuit, a passive low-pass filter circuit tuned to 100 Hz, and an operational amplifier of times five gain. A schedule of this process is shown in Figure 15.

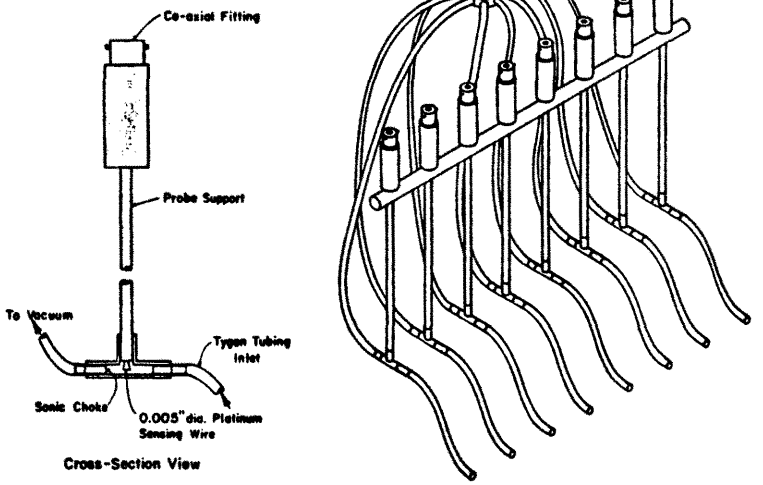

Figure 14. Hot-Wire Katharometer Probes

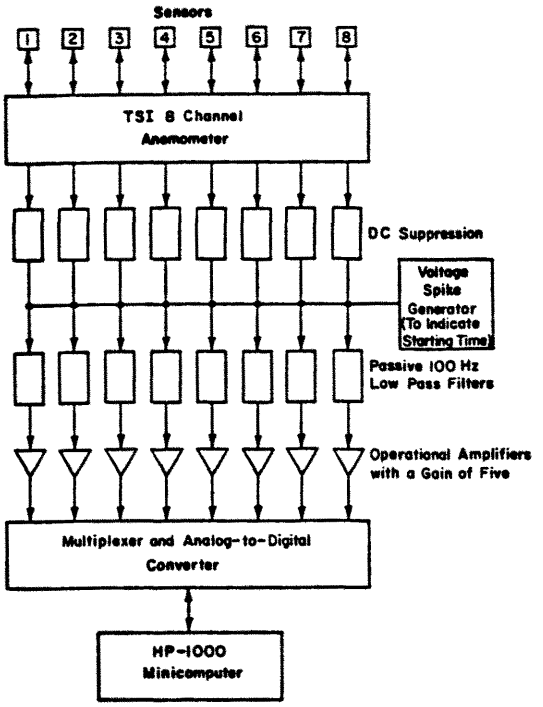

Figure 15. Block Diagram for Katharometer Data Reduction

The basic principles governing the behavior of aspirating hot-wire probes have been discussed by Blackshear and Fingerson [28], Netterville [29], and Kuretsky [30]. A vacuum source sufficient to choke the flow

through the small orifice just downwind of the sensing element was applied. This wire was operated in a constant temperature mode at a temperature above that of the ambient air temperature. A feedback amplifier maintained a constant overheat resistance through adjustment of the heating current. A change in output voltage from this sensor circuit corresponds to a change in heat transfer between the hot wire and the sampling environment.

The heat transfer rate from a hot wire to a gas flowing over it depends primarily upon the wire diameter, the temperature difference between the wire and the gas, the thermal conductivity and viscosity of the gas, and the gas velocity. For a wire in an aspirated probe with a sonic throat, the gas velocity can be expressed as a function of the ratio of the probe cross-sectional area at the wire position to the area at the throat, the specific heat ratio, and the speed of sound in the gas. The latter two parameters, as well as the thermal conductivity and viscosity of the gas mentioned earlier, are determined by the gas composition and temperature. Hence, for a fixed probe geometry and wire temperature, the heat transfer rate or the related voltage drop across the wire is a function of only the gas composition and temperature. Since all tests performed in this study were in an isothermal flow situation the wire's response was only a function of gas composition.

During probe calibration known compositions of either Argon-air or Freon 12-air mixtures were passed through a pre-heat exchanger to condition the gas to the tunnel temperature environment. These known compositions for the Argon-air calibration systems were drawn from bottles of prepared gas composition provided by Matheson Laboratories. For the Freon 12-air calibration system known compositions were produced

from pure Freon 12 and pure air passed through a Matheson gas proportioner. An overheat ratio (temperature of wire/ambient temperature) of 1.65 was used to maximize signal response while maintaining acceptable noise and signal drifting levels.

3.5.1.1 Errors in Concentration Measurements with Aspirating Probes

The effective sampling area of the probe inlet is a function of the probe's aspiration rate and the distribution of approach velocities of the gases to be sampled. The effective sampling area was approximately 0.5 cm^2.

The travel time from the sensor to the sonic choke limits the upper frequency response of the probe. At high frequencies the correlation between concentration fluctuations and velocity fluctuations (velocity fluctuations are a result of the changes of sonic velocity with concentration) at the sensor begin to decline. The CSU aspirated probe is expected to have a 1000 Hz upper frequency response, but to improve signal to noise characteristics the signal was filtered at 100 Hz. This is well above the expected frequencies for concentration fluctuations in this test program.

The accumulative error,[1] due to the combined effect of calibration uncertainties and nonlinear voltage drifting during the testing time for the different source gases used is estimated to be:

Source Specific Gravity	Source Composition	Error in Measurement Concentration Range (%)		
		0-1	1-10	10-100
1.38	Argon	±35%	±20%	±10%
1.79	25% Freon-12, 75% Air	±50%	±35%	±20%
2.59	50% Freon-12, 50% Air	±35%	±20%	±10%
4.18	Freon-12	±25%	±15%	±10%

[1]These errors are estimated ranges of approximately two to three standard deviations.

3.5.2 Gas Chromatograph

The Flame Ionization Detector (FID) operates on the principle that the electrical conductivity of a gas is directly proportional to the concentration of charged particles within the gas. The ions are formed by the hydrocarbon tracer in a gas sample being combusted in a hydrogen-air flame within the FID. The ions and electrons formed enter an electrode gap and decrease the gap resistance. The resulting voltage drop is amplified by an electrometer and fed to a Hewlett-Packard (HP) 3380 integrator. When no sample is flowing, a carrier gas (nitrogen) flows through the FID. Due to certain impurities in the carrier, some ions and electrons are formed creating a background voltage or zero shift. When the sample enters the FID, the voltage increases above this zero offset are proportional to the degree of ionization or correspondingly the amount of tracer gas present. Since the HP 5700 gas chromatograph used in this study features a temperature control on the chromatographs column and electrometer there is very low zero drift. The HP 3380 integrator compensates for any zero drift that does occur.

The lower limit of measurement is imposed by the instrument sensitivity and the background concentration of tracer within the air in the wind tunnel. Background concentrations were measured and subtracted from all data quoted herein.

3.5.2.1 Sampling System

The tracer gas sampling system consists of a series of fifty 30 cc syringes mounted between two circular aluminum plates. A variable-speed motor raises a third plate, which lifts the plunger on all 50 syringes simultaneously. A set of check valves and tubing are connected such that airflow from each tunnel sampling point passes over the top of each

designated syringe. When the syringe plunger is raised, a sample from the tunnel is drawn into the syringe container. The sampling procedure consists of flushing (taking and expending a sample) the syringe three times after which the test sample is taken. The draw rate is variable and generally set to be approximately 6 cc/min.

The sampler was periodically calibrated to insure proper function of each of the check valves and tubing assemblies. To calibrate the sampler each intake was connected to a manifold. The manifold, in turn, was connected to a gas cylinder having a known concentration of tracer gas. The gas was turned on, and a valve on the manifold was opened to release the pressure produced in the manifold. The manifold was allowed to flush for about 1 min. Normal sampling procedures were carried out to insure exactly the same procedure as when taking a sample from the tunnel. Each sample was then analyzed for tracer gas concentration. Percent error was calculated, and any "bad" samples (error > 2 percent) indicated a failure in the check valve assembly and the check valve was replaced or the bad syringe was not used for sampling from the tunnel.

3.5.2.2 Test Procedure

The test procedure consisted of: 1) setting the proper tunnel wind speed, 2) releasing a metered mixture of source gas from the release area source, 3) withdrawing samples of air from the tunnel designated locations, and 4) analyzing the samples with a Flame Ionization Gas Chromatograph. Photographs of the sampling system and the GC are shown in Figure 16. The samples were drawn into each syringe over a 300 s (approximate) time period and then consecutively injected into the GC.

The procedure for analyzing the samples from the tunnel is as follows: 1) a 2 cc sample volume drawn from the wind tunnel is introduced into the Flame Ionization Detector (FID), 2) the voltage output

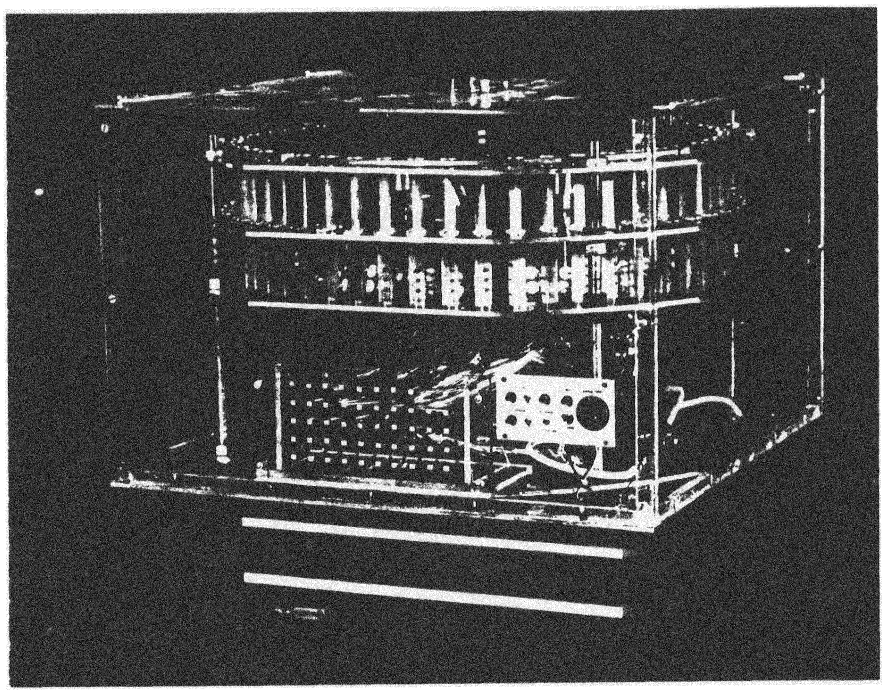

(a)

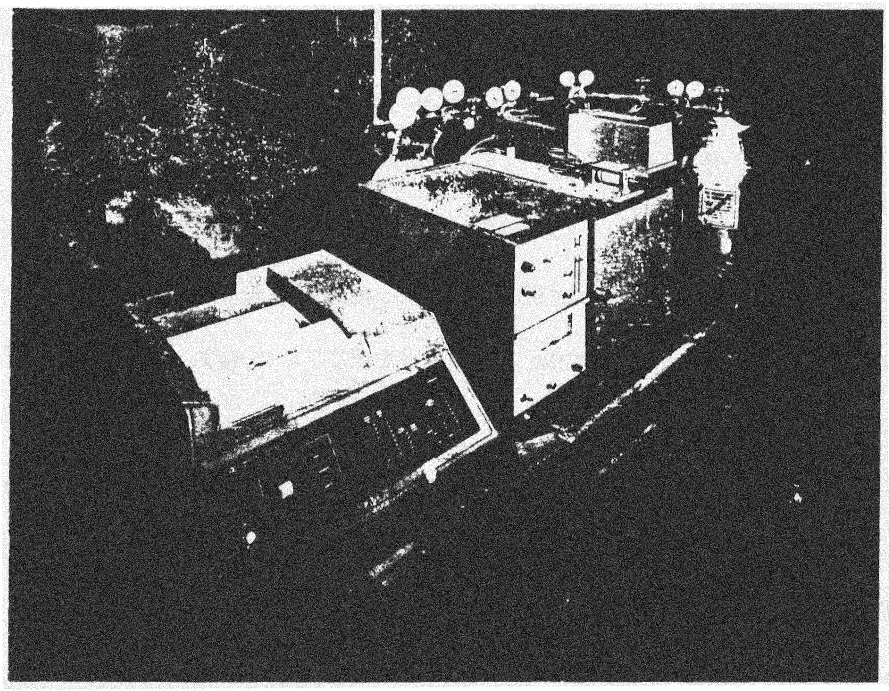

(b)

Figure 16. Photographs of (a) the Gas Sampling System, and (b) the HP Integrator and Gas Chromotograph

from the electrometer is sent to the Hewlett-Packard 3380 Integrator, 3) the output signal is integrated by the HP 3380, 4) this value $(\mu v\text{-}s)_{mea.}$ along with the response levels for the background $(\mu v\text{-}s)_{bg}$ and source $(\mu v\text{-}s)_{source}$ are converted into concentration by the equation

$$\chi = \frac{\chi_{mea.} - \chi_{bg}}{\chi_{source} - \chi_{bg}} = \frac{(\mu v\text{-}s)_{mea.} - (\mu v\text{-}s)_{bg}}{(\mu v\text{-}s)_{source} - (\mu v\text{-}s)_{bg}}$$

The tracer gas mixtures were supplied and certified by Scientific Gas Products.

3.5.2.3 Error in Concentration Measurements with the Gas Chromatograph

The error (~2-3 standard deviations) due to the combined effects of calibration, source strength, sampling, and instrument uncertainties is estimated at ±10%. The lower concentration limit for the different source gases used was:

Source Specific Gravity	Source Composition	Lower Concentration Limit
1.0	10% C_2H_6, 4.1% CO_2, 85.9% N_2	0.001%
1.22	19% CH_4, 81% A	0.002%
1.365	1.75% CH_4, 98.25% A	0.023%
1.5	3% C_2H_6, 97% CO_2	0.003%

Near these limits the error would be greater than ±10%.

4.0 TEST PROGRAM AND DATA

The dense plume measurement program was designed to provide a basis for the analysis of plume scaling laws, for the establishment of proper physical modeling techniques, for the development of a generalized laboratory plume which encompasses the behavior of all laboratory plumes, and to assist in the development and verification of analytical models. All tests were performed in the EWT described in section 3.1. The plumes were released from an area source mounted flush to the wind tunnel floor. The exit momentum in all tests was small. Source conditions and measurement systems are described in sections 3.2 and 3.5, respectively. The floor in the vicinity of the plume was always flat and smooth with no obstacles to cause wake effects. Two different upwind approach flow conditioning methods were employed as described in section 3.1. The mean velocity profiles described in section 4.4 were very similar, but the upper level turbulence in the visualization tests was decreased to insure that the plume outline remained visable far downwind. All concentration tests were performed in a typical atmospheric turbulence profile.

Section 4.1 reviews the run conditions and data obtained for all the visualization tests. Section 4.2 summarizes the run conditions and data obtained for all the continuous release concentration tests. Section 4.3 describes the run conditions and data obtained for all the transient release concentration tests. Section 4.4 discusses the approach wind field for all tests. Section 4.5 examines the results from the neutrally buoyant dispersion tests and considers the data implication with respect to Reynolds number invariance.

4.1 VISUAL PLUME DATA

The techniques employed to obtain the visual plume data are discussed in section 3.3, and an example of the plume appearance is shown in Figure 11. Table 1 contains the run conditions and data results for all forty-one visual plume tests. These tests included three different source gas specific gravities 1.38, 2.59 and 4.18, wind speeds at a height of 2.1 cm from 18.2-53.3 cm/s, and source flow rates from 40-346 ccs. The source diameter for all tests was 15 cm. Visual measurements of the upwind plume growth, L_u, the full plume width at the source, L_{H_o}, and the full plume width, L_{H_x}, at four different distances (61, 122, 244, 366 cm) downwind were made. The implications of this data set are discussed in Chapter 5. An empirical correlation which collapses the plume shapes to a single contour is presented in Chapter 6.

4.2 CONTINUOUS PLUME CONCENTRATION DATA

The techniques employed to obtain the concentration data are discussed in section 3.5. Runs 42 through 89 were all continuous release plumes. Runs 42 through 76 were measured with the aspirated hot-wire probes. Table 2 summarizes the test conditions and the mean ground level centerline concentration decay with downwind distance for each test. A separate appendix to this report gives a complete data listing of these runs. Since this data set was obtained with a fast response concentration measurement technique the peak concentration (approximately at the 1% probability level) and the root-mean-square concentration are reported along with the mean concentration. In runs 77 through 89 the gas-chromatograph flame-ionization measurement system was used to find mean concentrations. Table 3 summarizes the test

Table 1. Summary of Visual Plume Data

Run No.	Symbol[+]	Source Gas Specific Gravity ρ_s/ρ_a	Source Gas Flow Rate Q (ccs)	Wind Speed u@ 2.1 cm (cm/sec)	Upwind Plume Extent L_u (cm)	Lateral Plume Extent x=0 cm L_{H_o} (cm)	x=61 cm L_{H_x} (cm)	x=122 cm L_{H_x} (cm)	x=244 cm L_{H_x} (cm)	x=366 cm L_{H_x} (cm)
1	○	1.38	43	19.7	10	32.5	80	90	100	
2	◒	1.38	65	19.1	10	37.5	90	105	155	165
3	◔	1.38	107	20.5	14	54.5	110	150	157.5	190
4	◑	1.38	207	19.7	23.5	90	160	190	245	270
5	◕	1.38	72	29.5	8	25	65	80	95	105
6	◒	1.38	145	29.6	11.5	34.5	75	100	135	155
7	◔	1.38	207	27.9	15	50	100	120	160	185
8	◐	1.38	346	27.3	19	75	120	160	205	220
9	◕	1.38	85	39.8	8	20	50	65	100	125
10	●	1.38	170	38.9	10	30	70	85	115	140
11	⊖	1.38	330	38.3	14	45	100	125	150	190
12	⊘	1.38	83	53.3	7.5	15.5	35	50	75	
13	⊖	1.38	162	52.2	7.5	20	50	60	85	110
14	⊘	1.38	327	52	10	25	65	75	110	130
15	△	2.59	102	18.2	23.5	95	165	215	275	300
16	△	2.59	153	18.5	35	117.5	195	240	315	340
17	▲	2.59	205	18.8	50	142	250	280	335	340
18	▲	2.59	256	19.2	50	160	255	290	350	370
19	▲	2.59	86	32.3	19	60	105	140	175	
20	▲	2.59	173	31.3	27	98	145	185	225	250
21	▲	2.59	85	38.7	14	42	90	110	130	160
22	▲	2.59	123	38.5	17	57	105	135	155	190
23	▲	2.59	205	38.7	24	75	125	155	190	220
24	◬	2.59	80	50.4	10	30	65	75	95	
25	◬	2.59	160	49.9	12	41	90	105	140	165
26	◬	2.59	240	50.0	18	55	100	125	150	175
27	□	4.18	51	20.3	25	80	145	180		
28	▬	4.18	77	20.4	30	102.5	165	210		
29	◪	4.18	102	20.4	42	130	193	225	310	370
30	■	4.18	128	20.8	52	150	215	270	335	370
31	◪	4.18	43	32.4	12	42	100	125		
32	■	4.18	87	33.5	22	75	125	155	205	
33	◪	4.18	163	33.4	35	115	175	210	275	320
34	■	4.18	251	31.3	50	152	215	260	330	370
35	◪	4.18	61	38.4	14	45	95	105	155	
36	■	4.18	102	37.4	22	65	115	145	190	230
37	⊟	4.18	195	39.3	32	104	158	185	245	285
38	⊠	4.18	40	51.0	8	20	55	70		
39	⊟	4.18	80	50.5	12	36	80	90	130	
40	⊠	4.18	120	50.8	12	52.5	95	105	150	
41	⊞	4.18	192	49.9	17.5	72.5	110	140	170	190

[+]Symbols used in all figures unless noted differently on the figure
*Source Diameter for all tests = 15 cm
*Coordinate system referenced to source center
*Lateral distances are all full plume width values

Table 2. Continuous Release Concentrations Tests Taken with Hot Wire Aspirated Probes

Run No.	Symbol	Source Gas Specific Gravity ρ_s/ρ_a	Source Gas Flow Rate Q (ccs)	Wind Speed at 2.1 cm u (cm/sec)	$\bar{\chi}$ t x=30.5 (cm)	x=61 (cm)	x=122 (cm)	x=244 (cm)	x=366 (cm)
42+	○	1.38	170	20	0.189	0.103	0.050	0.018	0.012
43	◒	1.38	110	20.2	0.146	0.069	0.035	0.015	-
44+	◔	1.38	242	26.5	0.264	0.139	0.075	0.037	0.021
45+	◑	1.38	170	30	0.192	0.102	0.050	0.021	0.015
46+	◐	1.38	100	33.4	0.134	0.069	0.033	0.012	0.007
47+	◒	1.38	100	33.4	0.134	0.072	0.030	0.015	-
48+	◔	1.38	170	40	0.225	0.114	0.051	0.021	0.015
49+	◐	1.38	105	42.5	0.148	0.074	0.030	0.009	0.003
50+	◐	1.38	222	44	0.222	0.121	0.061	0.023	0.010
51+	●	1.38	170	50	0.201	0.100	0.041	0.017	0.007
52	⊖	1.38	340	51	0.273	0.152	0.074	0.031	-
53	◇	1.79	98	42.4	0.19	0.10	0.041	0.019	0.005
54	◈	1.79	144	48.1	0.22	0.115	0.055	0.026	0.012
55	◈	1.79	347	64.5	0.28	0.16	0.085	0.033	0.018
56	△	2.59	170	25	0.237	0.128	0.06	0.024	0.016
57	◬	2.59	87	30.1	0.13	0.068	0.032	0.014	-
58	◭	2.59	170	37	0.21	0.116	0.065	0.028	0.014
59	◭	2.59	224	41.2	0.238	0.125	0.071	0.036	0.022
60	◭	2.59	79	49.8	0.125	0.08	0.043	0.016	0.008
61	◬	2.59	170	51.5	0.206	0.112	0.061	0.029	0.017
62+	◭	2.59	170	63.5	0.18	0.109	0.056	0.025	0.01
63+	▲	2.59	204	68.1	0.20	0.11	0.055	0.021	0.013
64	◭	2.59	280	75.5	0.225	0.135	0.075	0.029	0.011
65	◬	2.59	170	77.5	0.201	0.114	0.049	0.012	0.005
66+	□	4.18	60.5	33.5	0.095	0.048	0.025	0.01	0.006
67+	▬	4.18	192	35	0.192	0.115	0.062	0.032	0.018
68+	◹	4.18	139	44.2	0.14	0.09	0.047	0.024	0.013
69+	◨	4.18	192	50	0.191	0.116	0.067	0.03	0.021
70	◪	4.18	55	55.4	0.085	0.05	0.024	0.01	0.005
71+	▬	4.18	310	58.4	0.255	0.14	0.081	0.05	0.028
72+	◹	4.18	192	70	0.191	0.104	0.06	0.025	0.017
73+	◧	4.18	126	73.1	0.13	0.075	0.04	0.013	0.005
74+	◪	4.18	192	86.5	0.166	0.091	0.049	0.017	0.006
75+	■	4.18	280	96.5	0.14	0.08	0.04	0.015	0.005
76	⊟	4.18	192	100	0.146	0.084	0.04	0.014	0.006

*Source Diameter for all tests = 15 cm
*Coordinate system referenced to source center
*All tests were isothermal, $T_a/T_s = 1$
*All tests are continuous release plumes
*For all tests concentrations were measured on half the groundlevel plane
+For these tests vertical concentration measurements were made at center line points downwind

Table 3. Continuous Release Concentrations Tests Taken with Gas Chromotograph System

Run No.	Source Gas Specific Gravity ρ_s/ρ_a	Source Gas Flow Rate Q (ccs)	Wind Speed at 2.1 cm u (cm/sec)	$\bar{\chi}_t$ x=30.5 (cm)	x=45.7 (cm)	x=61 (cm)	x=91 (cm)	x=122 (cm)	x=244 (cm)	x=305 (cm)	x=366 (cm)
77	1.0	182	21		0.184	0.13	0.083	0.042	0.014	0.013	
78	1.0	182	31.5		0.128	0.093	0.052	0.026	0.01	0.007	
79	1.0	364	31.5		0.192	0.15	0.069	0.044	0.018	0.013	
80	1.0	546	31.5		0.169	0.149	0.09	0.063	0.025	0.019	
81	1.0	182	47.3		0.10	0.065	0.034	0.018	0.007	0.005	
82	1.0	364	47.3		0.163	0.108	0.06	0.034	0.014	0.011	
83	1.0	546	47.3		0.138	0.118	0.045	0.031	0.015	0.008	
84	1.0	182	63		0.071	0.053	0.033	0.016	0.006	0.005	
85	1.0	364	63		0.126	0.092	0.06	0.033	0.013	0.01	
86	1.0	546	63		0.16	0.125	0.075	0.045	0.018	0.01	
87	1.22	77	25.4	0.1128		-		0.0291	0.0107		0.0053
88	1.365	98	32.7	0.1333		0.0722		0.0330	0.0139		0.0066
89	1.5	115	38.3	0.1572		0.0928		0.0406	0.0174		0.0089

*Source Diameter for all tests = 15 cm
*Coordinate system referenced to source center
*All tests were isothermal, $T_a/T_s = 1$
*All tests are continuous release plumes

conditions and the mean ground level centerline concentration decay with downwind distance for each test. Off centerline and vertical traverses at the centerline were also performed. The implications of this data set, runs 42 through 89, are discussed in Chapter 5, and empirical correlations which account for the effects of specific gravity, source strength, etc. are presented in Chapter 6.

4.3 TRANSIENT PLUME CONCENTRATION DATA

Runs 90-1 through 101-5 were for transient source conditions. Concentrations were measured by the aspirated hot-wire probes. Table 4 summarizes the test conditions and the peak ground level centerline concentration decay with downwind distance for each test. Twelve combinations of source specific gravity, source flow rate, and approach flow velocity were used. For each of the twelve combinations the behavior of five or six plumes with different source time durations were measured. A separate appendix to this report gives a complete data listing of these runs. This data set will not be discussed further in this report.

4.4 VELOCITY FIELD DATA RESULTS

The techniques employed in the acquisition of upwind velocity information are discussed in section 3.4. The major purpose for laboratory plume measurements is prediction at atmospheric scales. A critical requirement for accurate extrapolation is similarity in the distribution of upwind turbulent velocities. It is common to assume statistical stationarity[1] of these turbulent velocities. With this

[1]Statistical stationarity of a random variable, in this case the turbulent velocities, implies that the statistics of this variable do not change in time, i.e., the probabilistic moments such as signal mean, variance, etc. and the spectral distribution do not change in time. This assumption is valid for the wind field in the laboratory where large scale fluctuations are controlled, but in the atmosphere total wind field stationarity does not exist. To employ statistical techniques the assumption of approximate local stationarity over some time interval is commonly made.

Table 4. Transient Release Concentration Tests

Run No.	Source Gas Specific Gravity ρ_s/ρ_a	Gas Flow Rate Q (ccs)	Wind Speed at 2.1 cm U_H (cm/s)	Source Gas Time Duration Δt (s)	$(x_{peak})_L$ x=30.5 (cm)	x=91.5 (cm)	x=183.0 (cm)
90-1	4.18	140	30	4	0.090	0.037	0.014
90-2	"	"	"	7	0.126	0.061	0.023
90-3	"	"	"	10	0.148	0.074	0.030
90-4	"	"	"	15	0.180	0.086	0.041
90-5	"	"	"	25	0.193	0.095	0.044
90-6	"	"	"	40	0.200	0.103	0.048
91-1	4.18	255	37	4	0.161	-	0.018
91-2	"	"	"	7	0.206	0.070	0.028
91-3	"	"	"	10	0.244	0.083	0.037
91-4	"	"	"	15	0.246	0.090	0.046
91-5	"	"	"	40	0.267	0.109	0.058
92-1	4.18	140	60	2	0.051	0.016	-
92-2	"	"	"	4	0.094	0.031	0.011
92-3	"	"	"	7	0.125	0.051	0.023
92-4	"	"	"	10	0.146	0.058	0.025
92-5	"	"	"	40	-	0.071	0.039
93-1	4.18	255	74	2	0.123	0.046	0.015
93-2	"	"	"	4	0.156	0.073	0.033
93-3	"	"	"	7	0.178	0.079	0.043
93-4	"	"	"	10	0.190	0.084	0.046
93-5	"	"	"	40	0.207	0.104	0.056
94-1	2.59	280	30	4	0.183	0.052	0.018
94-2	"	"	"	7	0.240	0.077	0.033
94-3	"	"	"	10	0.263	0.093	0.040
94-4	"	"	"	15	0.284	0.112	0.050
94-5	"	"	"	40	0.293	0.121	0.063
95-1	2.59	280	44	4	0.102	0.038	0.013
95-2	"	"	"	7	0.125	0.053	0.022
95-3	"	"	"	10	0.137	0.055	0.026
95-4	"	"	"	15	0.148	0.055	0.030
95-5	"	"	"	40	0.160	0.061	0.036
96-1	2.59	130	33.5	4	0.077	0.024	0.010
96-2	"	"	"	7	0.135	0.038	0.018
96-3	"	"	"	10	0.163	0.058	0.023
96-4	"	"	"	15	0.177	0.062	0.028
96-5	"	"	"	40	0.174	0.071	0.038
97-1	1.38	110	20	4	0.05	0.018	-
97-2	"	"	"	7	0.102	0.025	-
97-3	"	"	"	10	0.112	0.032	-
97-4	"	"	"	15	0.132	0.039	0.017
97-5	"	"	"	40	0.146	0.050	0.021
98-1	1.38	295	28	4	0.171	0.044	0.022
98-2	"	"	"	7	0.237	0.066	0.032
98-3	"	"	"	10	0.273	0.084	0.044
98-4	"	"	"	15	0.282	0.102	0.043
98-5	"	"	"	40	0.286	0.109	0.055
99-1	1.38	295	48	4	0.230	0.076	0.025
99-2	"	"	"	7	0.290	0.091	0.049
99-3	"	"	"	10	0.308	0.112	0.047
99-4	"	"	"	15	0.311	0.136	0.064
99-5	"	"	"	40	0.330	0.124	0.062
100-1	1.38	100	33.5	4	0.075	0.020	-
100-2	"	"	"	7	0.117	0.038	-
100-3	"	"	"	10	0.143	0.042	-
100-4	"	"	"	15	0.137	0.047	0.020
100-5	"	"	"	40	0.160	0.054	0.024
101-1	1.38	170	65	2	0.035	-	-
101-2	"	"	"	4	0.052	-	-
101-3	"	"	"	7	0.104	0.035	-
101-4	"	"	"	10	0.130	0.031	-
101-5	"	"	"	40	0.154	0.048	0.017

*Source diameter for all tests = 15 cm
*Coordinate system referenced to source center
*All tests were isothermal, $T_a/T_s = 1$

assumption the turbulent velocity at a single spacial point may be described via probabilistic[2] and spectral[3] methods. Usually it is considered sufficient to measure and compare the first two moments of the turbulent velocity probability distribution. The first two moments are the mean velocity and the turbulent velocity variance (standard deviation, root-mean-square (r.m.s.) velocity) about this mean. Given a fully developed, stationary, spatially homogeneous flow variation of the turbulent velocities only occurs in the vertical direction. To demonstrate similarity between the model and prototype wind fields it is sufficient to compare the vertical variation of mean velocity, rms velocity, and spectral energy. Sections 4.4.1, 4.4.2, and 4.4.3 treat each of these topics for the longitudinal velocity component in a neutrally stable flow.

Comprehensive data has been obtained in the atmospheric boundary layer for a variety of different conditions [14,31,32]. Most correlations over this data base emphasize strong winds. The flow characteristics at lower wind speeds generally display a much greater variability. Nevertheless, to obtain some bases for comparative similarity the high wind speed empirical models are extrapolated here to the low wind speeds which are commonly of interest in plume dispersion studies.

4.4.1 Mean Wind Profiles

The mean wind speed profile is commonly described by either the log-linear relationship $u(z)/u_* = 2.5 \ln(z/z_o)$ where u_* is the friction

[2]A probabilistic description of a turbulent velocity involves the probability of occurrence of a velocity of a certain magnitude. The most probable velocity is the mean velocity.

[3]A spectral description of a turbulent velocity is the harmonic decomposition of the turbulent velocities magnitude or, more commonly, turbulent energy.

velocity at the wall and z_0 is the roughness length or the power-law relationship $u(z)/u_H = (z/H)^p$. The exponent, p, in the power law description and the roughness length, z_0, in the log-linear description are functions of the surface roughness conditions. Rougher boundary conditions (z_0 and p larger) increase the momentum deficit in the mean shear flow as depicted in Figure 17. Also shown with this figure is a summary of the variation in z_0 and p with the type of terrain [31]. Figures 18 and 19 show the variation of mean velocity with height for the range of conditions used in both visual and concentration tests.

Figure 18 indicates that the roughness length characterizing the wind tunnel shear profile was, $z_0 = 0.01$ cm. If length scaling were based upon this parameter[1] alone a model scale of 1:250 would be representative of farmland, a model scale of 1:1000 would be representative of a rural setting with a few trees, etc. This correspondence between scale and terrain type suggests a definite limitation to the ability of a wind tunnel to model a large release of heavy gas in an area of small surface roughness (ice, mud flats, calm open sea). The smallest z_0 that can be obtained in most wind tunnels is of the order of 0.001 cm.

Figure 19 which displays the power law correlation of the mean velocity profiles also suggests the scale constraint mentioned above. If the power index, p, could describe the entire profile then the terrain conditions predicted would be invariant with respect to the chosen length scale. As seen in this figure there is a systematic variation of the index p with height. p becomes larger with decreasing height which is essentially equivalent to the observed scale dependence of z_0.

[1] z_0 is not the only scaling length of importance. It characterizes the mean flow scale. Scales characteristic of the fluctuating velocities must also be considered.

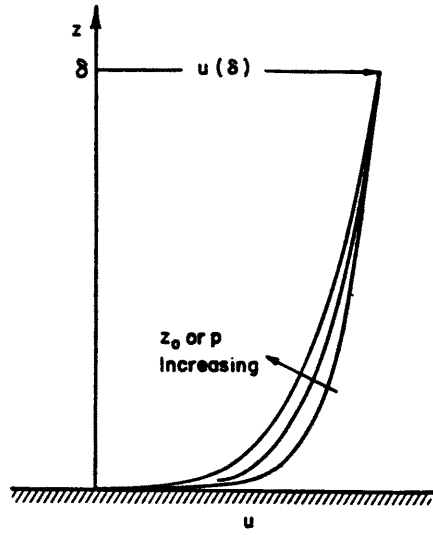

Terrain Type	z_o(cm)	p
Ice, Mud Flats	0.001	0.08
Calm Open Sea	0.01	
Sea, Desert	0.07	
Farmland Snow Cover	0.2	0.1
Short Grass	0.1-0.7	0.12
Rough Sea	2	
Grass Plains	2	0.13
Farm Crops	5	0.14
Rural	20	0.16
Small Towns	50	0.18
Forests	100	0.20
Large Cities	150-400	0.25-0.4

Figure 17. Mean Wind Shear Variation for Different Ground Roughness Conditions

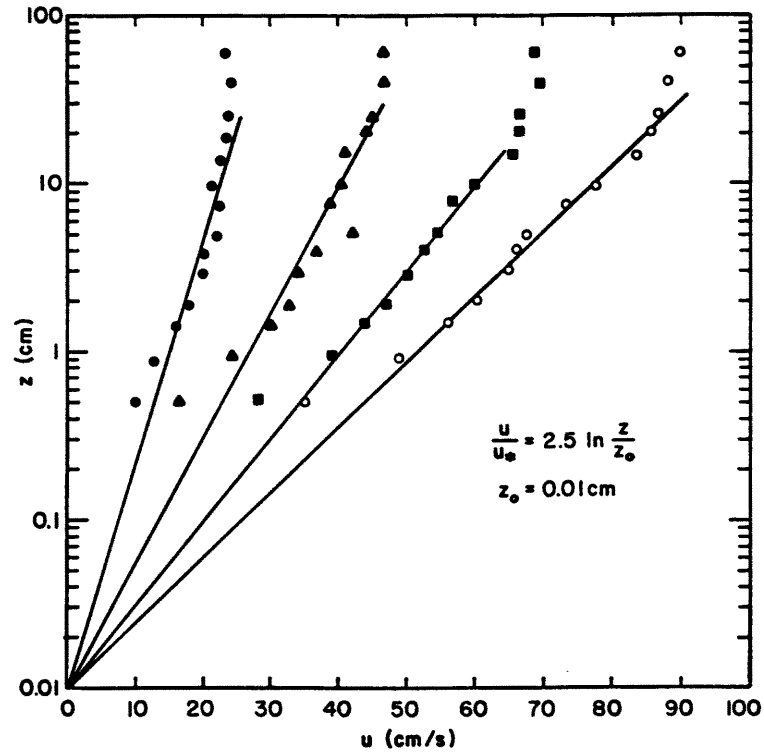

Figure 18. Log-Linear Description of Mean Velocity Variation with Height for the Model Boundary Layers

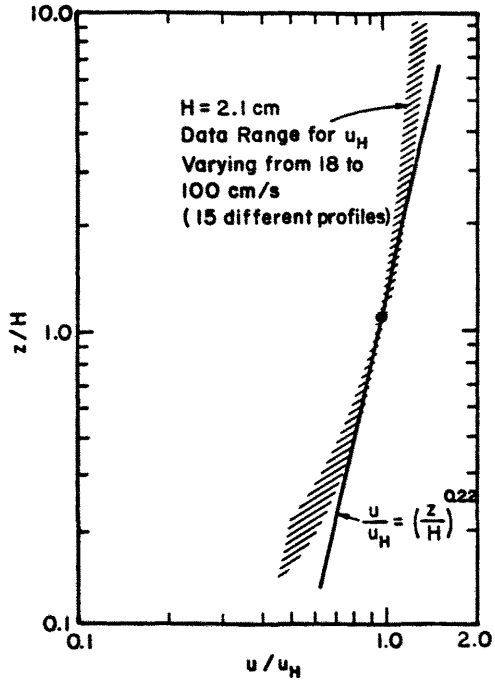

Figure 19. Power Law Description of Mean Velocity Variation with Height for the Model Boundary Layers

At smaller reference heights (larger model length scales) the power law index, p becomes larger. The table in Figure 17 shows that a larger p corresponds to a larger surface roughness. These observations indicate that the power law type representation should only be used over a portion of the shear layer. The solid line shown in Figure 19 which corresponds to p = 0.22 is provided to relate laboratory plumes of different length scales in section 5.3. A power law index of p = 0.22 relates the measured velocities over a length scale range of four centered around the reference velocity height.

The variation of mean wind speed at the reference height of 2.1 cm over the test sections crosswind and downwind directions was ±15% for runs with mean velocity below 30 cm/s and ±8% for runs with mean velocity above 30 cm/s.

4.4.2 Turbulent Intensity Profiles

The turbulent intensity of a turbulent velocity is defined as the rms velocity, σ_u divided by the local mean velocity, u. Figure 20 shows the variation in this turbulent intensity with height for both the visual tests and the concentration tests.

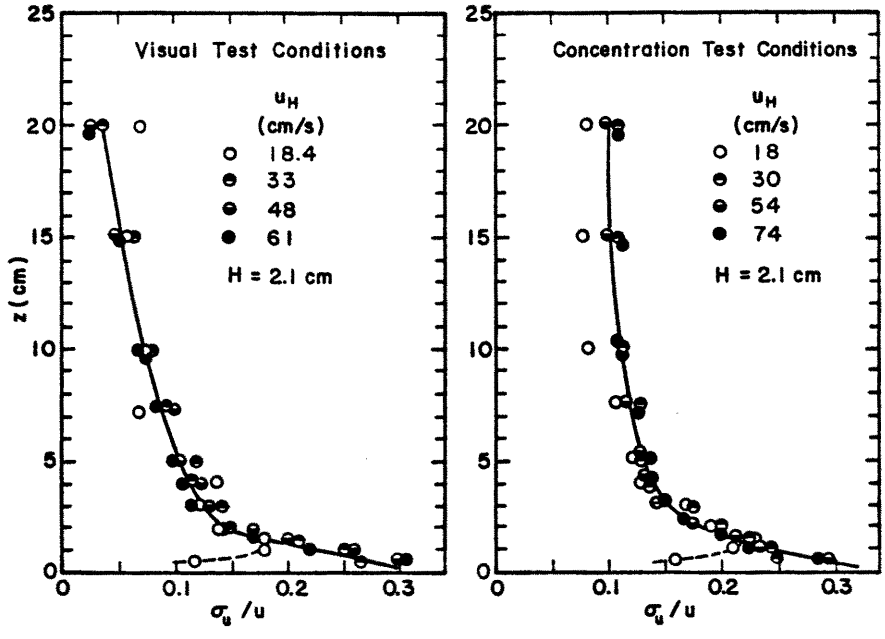

Figure 20. Local Longitudinal Turbulent Intensity Variation with Height for the Model Boundary Layers

The removal of the turbulence generators at the tunnel entrance section for the visual tests significantly reduces the upper level turbulent intensities; however, near the ground the turbulent intensity remains unchanged. As mentioned in section 4.4.1 the mean velocity profile for the two conditions was the same; thus the differences in intensity are

attributed solely to a change of magnitude of the rms velocity fluctuations. For the low wind speed tests ($u_H \cong 18$ cm/s) the turbulent intensity at 0.5 cm height drops to a lower value than at higher reference velocities. This is an indication that the boundary layer Reynolds number is not sufficient to maintain a highly turbulent flow near the boundary. To assess the impact of this deviation on the dispersion of a ground release plume several passive plumes were released into approach flows of different characteristic Reynolds numbers. These results are discussed in section 4.5.

The variation of turbulent intensity at the reference height of 2.1 cm over the test sections crosswind and downwind directions was ±17% for runs with mean velocity below 30 cm/s and ±8% for runs with mean velocity above 30 cm/s.

By correlating strong wind atmospheric data over a large variety of different roughness condition ESDU [32] concluded that the variation of turbulent intensity with height, z, up to 100 meters is:

$$\frac{\sigma_u}{u} = \frac{[0.867+0.556\ \log_{10}z-0.246(\log_{10}z)^2]\cdot B}{\log_e(z/z_o)} \ ,$$

where $B = 1.0$ for $z_o \leq 0.02$ m

$B = 0.76/z_o^{0.07}$ for $0.02 < z_o \leq 1.0$ m

$B = 0.76$ for $z_o \geq 1.0$ m .

Ninety percent of the data utilized fell within ±15% of the values given by this equation. Figure 21 is a comparison of the model data scaled by several different length scales to this atmospheric data relation.

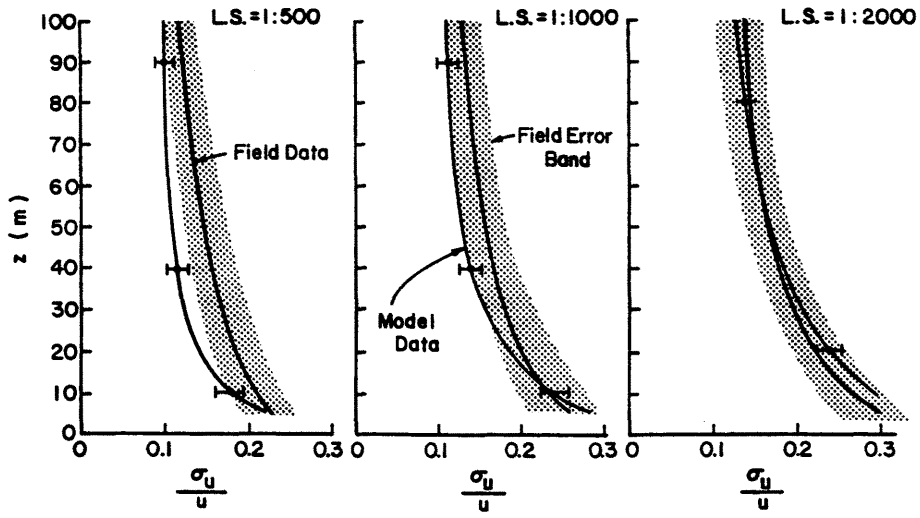

Figure 21. Field to Model Comparisons of Local Longitudinal Turbulent Intensity Variation with Height for Different Length Scale Ratios

It appears from these comparisons that a model length scale of ~1:2000 gives the best fit to the variation of turbulent intensity over the height of the entire surface layer. Since the present problem is to simulate the near field dispersion of a heavy gas plume released at the ground level it is only necessary that there be a good comparison of the turbulent intensities near the ground. It would appear that a length scale ratio of 1:1000 is more appropriate for ground level plumes. The spectral distribution of the turbulent velocities in both boundary layers are also analyzed in section 4.4.3. Consistency is sought between optimum scales for mean velocity, turbulence intensity, and spectra.

Since the ESDU atmospheric correlation is for strong wind conditions the extrapolation to low wind speed conditions may lead to errors of unknown magnitude. It is important that low wind speed velocity data be taken over any dispersion site prior to a physical modeling study.

4.4.3 Power Spectrum of Turbulent Velocity Fluctuations

A measure of the turbulent kinetic energy associated with the fluctuating velocity component, u' is $\overline{u'^2}$. The seemingly random variation of this energy measure, $\overline{u'^2}$ can be harmonically decomposed into the sum of cosine and sine waves of varying amplitudes and frequencies through the technique of Fourier Integral Transformations [33]. It is convenient to present this energy measure at frequency n as the integral of power over an incrementally small frequency range, dn. Or phrasing it mathematically, $S_u(n) = d(\overline{u'^2}(n)/dn$ where $S_u(n)$ is the longitudinal power spectral density and $\overline{u'^2}(n)$ is the energy density at frequency n. Integrating $S_u(n)$ over all frequencies yields the total mean square velocity fluctuation, $\sigma_u^2 = \overline{u'^2}$. The characteristics of the rms velocity fluctuation, σ_u were discussed in the previous section 4.4.2.

It is common to present spectral data in a normalized form such that equal areas on a graph represent equal fractional energies. The steps leading to this dimensionless form are summarized below:

1. Since the frequency usually varys over several orders of magnitude it is convenient to present the power spectral information as $S_u(n)$ versus $\log_e n$ but in order to maintain equal areas under the curve as having equal energies it is necessary to plot $nS_u(n)$ vs. $\log_e n$, i.e.

$$d(\overline{u'^2}(n))/d(\log_e n) = n\,\frac{d(\overline{u'^2}(n))}{dn} = nS_u(n).$$

2. When one is interested in only the frequency distribution of turbulent kinetic energy and not the total energy a normalization $nS_u(n)/\overline{u'^2}$ is commonly employed, where

$$\overline{u'^2} = \int_0^\infty nS_u(n)\,d(\log_e n).$$

3. One may use Taylor's hypothesis that turbulence is advected along with the mean flow in an undistorted manner ($\partial/\partial t = -u\ \partial/\partial x$, [7]) to transform the frequency axis, n, to that of the wave number,[1] $n/\bar{u}$. This transformation allows one to interpret the energy distribution in terms of the wavelength, $\lambda = \bar{u}/n$, which can be loosely associated with the size of turbulent eddy-like motions. Taylor's hypothesis is not strictly valid for small wave numbers [34]; thus any physical interpretation of the spectrum should be viewed cautiously at small wave numbers (for the atmosphere, $n/\bar{u} < \sim 0.003\ m^{-1}$).

4. The turbulent energy spectrum can be broken up into four broad regions (see Figure 1) [7]:
   a) A low frequency (large wavelength) production region where energy is transferred to turbulent motion from the mean flow.
   b) A range of wavelengths somewhat smaller than those of the production range which are characteristic of the energy containing eddies.
   c) An inertial subrange where the energy containing eddies are broken into eddies of smaller and smaller wavelength. Equilibrium cascading of turbulent energies results in the proportionality, $nS_u(n) \propto n^{-2/3}$.
   d) A final region where the eddies are small enough to be dissipated by viscosity and energies fall off more rapidly than in the inertial subrange.

To summarize in a presentation of $nS_u(n)/\overline{u'^2}$ versus $n/\bar{u}$ on log-log paper the magnitude of the function is the ratio of the turbulent energy at a specific wave number (or wavelength characteristic of a turbulent eddy) to the total turbulent energy of the flow. The inertial subrange will appear as a straight line with a slope of -2/3 when plotted in this manner, and the wavelength, λ_p, characteristic of the eddies of largest energy will be at the peak of the curve.

Figure 22 displays the spectral distribution of this normalized turbulent energy for a range of velocities at one centimeter height that encompass the test conditions under which concentration data were obtained. The distribution of turbulent energy changes quite consistently with changing velocity and thus changing Reynolds number. This

[1]Wave number is actually defined as $2\pi n/\bar{u}$, but to simplify the conversion to wavelength, $\lambda = \bar{u}/n$, the 2π term will be dropped from its definition for the remainder of the report.

characteristic fall off of spectral energy distribution with decreasing Reynolds number is discussed in section 2.1.1 and Figure 1 earlier in this report. The falloff is due to the narrowing of the inertial subrange with Reynolds number bringing the production range closer to the viscous dissipation range. It appears that there is no inertial subrange for the lower velocity tests. Batchelor as cited by Raine [34] gives as a criterion for the existence of the inertial subrange as $(Re_{\lambda_p})^{3/8} >>> 1$ where $Re_{\lambda_p} = \frac{\sigma_u \lambda_p}{\nu}$. The range of $(Re_{\lambda_p})^{3/8}$ for the data shown in this figure is from 13.8 to 23. The impact of this Reynolds number effect on the dispersion of plumes is difficult to evaluate. There is still a somewhat nebulous connection between this Eulerian spectral energy distribution and the more pertinent Lagrangian spectral energy distribution.

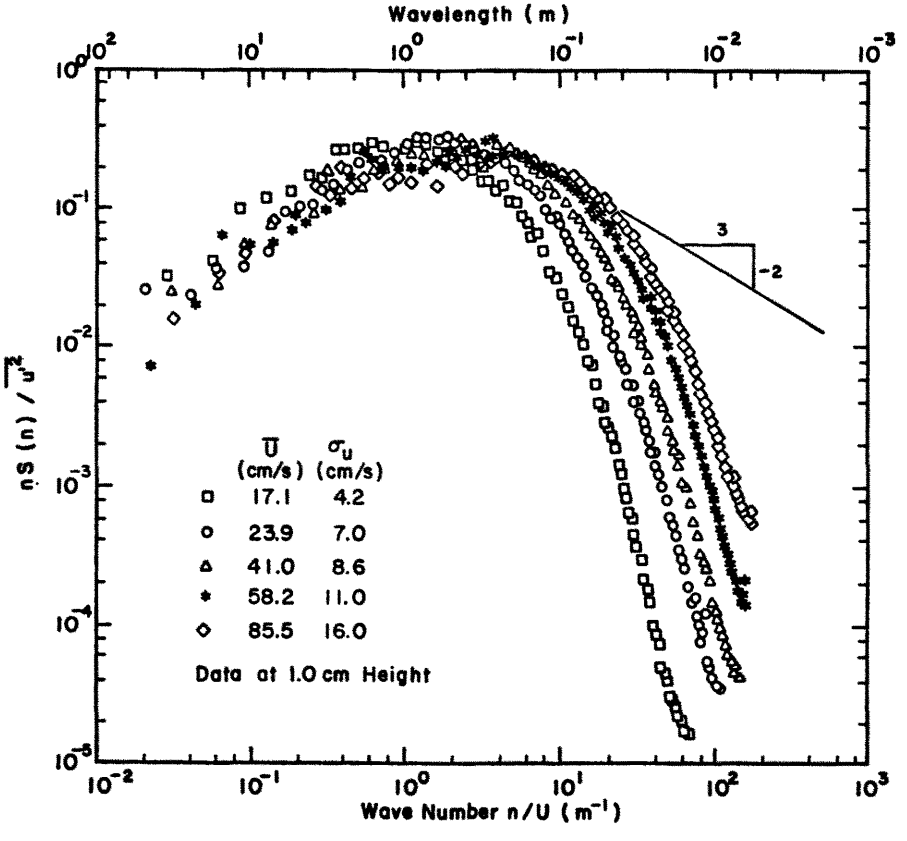

Figure 22. Power Spectrum of Turbulent Velocity Fluctuations within the Model Boundary Layers

To interpret wavelengths in Figure 22 as being proportional to the scales of turbulent motions which control dispersion may be conceptually misleading,[1] but the idea is pursued here to obtain an estimate of the impact of spectral energy variations on the laboratory plumes. The plumes tested had characteristic dimensions of the order of 4.0 meters downwind, 1.0 meter laterally, and 0.03 to 0.3 meters in height. Since turbulent scales much smaller than the plume scales just mix plume gases back and forth within the plume and turbulent scales much larger than the plume scales cause plume meandering[2] it is concluded that the turbulent scales affecting plume dispersion are of the same order as the plumes dimensions. The longitudinal integral scale of turbulence, L_{u_x}, may be approximated as $L_{u_x} = \lambda_p/2\pi$ [31]. This length scale is considered proportional to the size of the average energy containing eddies. The constant of proportionality between the wavelengths shown on the figure and the characteristic length scale of the turbulent motions is $1/2\pi = 0.16$. Multiplying the wavelength axis in Figure 22 by 0.16 and comparing the magnitude of the turbulent energy for the different Reynolds numbers tested over the converted scale range of 0.03 meters to 4 meters shows that within this range the comparisons appear acceptable expect for the lowest velocity case (lowest Reynolds number).

Empirical expressions have been proposed to correlate atmospheric spectral data [14,31,32,34]. The predictions of several of these expressions for the spectral distribution of turbulent energy for a

[1]The large eddies considered here are anisotropic. A one-dimensional spectrum cannot account for this three-dimensional character. It would be more appropriate to use a three-dimensional spectrum, but these are experimentally difficult to obtain.

[2]Meandering scales are not normally present in wind tunnels.

strong-wind neutrally-stable atmosphere at a ten meter height are presented in Figure 23. There is a fairly large scatter among these correlation curves let alone the original data base. The Harris, Davenport, and Kaimal curves do not predict any variation in the spectral distribution with changing surface roughness (variable z_0), but the ESDU curves do predict a spectral variation with changing z_0. Kaimal [14] reported that atmospheric spectra rapidly change character with the slightest onset of unstable density gradients. He proposed a neutral expression as the limit to stable distributions, and he included the shaded area presented in the Figure 23 as a highly variable range of the spectral distributions for neutral or undetectability unstable conditions. All the expressions predict the -2/3 decay characteristic of the equilibrium nature in the inertial subrange.

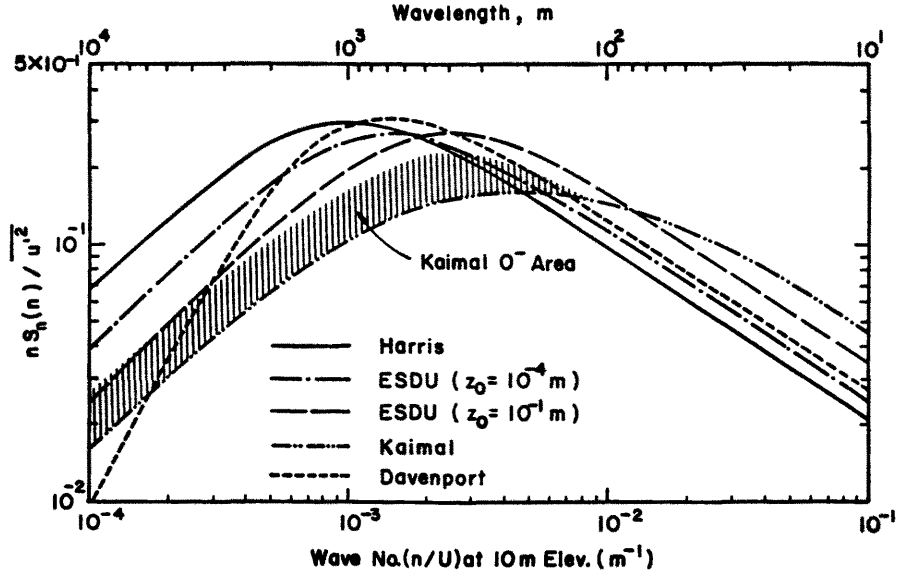

Figure 23. Different Descriptions of the Power Spectrum of Turbulent Velocity Fluctuation for the Atmospheric Boundary Layer

To use these curves as a basis for determining the approximate length scale relationship between the wind-tunnel boundary layer and the atmospheric boundary layer the peak wavelength representative of the energy containing eddies should be used. In Figure 23 λ_p ranges from 200 to 1000 meters with the majority of predictions in the neighborhood of 500 meters. In Figure 22 λ_p ranges from 0.4 to 0.7 meters with 0.5 meters as the best estimate. The ratio of these values yields a length scale ratio which ranges from 1:285 to 1:2500 with the best representation at 1:1000. The data in Figure 22 was taken at a 0.01 meter height, and the data in Figure 23 is representative of a 10 meter height. One concludes the relationship between the heights of reference is also proper; 10/0.01 = 1000.

The large variability found in the peak wavelength is due to the fairly flat variation of spectral energies at peak wavelengths and the large variations in predicted atmospheric spectral behavior. The flatness of the spectral distribution is natural; thus there should be some flexibility in choosing the representative model length scale ratio. The large variations in atmospheric spectral behavior is undoubtably due to the grouping together of measurements taken at many different sites. Site specific velocity information is essential for accurate selection of a model length scale ratio.

Figure 24 compares the ESDU atmospheric spectra correlations scaled down by three different length scale ratios to the wind tunnel spectral energy distribution. All evidence supports the conclusion that the wind-tunnel boundary layer has a 1:1000 length scale ratio. Since the model's roughness length was of the order of 0.01 centimeters, the wind tunnel's ground level roughness is representative of farm crops or a rural setting ($z_o \tilde{\sim}$ 10 cm, see Figure 17).

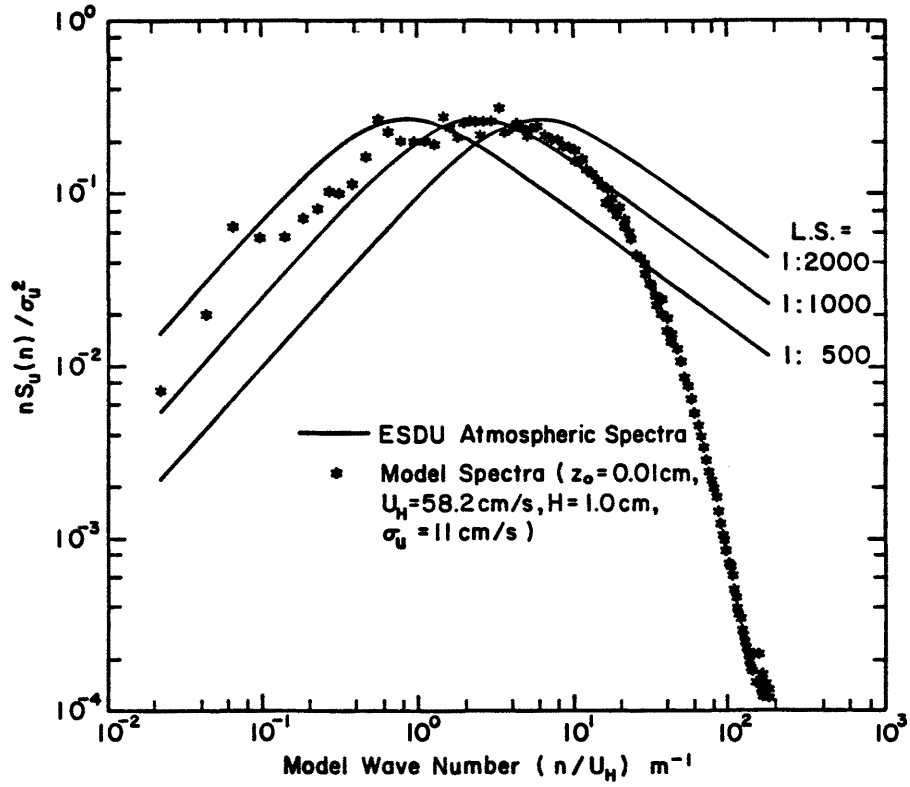

Figure 24. Field to Model Comparisons of the Power Spectrum of Turbulent Velocity Fluctuations for Different Length Scale Ratios

This length scale relationship between atmospheric and wind tunnel boundary layers is based on strong-wind atmospheric data. The extrapolation of this data base to low velocity atmospheric winds may lead to large errors. Indeed, in a recent wind tunnel simulation of LNG spills at China Lake, California, [5] plumes released in this same wind tunnel boundary layer were found to be in good agreement with field concentration measurements at a scale of 1:85. At this scale the mean velocity profile was properly matched and the turbulent intensity near the ground was also matched. Perhaps dense plume dispersion in the near field is not sensitive to the length scale ratio of the background turbulence.

4.5 PASSIVE PLUME DISPERSION TEST RESULTS

Downwind concentration measurements were obtained for ten neutrally buoyant plumes (source gas specific gravity of 1.0). The conditions for these tests and plume centerline concentration values are summarized in Table 3. The source configuration, a ground level circular area source of 15 cm diameter, was identical to that for all the heavy plume tests.

The passive plume tests were performed for three reasons. First, it was necessary to determine when there existed an effect of source gas initial momentum (or u_H/W) on the resultant concentration field. Second, to investigate the effects of different approach flow Reynolds numbers on a passive plume. Third, passive plume concentration fields provide a convenient reference for interpretation of heavy plumes.

Source Gas Momentum Effects

The source diameter was 15 cm. The vertical velocity of the source gas is $W = 0.00566\ Q$; hence we can calculate u_H/W from data in Table 3, i.e.:

Run No. =	77	78	79	80	81	82	83	84	85	86
u_H/W =	20.4	30.6	15.3	10.2	45.9	23.0	15.3	61.2	30.6	20.4

The normalized centerline concentrations (see section 2.2.2 for a discussion of the implications of this normalization) are plotted versus downwind distance in Figure 25. The data for runs 79, 80, and 83 fell short of the line correlating most of the data (note that data for runs 79, 80, and 83 are already removed from Figure 25). These runs had the lowest u_H/W ratios; thus for velocity ratios, u_H/W, less than 17 there was increased plume dispersion due to source momentum effects. Values

of the velocity ratio $u_H/W > 17$ were maintained throughout all dense plume tests reported. A heavy plume has more vertical momentum at the same velocity ratio; hence, the value of 17 may be nonconservative. Nonetheless, it was felt that this effect will be compensated by the large negative buoyancy forces causing the plume to collapse back on itself.

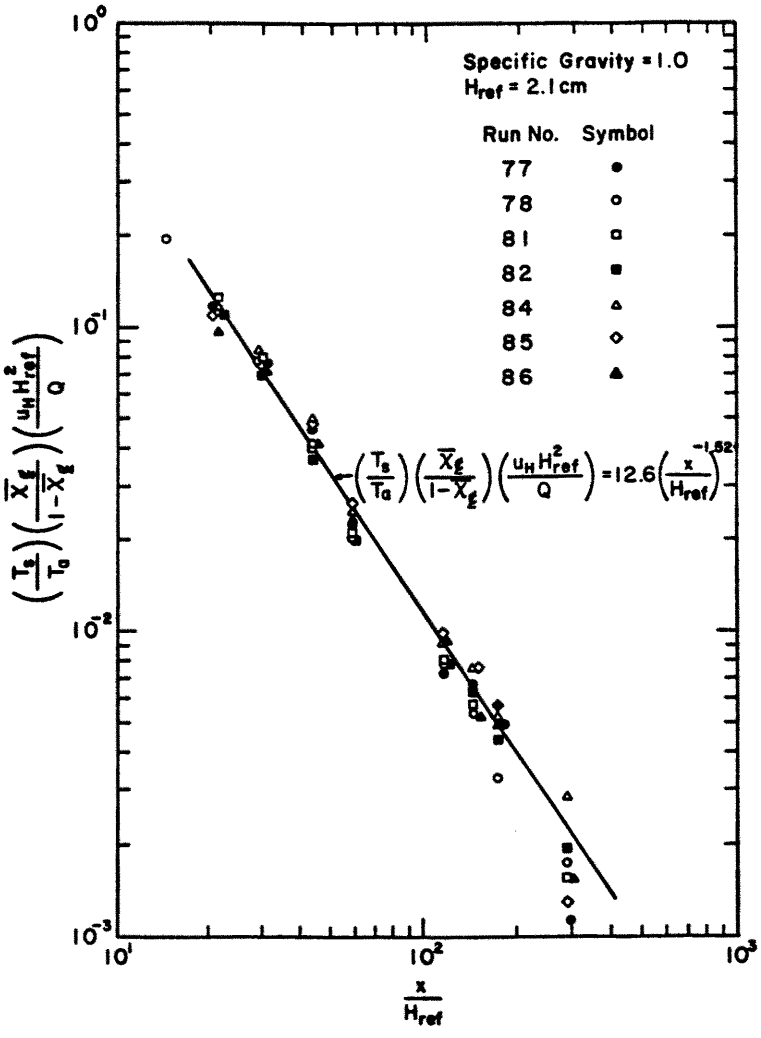

Figure 25. Normalized Centerline Concentration Decay with Downwind Distance for the Passive Dispersion Tests

Reynolds Number Invariance

It was suggested in section 2.1.1 and again in section 2.2.2 that an appropriate test for Reynolds number invariance is to release passive plumes of varying Reynolds numbers and normalize the concentrations

measured within the plumes by the technique developed in section 2.2.2. If the plumes truly are passive (no source momentum effects) then the entrainment physics and downwind concentration profile distributions[1] will be equivalent provided there is Reynolds number invariance.

In Figure 25 the normalized centerline concentration decay with downwind distance is plotted for the seven neutrally buoyant plumes that displayed no momentum effects. Sufficient agreement is obtained to conclude that the approach flow turbulent behavior is invariant with Reynolds number for velocities greater than 21 cm/s at a 2.1 cm height. These results suggest that the measured falloff in turbulent intensity at the 0.5 cm height (see section 4.4.2) and variations in the spectral energy distribution (see section 4.4.3) with decreasing Re do not significantly effect passive plume dispersion for the range of dense plume tests reported herein.

Since a heavy plume will alter the ambient turbulent velocity fluctuations within the plume the passive dispersion test for approach flow Re invariance by no means guarantees Re invariance for heavy plumes. To demonstrate Re invariance for heavy plumes it is necessary to take measurements on rigidly similar (no source density or volume distortion) plumes in boundary layers of different characteristic length scales. This was attempted during the model simulations of LNG spill tests performed at China Lake, California reported in [5,35]. Unfortunately, full scale wind field nonstationarity, lack of ensemble or statistical averages during field experiments and necessary modeling

[1]Note that when reference is made to a distribution it is intended that it is independent of actual magnitudes, i.e., the profile has been normalized by the magnitude of interest at some position within the profile.

approximations to the source conditions permit only qualitative conclusions with regard to the invariance. Forty cubic meter LNG spills at reference wind velocities greater than 6.3 m/s at 3 meters height were simulated "closely".[1] Low wind speed tests were not conclusive.

[1] "Closely" is, of course, a matter of judgement. The reader is referred to the original reports [5,35] for details.

5.0 ANALYSIS AND VERIFICATIONS OF HEAVY PLUME SCALING LAWS

Chapter 2 reviews atmospheric flow similarity and its interaction with plume dynamics. Under the most rigid scaling procedure there is a one-to-one correspondence between the control variables (L,u,Q,ρ_s) for the model and the field. For some classes of plume behavior it is felt that rigid scaling is overly restrictive; thus several different enhanced scaling schemes are discussed in sections 2.2.1.1, 2.2.1.2, and 2.2.1.3. These schemes include the relaxation of source density equality, the use of Flux Froude Number $(\dot{F}r = \frac{u^3 L}{Qg'})$ as the only significant plume parameter, and the variation of plume length scale within a fixed velocity field scale. An enhanced scheme permits a multiple correspondence between the control variables (L,u,Q,ρ_s). The advantages of enhanced schemes are:

1) Measurements on a single plume at a modeling or atmospheric scale can be used to predict the structure of other plumes at this same scale.
2) The range of field situations that can be physically modeled is increased (i.e., low winds speeds, large source gas releases).

The remainder of this chapter discusses the scaling implications of the data presented in sections 4.1 and 4.2. Section 5.1 discusses the effect of density ratio relaxation, section 5.2 discusses the similarity between plumes for which only $\dot{F}r$ equality is maintained, and section 5.3 discusses the similarity between plumes for which $\dot{F}r$ equality is maintained but the characteristic length scale, L, associated with the fixed velocity field is allowed to vary.

5.1 EFFECT OF DENSITY RATIO RELAXATION ON PLUME SIMILARITY

When the density ratio equality between two plumes is relaxed several of the other parameters listed in section 2.1 also vary. One must select which of these remaining parameters are dominant and

maintain their equality. For the data presented in sections 4.1 and 4.2 the plumes vertical momentum may be neglected. Previous studies suggest that [5,17] the plumes mass ratio may also be relaxed. The remaining parameters are then the Densiometric Froude Number ($Fr = \frac{u^2}{g'L}$) and the Volume Flux Ratio ($V = \frac{Q}{uL^2}$). Since the Flux Froude Number ($\dot{F}r = \frac{u^3L}{g'Q}$) is the ratio Fr/V its equality is guaranteed when equality in Fr and V are stipulated.

An alternate enhanced scheme might be to maintain the equality of $\dot{F}r$ and Mass Ratio ($M = \frac{\rho_s Q}{\rho_a uL^2}$). This scheme appears logical because it is the relationship between the inertia of the approach flow and the inertia of the plume which determines how rapidly the plume gases are accelerated to approach wind speeds (see Figure 26). Hence one might logically require equality of $\dot{F}r$ and M in an enhanced scheme.

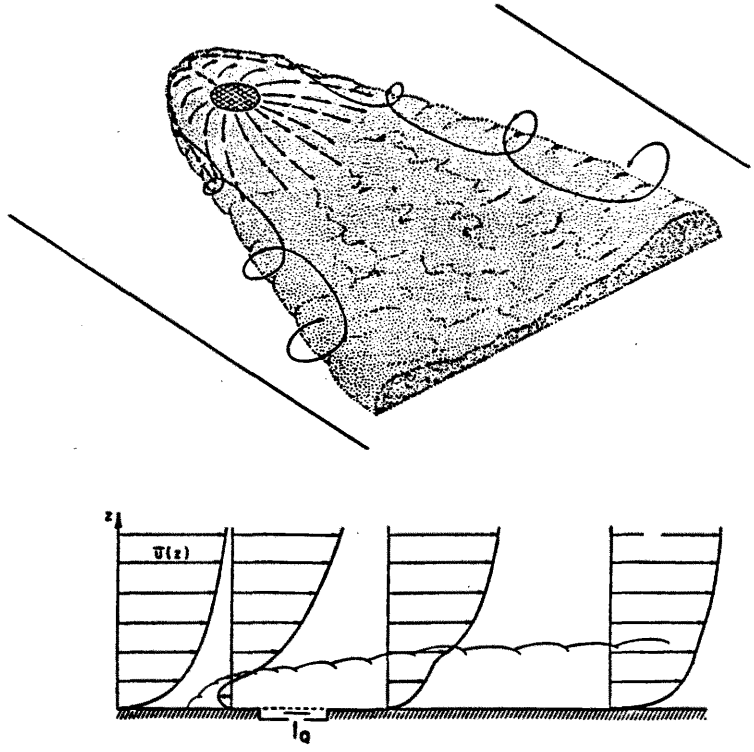

Figure 26. Qualitative Description of Velocity Field within a Heavy Gas Plume

Both of these schemes were evaluated. The table below summarizes the appropriate density distortion tests also listed in Tables 2 and 3 of section 4.2.

Run No.	Source Gas Specific Gravity	Source Gas Flow Rate (ccs)	Wind Velocity (cm/s)	ℓ_b (cm)	Type of Scaling
87	1.22	77	25.4	1	Fr & $V \equiv$
46,47,88	1.37	98	32.7	1	"
89	1.50	115	38.3	1	"
54	1.79	144	48.1	1	"
63	2.59	204	68.1	1	"
43	1.38	110	20.2	5	Fr & $V \equiv$
59	2.59	224	41.2	5	"
71	4.18	310	58.4	5	"
46,47,88	1.38	98	32.7	1	$\dot{F}r$ & $M \equiv$
53	1.79	98	42.4	1	"
60	2.59	79	49.8	1	"
70	4.18	55	55.4	1	"
43	1.38	110	20.2	5	$\dot{F}r$ & $M \equiv$
57	2.59	87	30.1	5	"
66	4.18	60.5	33.5	5	"

Figure 27 shows the centerline concentration decay with downwind distance for each of the four cases listed above. Section 2.2.2 justifies the ordinate and abscissa scales used in these figures. If the plumes are similar (in this enhanced sense) the data should fall onto a single line. The results from the passive plume tests for the same source configuration are presented in each of these figures for a reference. Figure 28 shows the two percent ground level concentration contour for the first group of runs (87,46,47,88,89,54,63).

It is clear that neither of the enhanced modeling schemes tested (Fr & $V \equiv$ and $\dot{F}r$ & $M \equiv$) are valid over the full range of source specific gravities. Both methods suggest that as the source specific gravity decreases the dispersion of the plume increases. For the cases in which $\ell_b = 1$ and the source specific gravity is greater than 2 there is

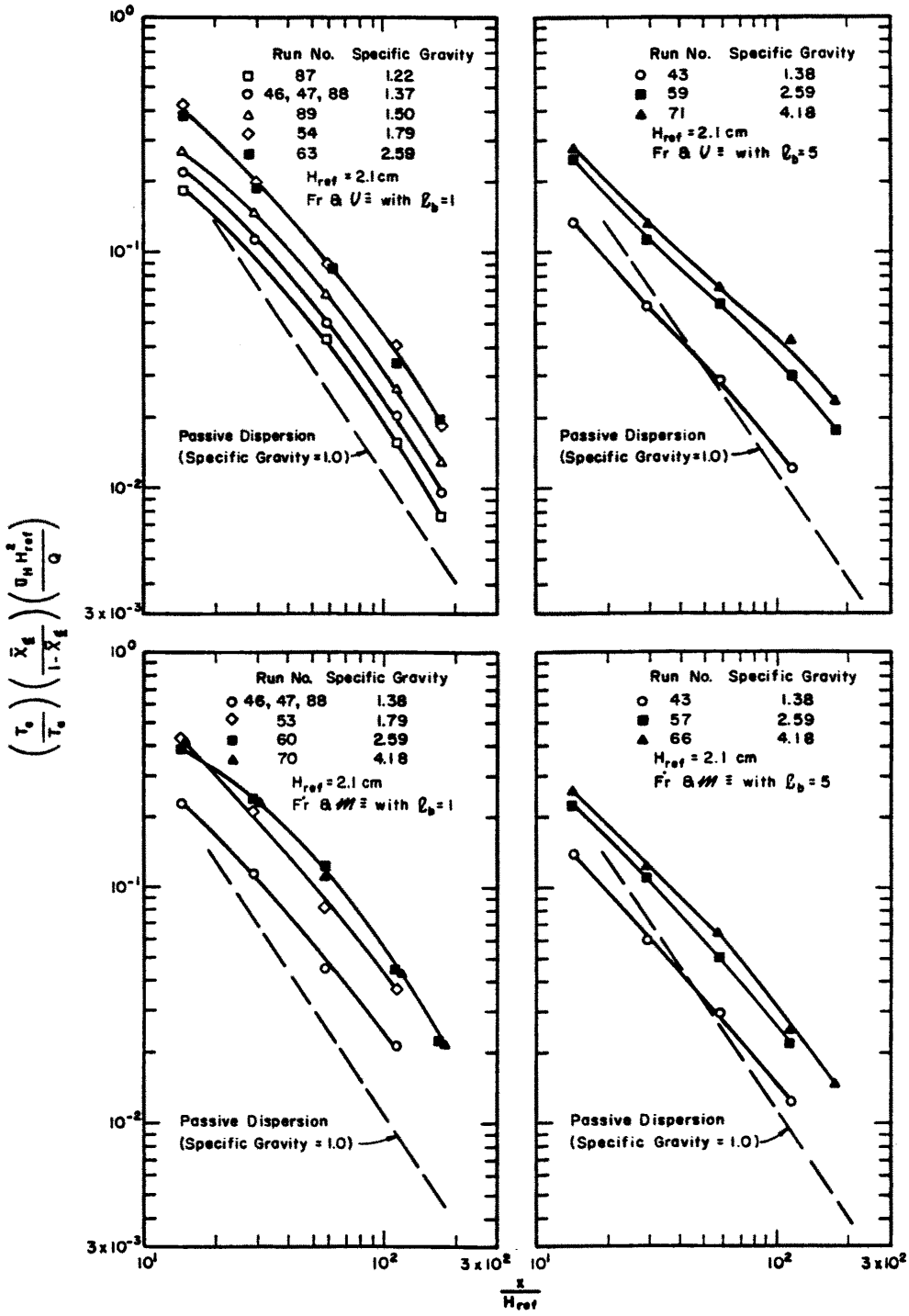

Figure 27. Normalized Centerline Concentration Decay with Downwind Distance for Source Specific Gravity Relaxation Tests

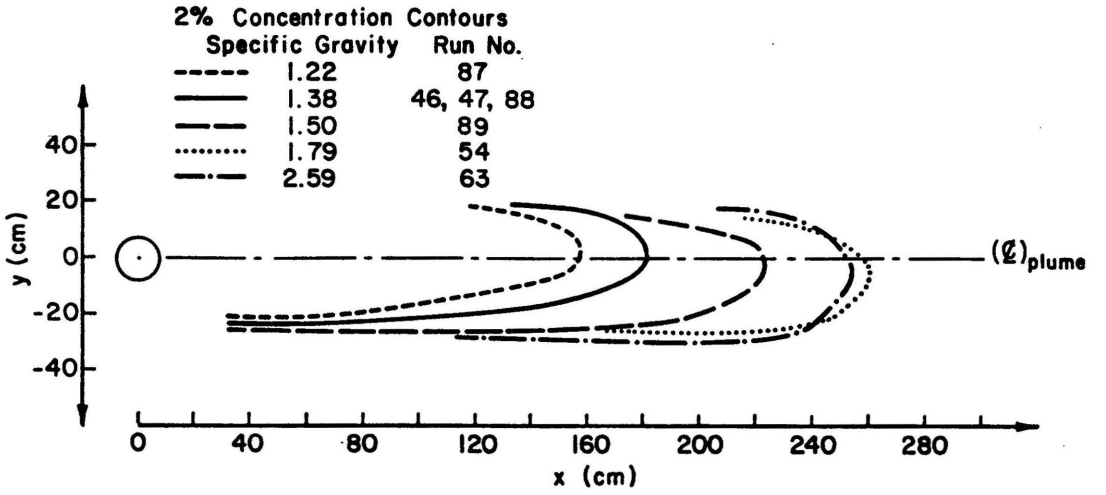

Figure 28. Ground Level Two Percent Concentration Contours for Source Specific Gravity Relaxation Tests

satisfactory similarity for either enhancement scheme. Neither scheme works well in other situations.

A plausible explanation for the behavior discussed above relates to suppression of turbulence by stable density gradients. The entrainment rate on the plumes upper surface is governed by the turbulent vertical velocity fluctuations, w'. The vertical density gradient, $\nabla\rho$, within a heavy plume will alter the magnitude of w' from that of the approach flow. As $\nabla\rho$ increases it will effectively dampen out w'. The largest effect of $\nabla\rho$ on plume entrainment rate will be near the source. For plumes in which the source specific gravity ratio is small $\nabla\rho$ will be small, and the dilution near the source will be large. For plumes in which the source specific gravity ratio is large $\nabla\rho$ will be large, and the dilution near the source will be small.

5.2 SUFFICIENCY OF FLUX FROUDE NUMBER MODELING FOR PLUME SIMILARITY

When equality of Fr, V, and ρ_s/ρ_a is specified along with the proper approach flow characteristics (geometric scale, Reynolds number invariance, etc.) plume structure will be rigorously similar. In

practice this leads to such restrictive conditions that it diminishes the range of application for physical modeling. Since the Flux Froude number, $\dot{F}r = Fr/V$, properly matches plume buoyancy and approach flow inertial forces maintaining only its equality increases the range of plumes which will exhibit similar structure. It would be helpful to know the extent to which V (or Fr) can be varied without changing plume similarity significantly.[1]

Data in sections 4.1 and 4.2 were grouped by equality in the Flux Froude number ($\dot{F}r = U_H^3 L/Qg' = L/\ell_b$). Since L is a characteristic length describing the total geometric setting of the plume (i.e., scale of the turbulence, scale of the topography, etc.) it will be constant for all plumes released into the same boundary layer. Comparing plume structure between tests of equal buoyancy length scales, $\ell_b = Qg'/U_H^3$, determines similarity limits for volume ratio distortion.[2] Figures 29 and 30 are plots of upwind and lateral plume extent versus ℓ_b respectively (refer to Table 1 to identify the run conditions for each symbol in these figures[3]). There is a definite tendency at a constant ℓ_b for increased plume growth with increasing volume flux ratio, V (or equivalently decreasing Fr). The magnitude of error incurred by this variation in V is unknown because of the large experimental error associated with estimation of ℓ_b (±45 percent). This large error is

[1]In section 5.1 it was shown that relaxation of the source density ratio results in a significant loss in plume similarity. Throughout the remainder of this section a distinction between the different source specific gravities tested will be maintained even though they are occasionally grouped on the same graph.

[2]Note that since g' = constant if the source specific gravity is not modified the line of enhancement by this technique would be $Q \propto U^3$.

[3]Figure 34 of section 5.3 is also useful in this context.

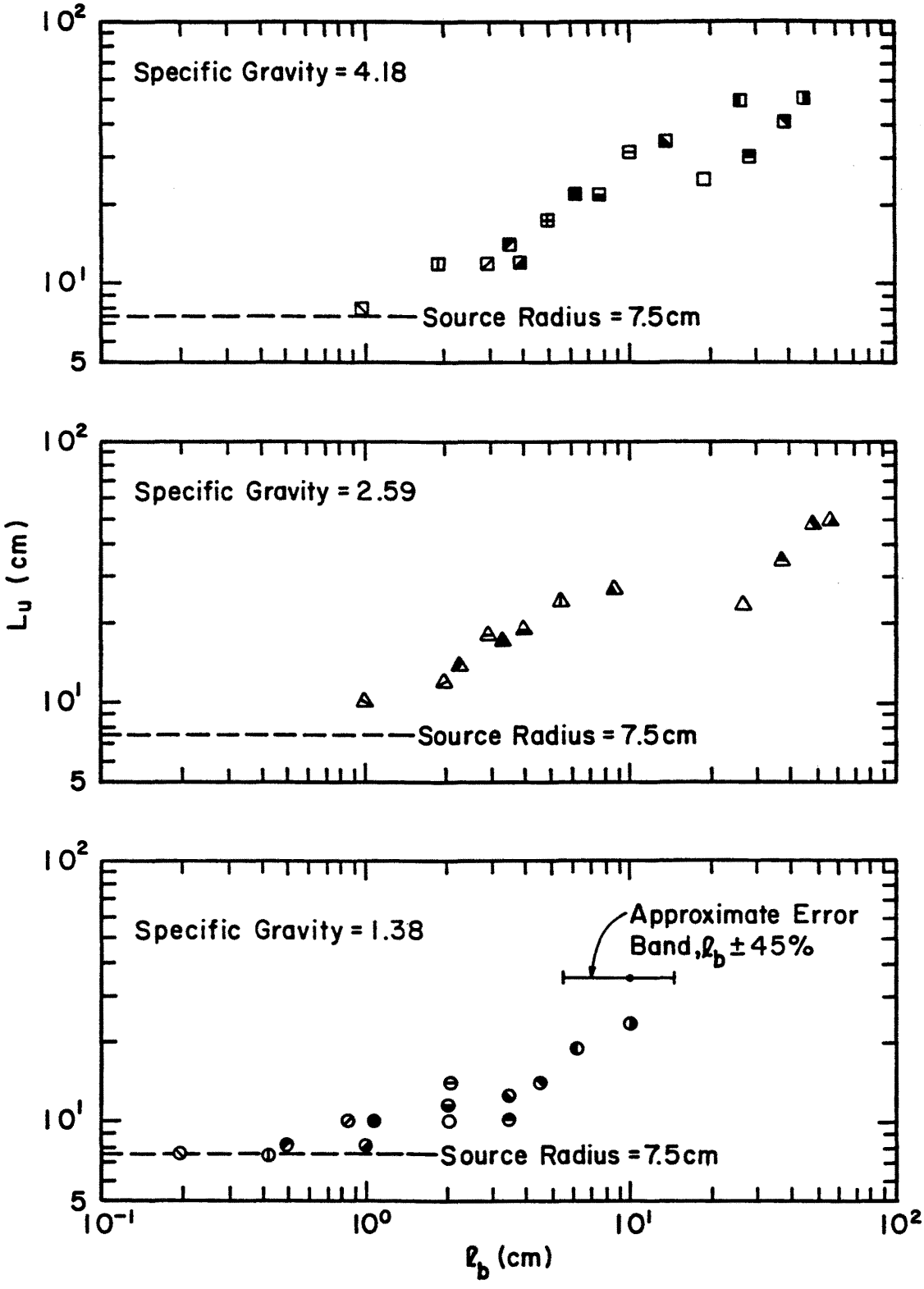

Figure 29. Plume Upwind Growth versus Buoyancy Length Scale

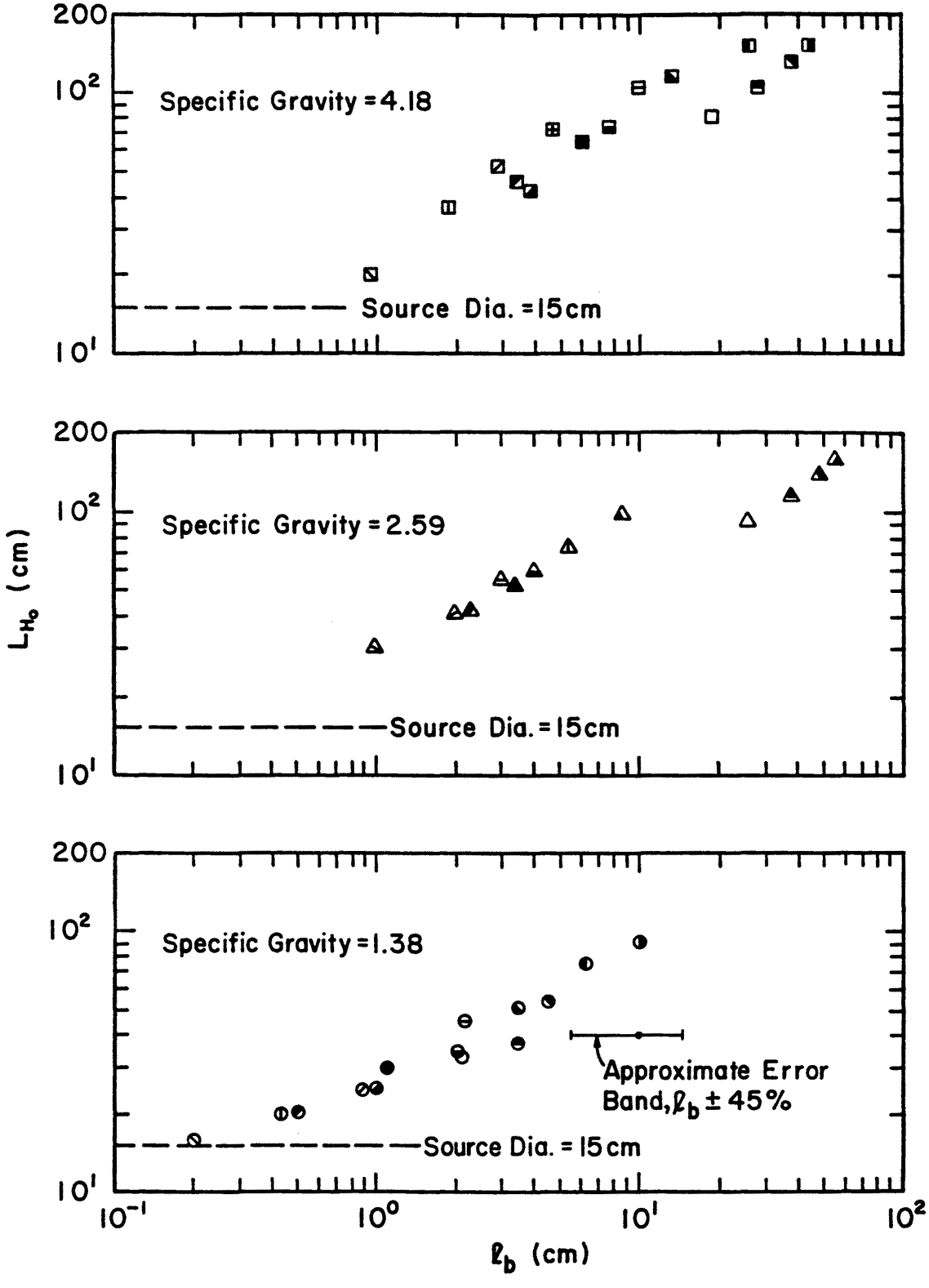

Figure 30. Plume Growth Lateral to the Source versus Buoyancy Length Scale

primarily due to the cubic dependence on the mean velocity which is accurate to ~±15 percent. If the trends in the data are assumed to be solely caused by variations in γ then within a volume ratio distortion range of 1.5 there is no appreciable change in lateral or upwind plume extent.

There is also a significant deviation in Figures 29 and 30 for the plumes of specific gravities 2.59 and 4.18 at the lowest wind speeds, ~20 cm/s. This behavior may be attributed to a systematic error in the velocity setting or a loss of Reynolds number invariance. At these low wind speeds the generation of turbulence from the wind shear is not strong enough to overcome the dampening influence of the density gradients.

Figures 31, and 32 show centerline concentration function $\left(\frac{T_s}{T_a}\right)\left(\frac{\chi_{\ell}}{1-\chi_{\ell}}\right)\left(\frac{U_H H^2}{Q}\right)$ versus downwind distance, x/H, for the specific gravities 1.38, 1.79, 2.59, and 4.18. Section 2.2.2 discussed the derivation and limitations of this function. Since it is hypothesized that plumes of equal ℓ_b are similar, normalized concentration variations with downwind distance should be similar. Within groups of constant ℓ_b there is definite similarity between centerline concentration decay curves for volume ratio distortions up to 1.5.

There is sufficient similarity between heavy plumes when the Flux Froude number ($\dot{F}r = U^3L/Qg'$) and source gas specific gravity (ρ_s/ρ_a) equality are specified and the distortion in volume flux ratio ($\gamma = Q/UL^2$) is limited to use it as an enhanced modeling technique. This allows the range of conditions for physical modeling to be significantly extended.

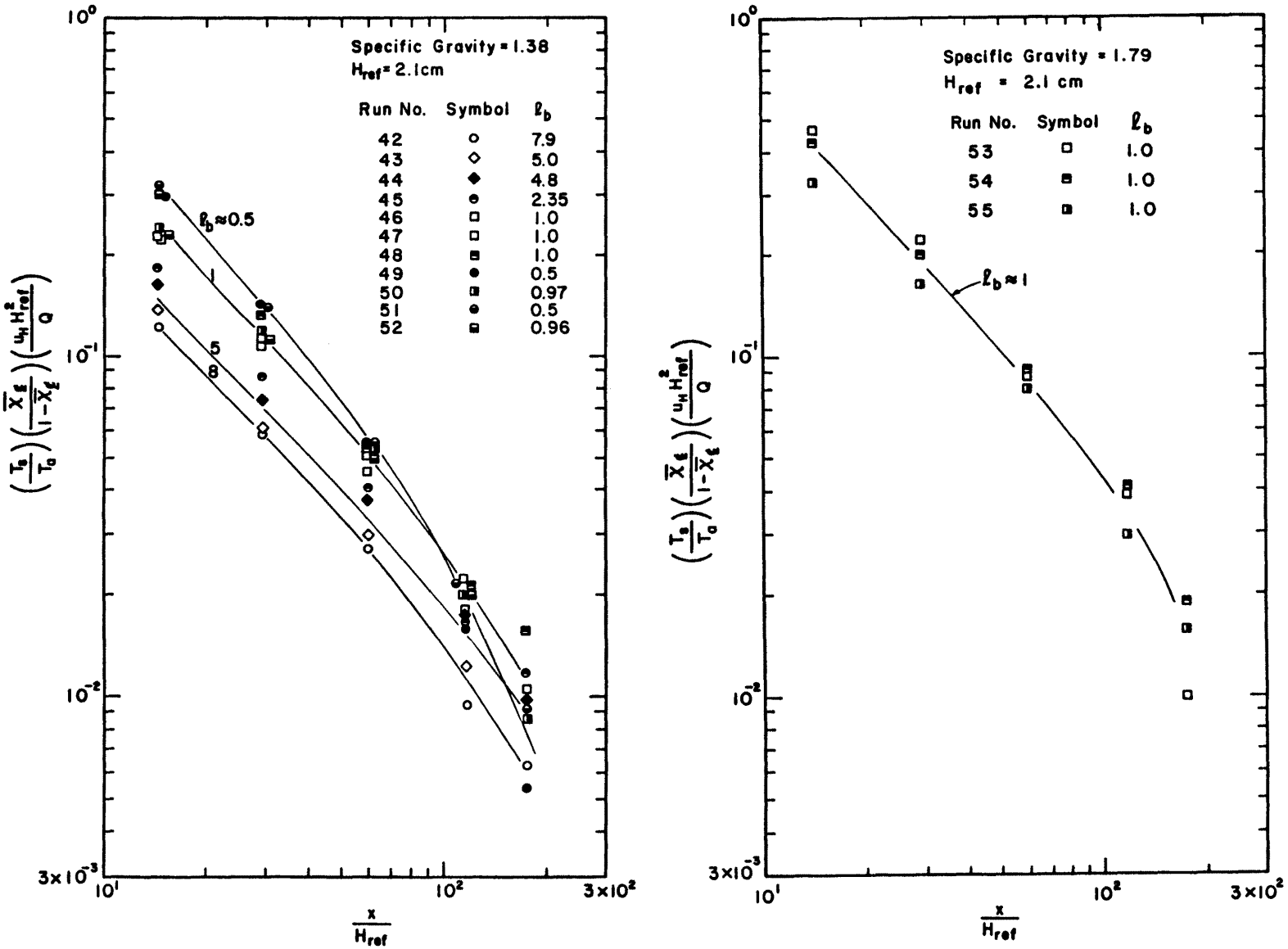

Figure 31. Normalized Centerline Concentration Decay with Downwind Distance for Source Specific Gravities 1.38 and 1.79

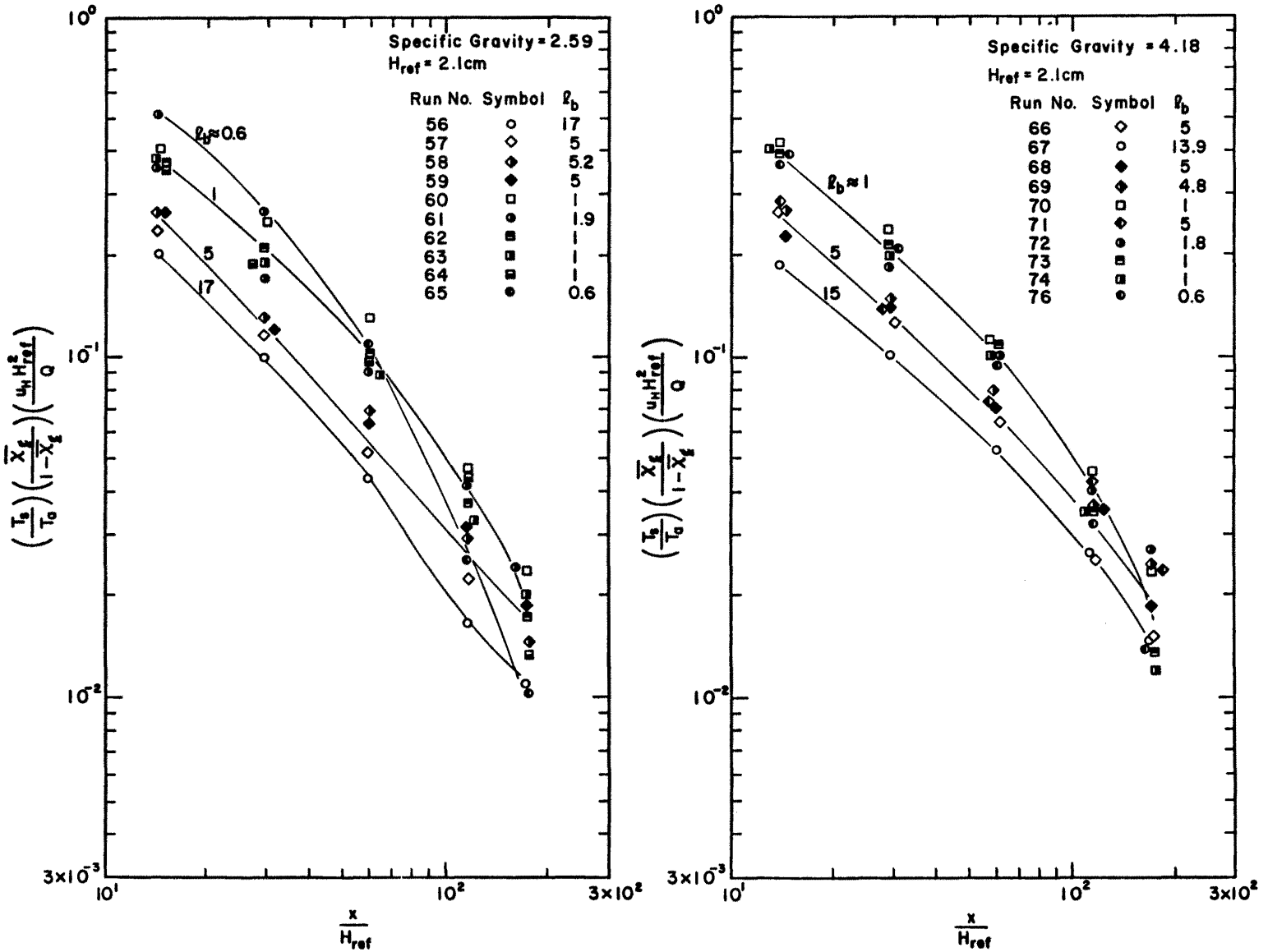

Figure 32. Normalized Centerline Concentration Decay with Downwind Distance for Source Specific Gravities 2.59 and 4.18

5.3 SIMILARITY OF PLUMES WHEN THE VELOCITY FIELD LENGTH SCALE HAS BEEN DISTORTED

Section 2.2.1.3 discusses the variability in the length scale relationship which exists between a wind-tunnel boundary layer and the atmospheric boundary layer. Such variability may permit one to examine different plumes in the same velocity field and demonstrate that partial similarity exists. This technique would work only over a limited range of length scale distortions, because as the scale distortion increases a plume would be exposed to different mean velocities and turbulence intensities over its height. Figure 5 in section 2.2.1.3 shows the approximate magnitude of wind shear distortion between two boundary layers with a length scale ratio of two.

In section 5.2 it is shown that if the Flux Froude number, $\dot{F}r = U^3L/Qg'$, is the dominate parameter then the plume's scaling length is the buoyancy length scale, $\ell_b = Qg'/U^3$. To maintain plume similarity $\dot{F}r$ $(= L/\ell_b)$ must remain a constant. L is some characteristic length scale associated with the velocity field. If we allow ℓ_b to vary then the length scale L must also vary in the same manner, but if L is a fixed velocity length scale then its distortion results in a partial simulation.

All reference velocities were measured at a constant height of 2.1 centimeters. To relate plumes of different geometric scale via this technique the height at which the reference velocity is evaluated must be scaled appropriately due to the presence of wind shear.[1] This can be accomplished by assuming that all the velocity profiles for the data set

[1] If all velocity profiles exhibit the same power law variation with height then the velocity at some height will characterize the entire velocity profile. Thus $U_H \propto$ Bulk Velocity over H, $U_H^2 \propto \frac{1}{H}\int_0^H U^2 dz$, etc.

follow the same power law velocity variation with height (see section 4.4.1 for further discussion). Let $U@(\ell/\ell_r)H = U_H(\ell/\ell_r)^p$ and define $\ell/\ell_r = [\ell_b/(\ell_b)_r]_c = [Qg'/(U@(\ell/\ell_r)H)^3]/[Qg'/U_H^3]_r$ then one can solve for ℓ/ℓ_r explicitly yielding[1,2]

$$(1) \qquad \frac{\ell}{\ell_r} = \left(\frac{\ell_b}{(\ell_b)_r}\right)^{1/(1+3p)} = \left[\frac{\ell_b}{(\ell_b)_r}\right]_c \quad .$$

Figure 33 explains some of these concepts. Outlines of two different plumes are drawn which are related by the length scale ratio $(\ell/\ell_r) = 2$. Also shown are the velocities that must be used to define the buoyancy length scale for each plume such that $(\ell/\ell_r) = [\ell_b/(\ell_b)_r]_c$. It is most imperative that velocity be evaluated at such scaled heights if one wishes to investigate geometric similarity for different plumes. Previous investigations have neglected this point [36,37]. Even for rigorous plume similarity the length scale relationship between plumes must be $[\ell_b/(\ell_b)_r]_c$. From Figure 19 of section 4.4.1 the value for the power law exponent, p, chosen for the present test is p = 0.22. The exponent in Equation 1 above is then 1/(1+3p) = 0.6.

To evaluate the implications of the data sets presented in Tables 1 and 2 with regards to this proposed partial simulation technique it is important that the test conditions be presented in such a manner as to display the magnitude of length scale and volume distortion differences between the difference tests. We have shown that the length scale relationship between the different tests is given by $\frac{\ell}{\ell_r} = \left(\frac{\ell_b}{(\ell_b)_r}\right)^{0.6}$, or

[1]Through the remainder of this section whenever there is a subscript c outside of a bracketed parameter then all velocity terms within that parameter are evaluated at the relative height $(\ell/\ell_r)H$. Whenever the subscript c is absent then it can be assumed the velocity term is evaluated at H = 2.1 centimeters.

[2]Remember that for Fr equality any length dimension characteristic of the plume size is proportional to ℓ_b.

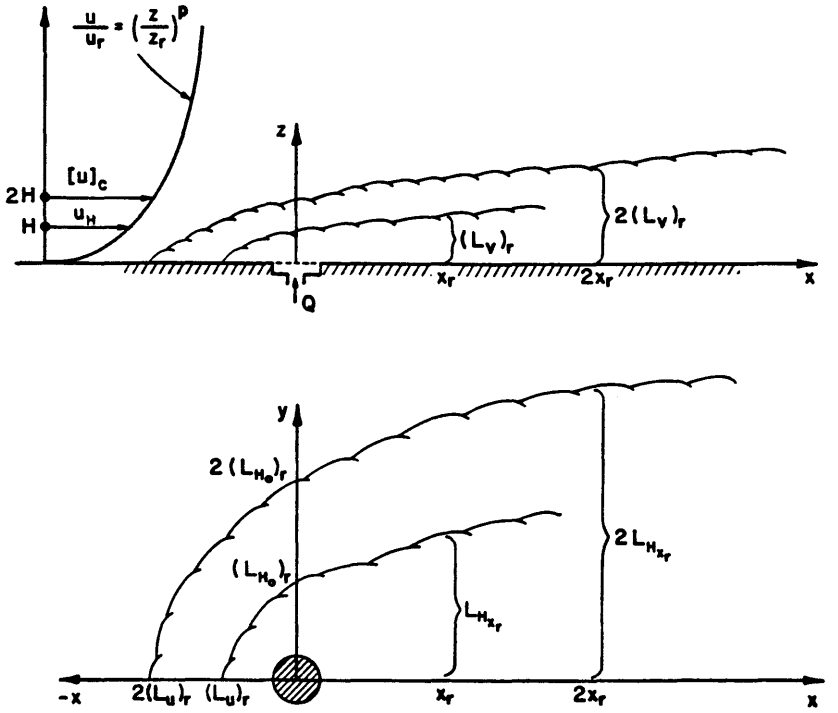

Figure 33. Explanatory Diagram for Plume Length Scaling Discussions

choosing the reference conditions such that $(\ell_b)_r = 1$ yields $\ell = [\ell_b]_c = \ell_b^{0.6}$. A similar scaling procedure used to evaluate the appropriate height for the velocity term in the volume flux ratio V yields,

$$[V]_c = \frac{Q}{(U@(\frac{\ell}{\ell_r})H)(\frac{\ell}{\ell_r}L)^2} = \left(\frac{Q}{U_H L^2}\right)\left(\frac{\ell}{\ell_r}\right)^{-(p+2)} = V\left(\frac{\ell_b}{(\ell_b)_r}\right)^{-(p+2)/(3p+1)}$$

Reference conditions of $(\ell_b)_r = 1$, $L = 1$, and $p = 0.22$ yields $[V]_c = V(\ell_b)^{-1.337}$.

Figure 34 plots $[V]_c$ versus $[\ell_b]_c$ for the visualization tests and for the concentration tests. In these figures if two tests are related by $[V]_c$ = constant then there is both Fr and V equality, and they are related by the length scale ratio $[(\ell_b)_1]_c/[(\ell_b)_2]_c$. If two tests are related by $[\ell_b]_c$ = constant then they are both at the same length scale,

have $\dot{F}r$ equality, and their volume ratio distortion is given by $[V_1]_c/[V_2]_c$ (this is the case considered throughout section 5.2). When tests are not along either of these lines then there is distortion in length scale and volume flux ratio; however, all points can still be related by the single parameter $\dot{F}r$. One wishes to evaluate the limits of length scale and volume ratio distortion for which there is still similar plume structure.

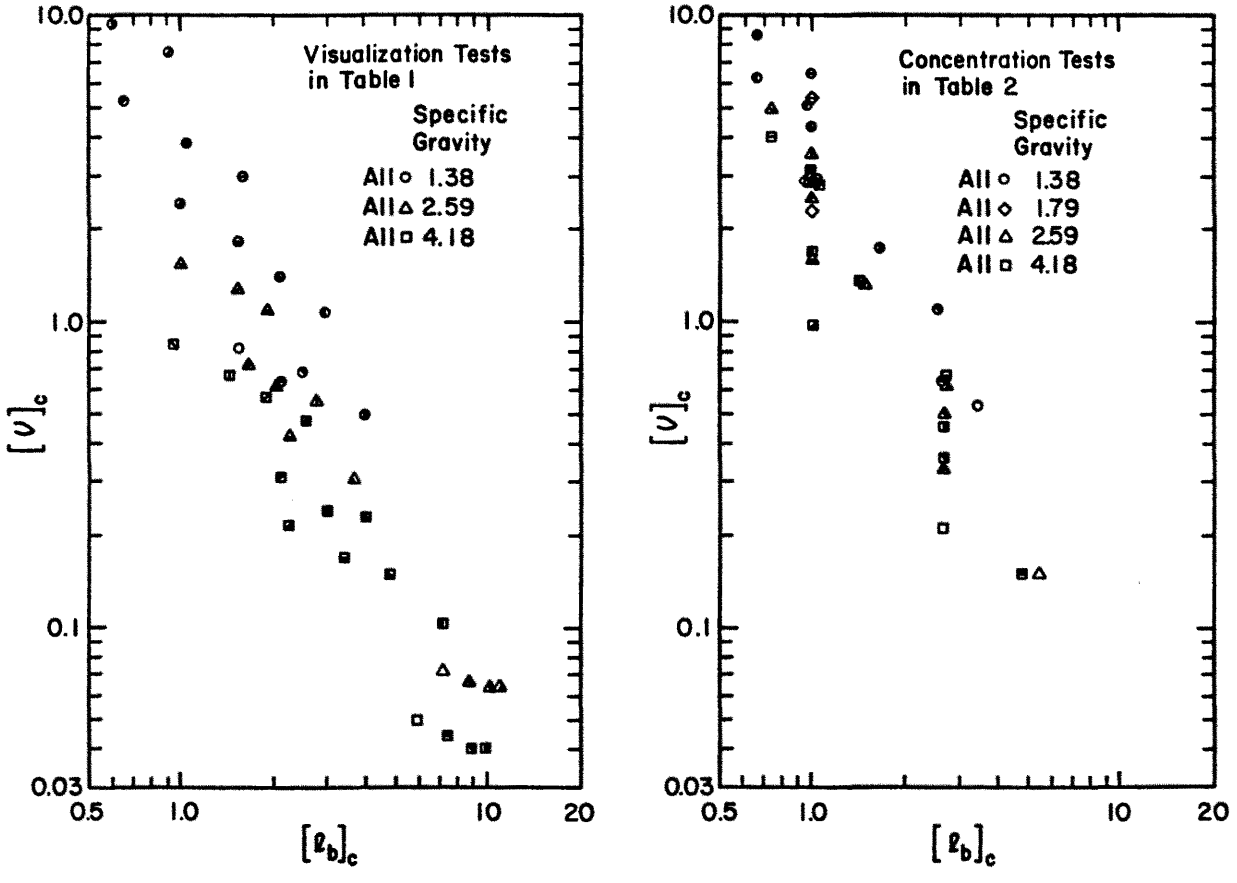

Figure 34. Test Condition Parameter Plots

Figure 35 considers the upwind and lateral plume extents at the source versus the length scaling parameter $[\ell_b]_c$. The runs for specific gravities of 2.59 and 4.18 at the lowest wind speed, ~20 cm/s, have been excluded from these two figures because of the low Reynolds number effects mentioned in section 5.2. These figures, demonstrate that the scaling length $[\ell_b]_c$ is linearly related to these plume dimensions over a fairly large range of test conditions. The scatter in the data shows the same tendency to produce less plume growth with declining volume flux ratios as discussed in section 5.2. Figure 36 shows the lateral plume growth with downwind distance. Both these plume dimensions are normalized by the scaling length $[\ell_b]_c$. The correlation of plume dimensions with length scale, $[\ell_b]_c$, is excellent. Downwind of the source further plume growth is not seriously affected by changing volume flux ratios. Britter [37] states that a simple balance of wind advection and buoyancy spreading predicts the lateral plume growth should go as $(L_{H_x} - L_{H_o})/[\ell_b]_c \alpha (x/[\ell_b]_c)^{2/3}$. Indeed this is what Figure 36 demonstrates to be true.

Figure 34 shows that a change of length scale between two tests usually results in a change in the volume flux ratio. In Figure 35 and earlier in section 5.2 it is observed that the near source behavior is affected by the volume flux ratio; hence a definite maximum magnitude for permissible length scale distortion is not retrievable from the data. A general overview of these figures suggests a length scale distortion of 1.5 has little effect.

In Figures 35 and 36 a good correlation appears to exist between the different specific gravities tested. This seems to contradict what was found earlier in section 5.1 for plumes of different specific

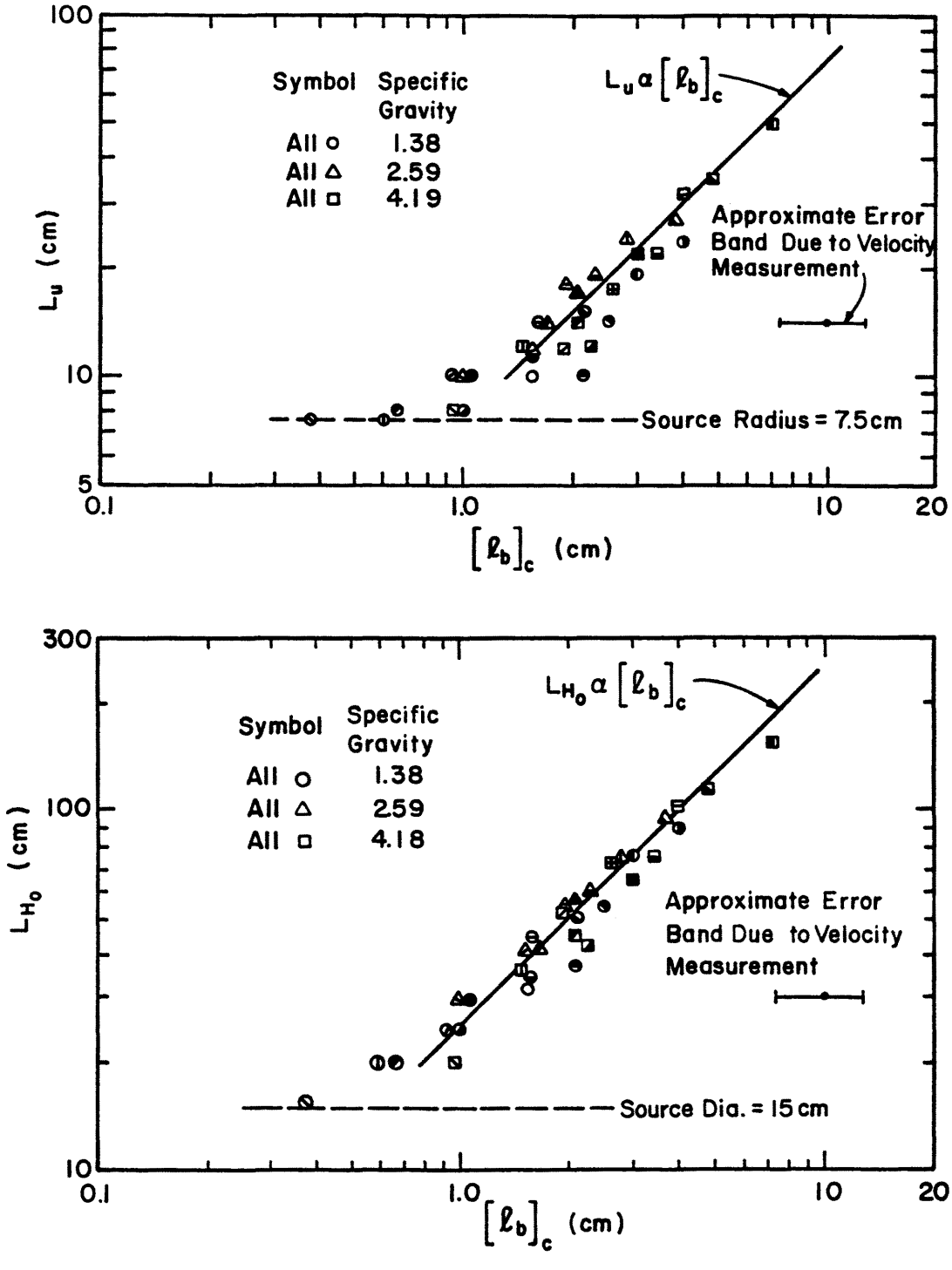

Figure 35. Near Field Plume Growth versus Velocity Corrected Buoyancy Length Scale

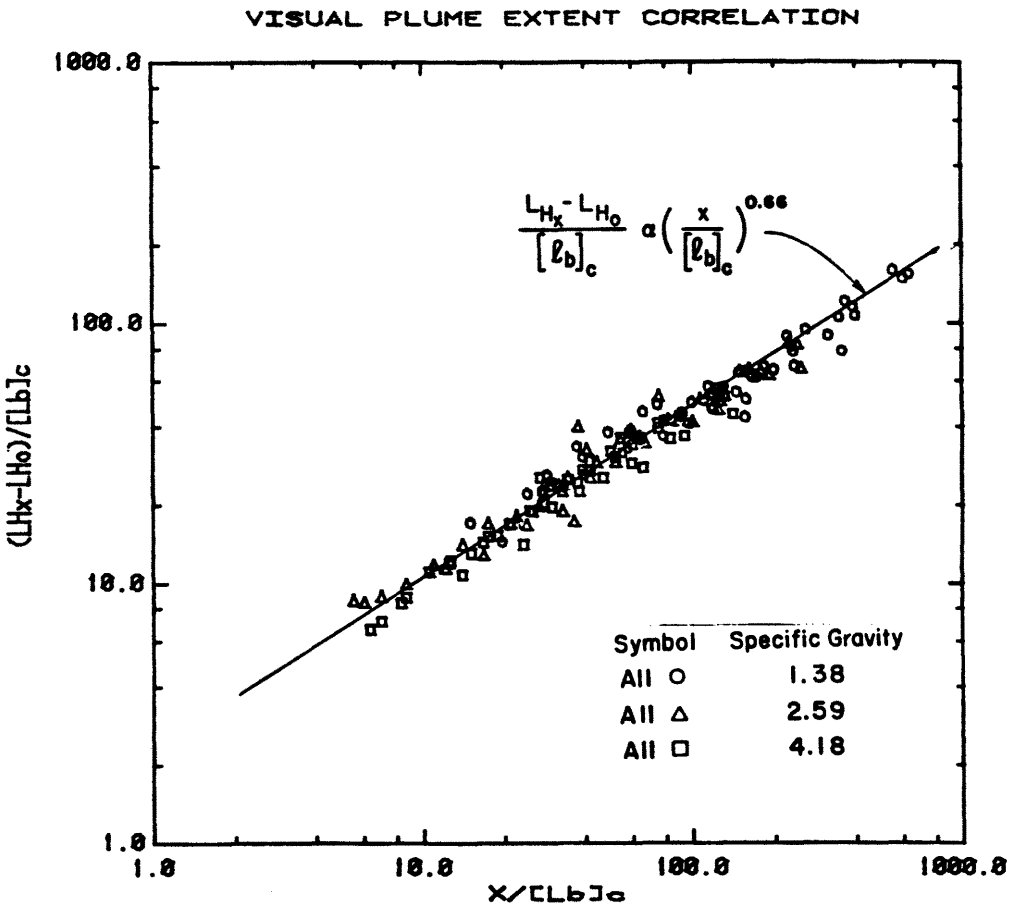

Figure 36. Lateral Plume Growth versus Downwind Distance Normalized with respect to Velocity Corrected Buoyancy Length Scale

gravities for which equality of both Fr and V were maintained. Actually the presentation in Figures 35 and 36 overshadows these differences between specific gravities. Basing V and Fr on the known plume length scale, L_{H_o}, yields $[V]_c = Q/(U@_{(L_{H_o})_r}H)L^2$ and $[Fr]_c = (U@_{(L_{H_o})_r}H)^2/g'L_{H_o}$. To estimate the velocities at different heights a cubic fit through the shaded region of Figure 19 was used rather than the power law expression. Choosing $(L_{H_o})_r$ = 30 cm and plotting this new $[V]_c$ versus $[Fr]_c$ results in Figure 37. Plumes with source-gas specific gravity 1.38 now do not correlate with plumes of specific gravities 2.59 and 4.18. This figure also displays the magnitude of deviation that occurs as the result of volume distortion when comparing plumes based on $\dot{F}r$ only.

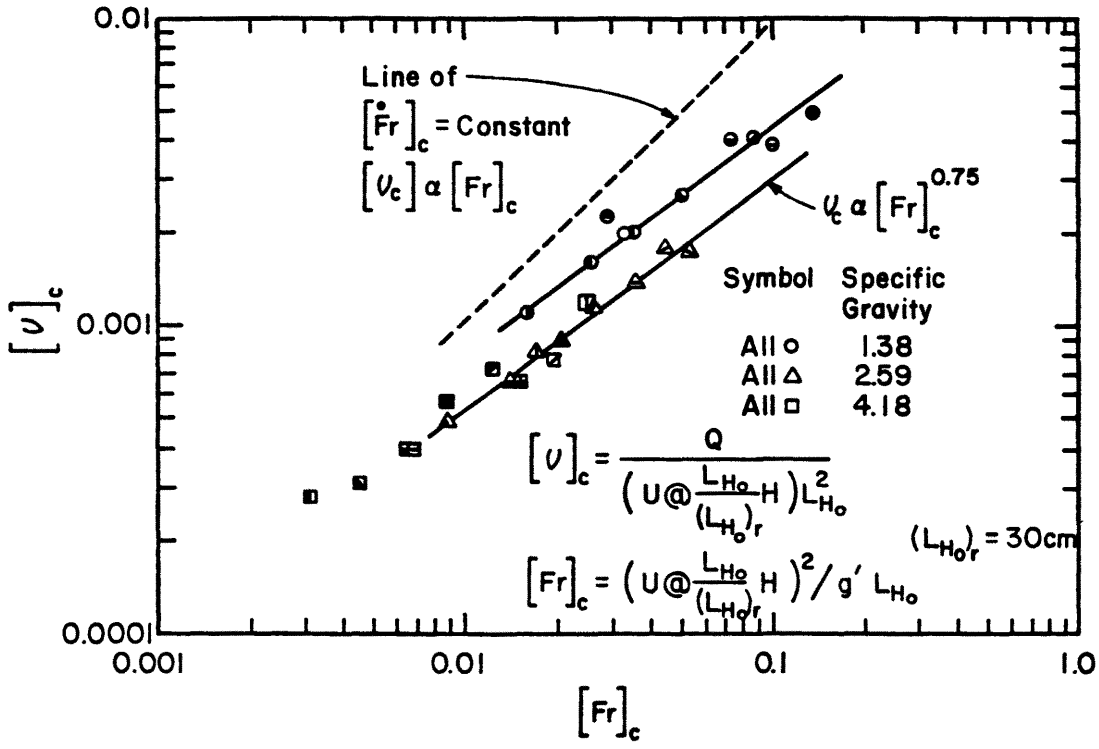

Figure 37. Volume Flux Ratio versus Densimetric Froude Number where Velocity Terms in Both Parameters are Referenced to a Height Proportional to the Measured Plume Width at the Source

So far we have only looked at the visual test results to determine what sort of length scale distortions are permissible. A more complete picture of changes in plume structure may be obtained by observing the centerline concentration data. The normalized concentration $K(x) = \left(\frac{T_s}{T_a}\right)\left(\frac{\chi_t}{1-\chi_t}\right)\left(\frac{U_H L^2}{Q}\right)$ and the downwind distance x must be properly scaled. Using the methodology presented earlier and requiring $(\ell_b)_r = 1$ we obtain the necessary form $\left(\frac{T_s}{T_a}\right)\left(\frac{\chi_t}{1-\chi_t}\right)\left(\frac{U_H H^2}{Q}\right)(\ell_b)^{1.337}$ versus $(\frac{x}{H})(\ell_b)^{-0.6}$. Figure 38 presents the data for source specific gravities 1.38 and 2.59 in this format. There is a distinctive separation between the different tests according to their associated scaling lengths, $[\ell_b]_c$. This seems to indicate that the distortion in the mean shear profile by the proposed modeling enhancement technique is not permissible, but for a

majority of the data a change in scaling length, $[\ell_b]_c$, results in a volume ratio distortion. To try to separate these two different influences on the data the Y coordinate of Figure 38 was divided by the X coordinate raised to the -1.25 power and plotted versus the volume flux ratio, $[V]_c$ in Figure 39. This figure provides an estimate of the amount of error incurred, ±10 percent, if a 1.5 factor in volume ratio distortion is allowed. Within the limitation of this volume ratio distortion it appears that a length scale distortion factor of 1.5 is permissible.

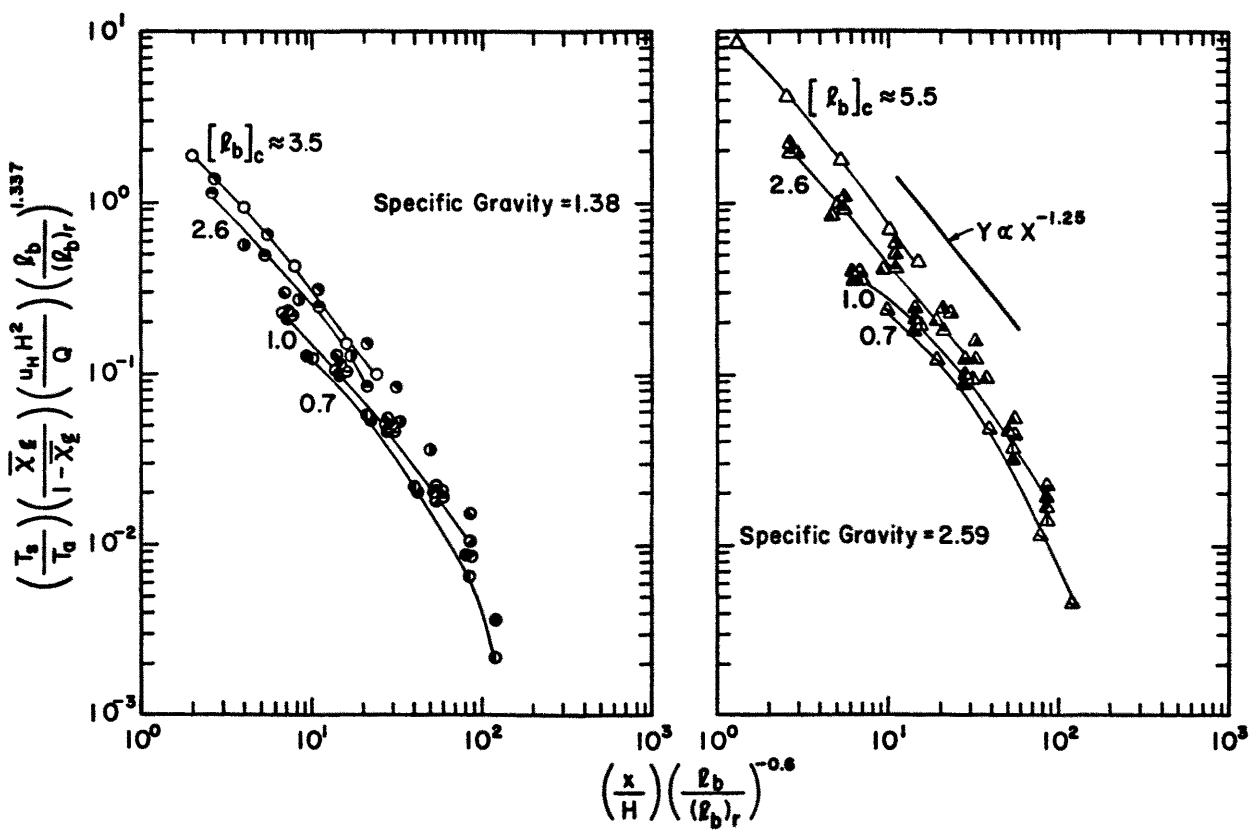

Figure 38. Length Scale Adjusted Normalized Centerline Concentration Decay versus Length Scale Adjusted Downwind Distance

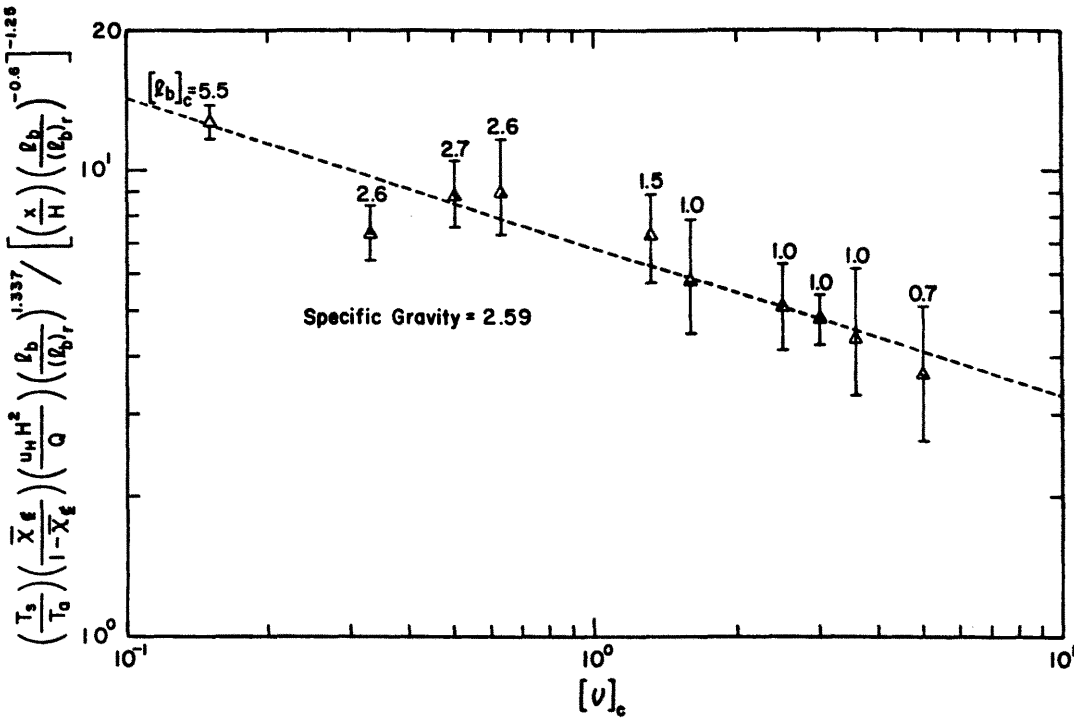

Figure 39. Effects of Length Scale and Volume Flux Ratio Distortion on Length Scale Adjusted Normalized Centerline Concentration Decay

6.0 EMPIRICAL MODELS FOR CONTINUOUS RELEASE HEAVY PLUMES

6.1 LABORATORY SCALE EMPIRICAL MODELS

This section proposes a coordinate system which collapses all the continuous heavy plume test data onto a single set of plume outline and plume concentration contours. Dimensionless parameters were sought which correlated the dependent variables (plume extent and concentration) with low variance.

The plume variables of interest are Q, ρ_s/ρ_a, u_H and L. Since the plume structure will be dominated by a balance of buoyancy to inertial forces these variables were grouped into a Flux Froude number, $u_H^3 L/Qg' = L/\ell_b$ where $g' = g(\rho_s/\rho_a - 1)$ (see section 2.2 for further details). If this were the only parameter governing the structure of a set of heavy plumes and if there was no shear in the approach flow then the buoyancy length scale, ℓ_b, would be proportional to any characteristic length defining the plume structure, i.e., upwind plume extent, L_u, lateral plume width at the source, L_{H_o}, a distance to a centerline concentration, etc. Since there normally is wind shear in the approach flow and there are other parameters beside $\dot{F}r$ that have an effect on plume structure the plumes characteristic length scale, ℓ_b, must be modified. A convenient way to do this is to adjust ℓ_b by a nondimensional grouping of the variables g', Q, and u_H raised to some power. The nondimensional grouping, $f = Q^{1/2} g'/u_H^{5/2}$, was chosen. This modified characteristic scale is now $L \alpha \ell_b/f^c$.

The best value for the exponent, c, determined by performing a least square regression upon the visual test data summarized in Tables 1 and 2 of section 4.2, is 0.8. The quality of this empirical fit is apparent in Figure 40 for the upwind plume extent (top figure) and the

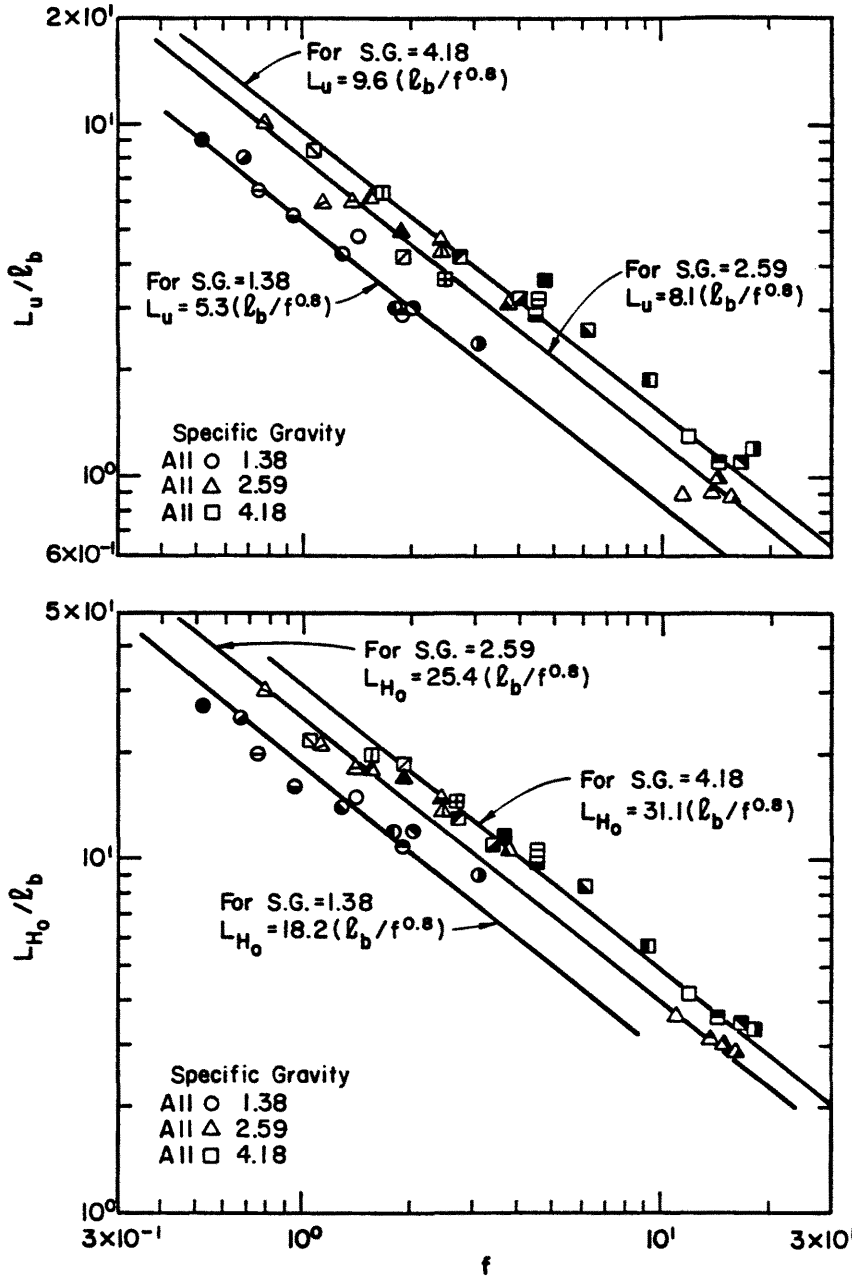

Figure 40. Near Field Plume Extent Data Correlations

lateral plume width (bottom figure) at the source.[1] Figure 41 displays the lateral growth of the visual plume extent in the downwind coordinate direction using this same length scaling criteria for each source specific gravity group. These figures demonstrate that the length scale $\ell_b/f^{0.8}$ $(= Q^{0.6}g'^{0.2}/u_H)$ satisfactorily correlates the ground plane visual extent of laboratory plumes that have a common source gas specific gravity. Neither correlation nor any other system examined eliminated the spread in data associated with specific gravity. This phenomenon is consistent with the observations made in section 5.1 that plumes of different source specific gravity are not physically similar. Since attempts to correlate all data with one correlation were ineffectual different generalized plume formulae are proposed for each of the major specific gravity groups tested; 1.38, 2.59, and 4.18.

In section 2.2.2 the normalized concentration scaling function $K(x) = \left(\frac{T_s}{T_a}\right)\left(\frac{\chi}{1-\chi}\right)\left(\frac{u_H L^2}{Q}\right)$ is derived. K(x) has a universal form for plumes that have similarity in their entrainment physics and normalized concentration variation in plume cross-sections. Both of these conditions are approximately met for the laboratory heavy plumes tested when one separates the tests by the source specific gravity and uses the scaling length $(\ell_b/f^{0.8})$ to describe their physical size. Inserting this characteristic length in the above expression for K(x) we obtain

$$\left(\frac{T_s}{T_a}\right)\left(\frac{\chi}{1-\chi}\right)\left(\frac{u_H(\ell_b/f^{0.8})^2}{Q}\right) = K(x)$$

Figure 42 displays normalized concentration decay, K(x), versus normalized downwind distance, $x/(\ell_b/f^{0.8})$, for plume centerline

[1]The data for runs 9, 12, 13, and 14 are not included in the regression or the figures since there is insufficient gravitational spreading in these runs to overcome the effect of the source diameter (D = 15 cm).

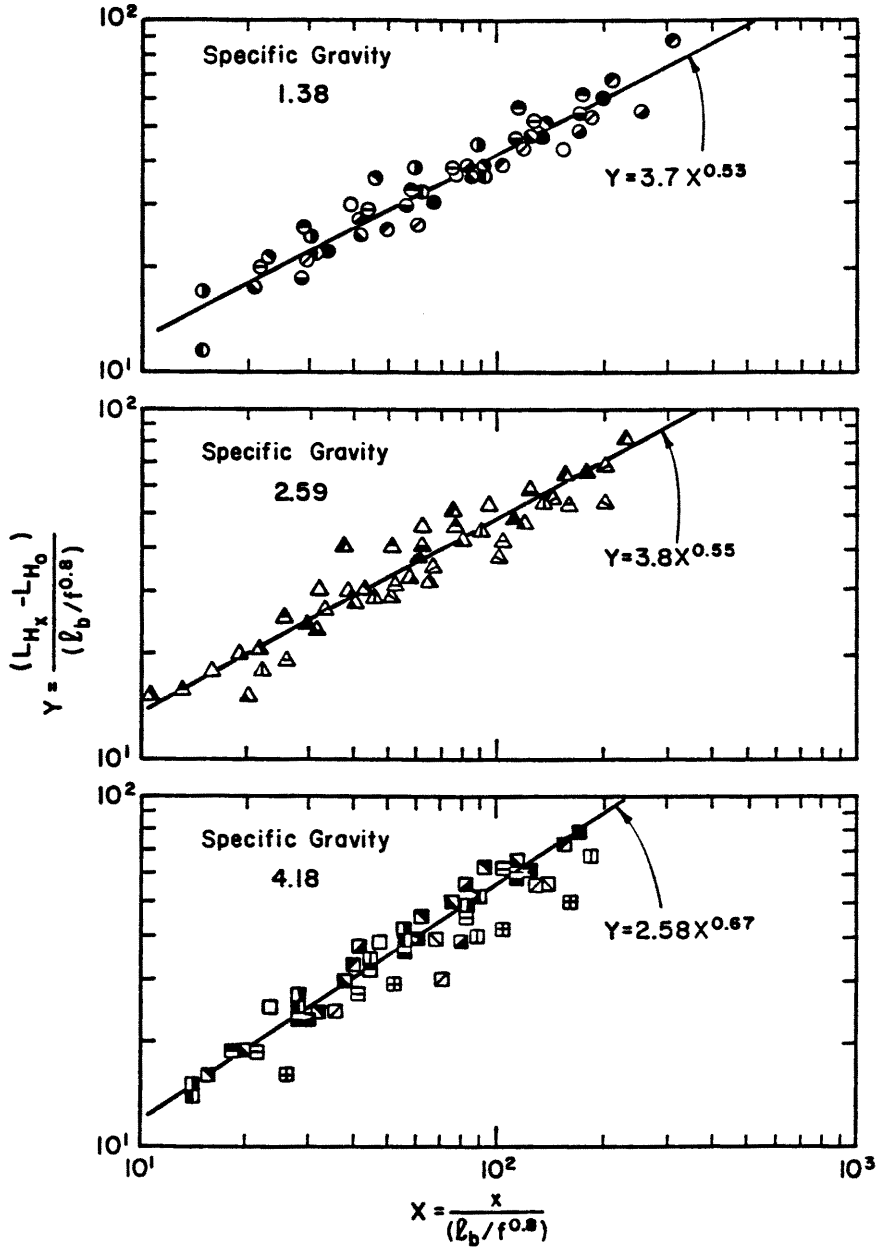

Figure 41. Lateral Plume Growth versus Downwind Distance Data Correlations

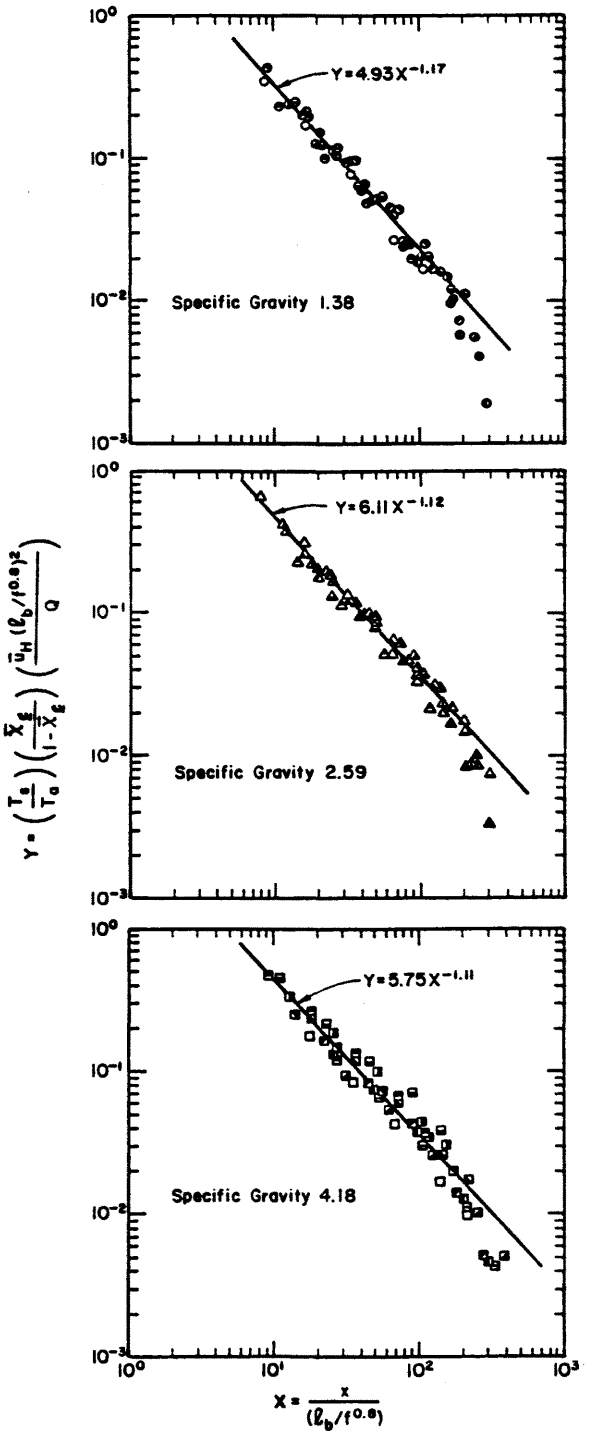

Figure 42. Normalized Centerline Concentration Decay versus Downwind Distance Data Correlations

concentrations only. The length scaling ($\ell_b/f^{0.8}$) satisfactorily collapses the data, particularly for the specific gravity groups 1.38 and 2.59.

The variance of plume width about its centerline, $\sigma_y = (\int \chi y^2 dy / \int \chi dy)^{1/2}$, was computed for each crosswind profile for all the concentration tests shown in Table 2. The normalized plume variance, $\sigma_y/(\ell_b/f^{0.8})$ versus normalized downwind distance, $x/(\ell_b/f^{0.8})$ is shown in Figure 43 for each source specific gravity group. Again the results are acceptably consistent with the exception of the highest wind speed tests in the specific gravity groups 2.59 and 4.18. The complete profile variation in these crosswind plume sections, $\chi(x,y)/\chi(x,0)$ versus y/σ_y was plotted for each downwind cross section for all the runs (Figure 44). This plot also displays reference profiles that would be obtained in passive dispersion (the Guassian Distribution) and in uniform mixing (the Slab Type Distribution). The profiles vary greatly but generally lay somewhere between the Guassian and the Slab type distributions. A cubic equation was fit to the curve most characteristic of the majority of the profiles. This curve will be used to describe the lateral concentration field for the generalized plume models developed in the following paragraphs. The simple empirical models purposed cannot account for plume bifurcation.[1] These models should be used with discretion close to the source where bifurcation may exist.

[1]Figure 26 in section 5.1 demonstrates the formation of plume bifurcation. In this figure it is seen that a large amount of the sources gas is funneled out into a horseshoe pattern around the source. When the buoyancy forces are very small the plume is advected rapidly away from the source producing very little bifurcation. When the buoyancy forces are large the plume spreads out fairly uniformly in the near field and behaves like a line source. When the buoyancy forces are intermediate the source gas is confined within a tight horseshoe pattern causing plume bifurcation in the near field. Measurements indicate that this bifurcation soon decays with increasing downwind distance and centerline concentrations become the profile maximums.

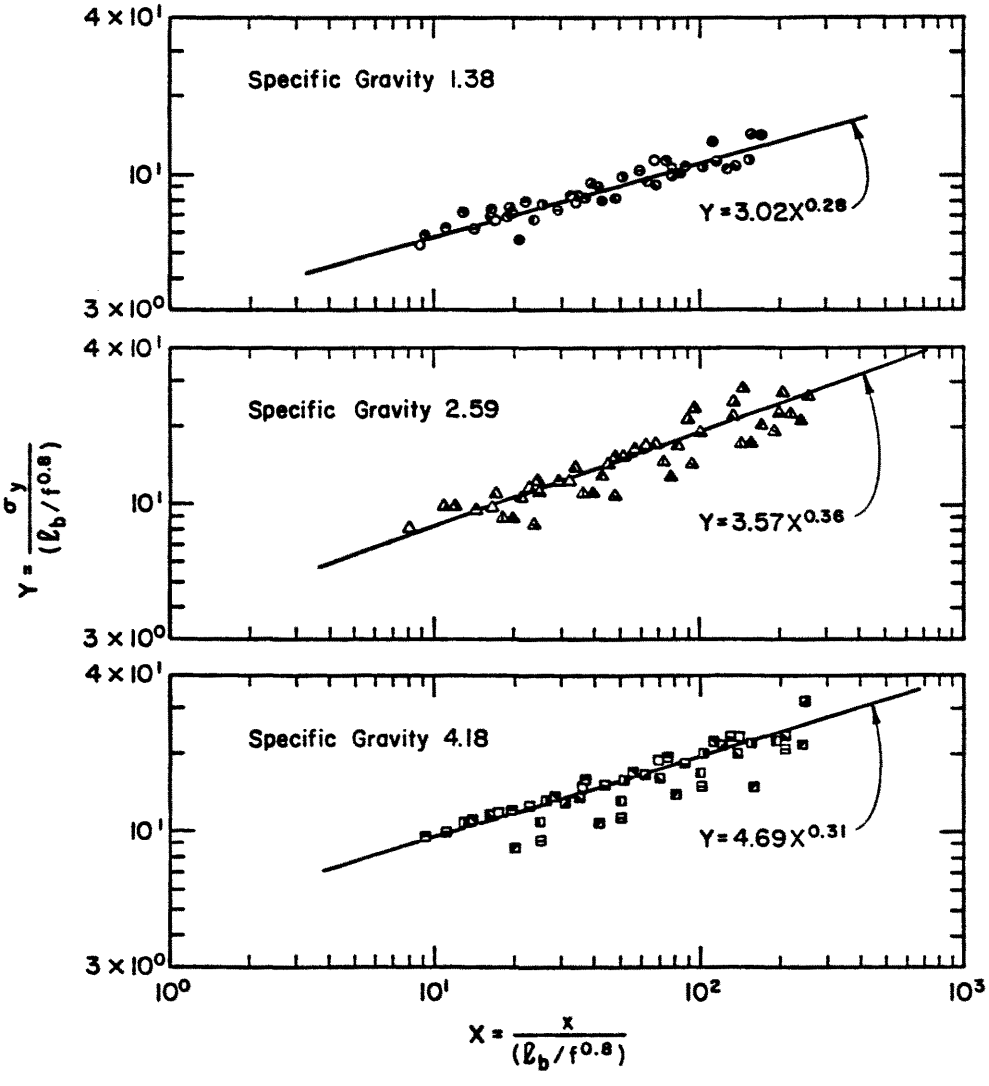

Figure 43. Standard Deviation of Plume Width versus Downwind Distance Data Correlation

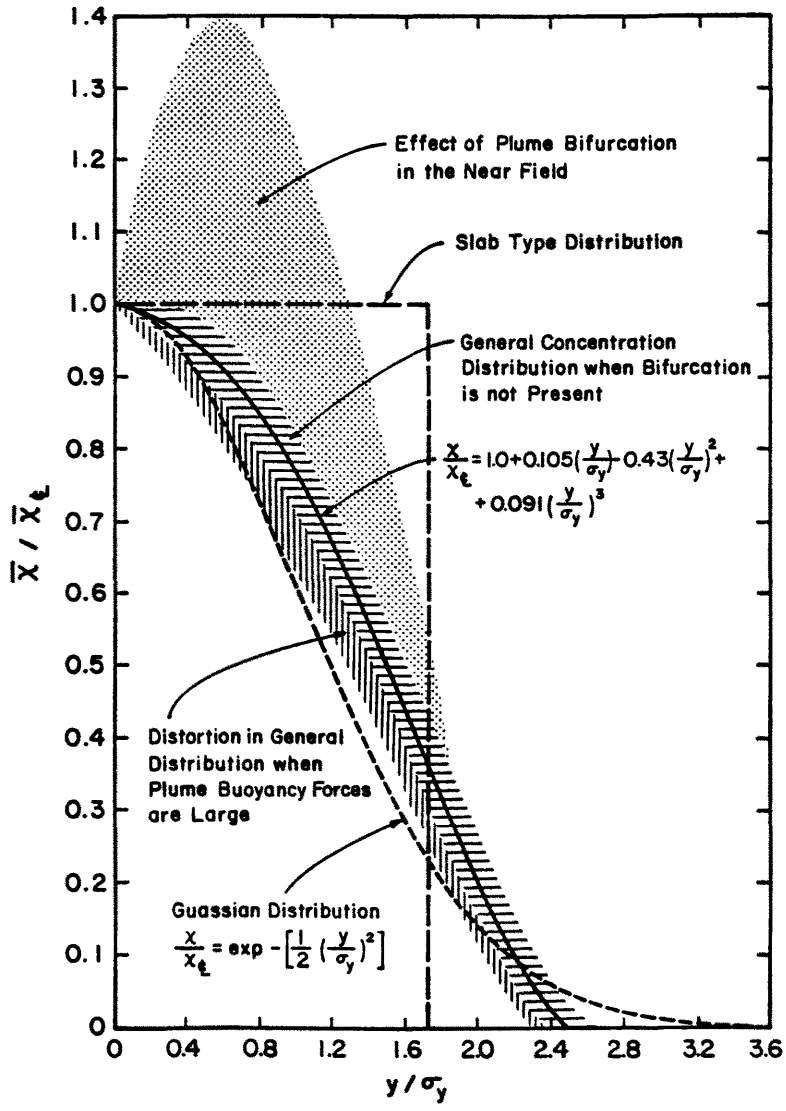

Figure 44. Plume Normalized Lateral Concentration Profiles

Combining descriptions of upwind plume extent, lateral plume extent, centerline concentration decay, and lateral concentration variation for each specific gravity group we obtain a generalized ground plane description for all the continuous release laboratory tests performed. Figures 45, 46, and 47 present these generalized plumes for the source specific gravity tests 1.38, 2.59, and 4.18 respectively. The construction, the assumptions employed, and the error bounds for these curves are reviewed below for the specific gravity test group of 1.38.

From Figure 40 it was found that the data for upwind plume extent and lateral plume width at the source can be represented by $L_u/(\ell_b/f^{0.8}) = 5.3$--(standard deviation of ±8.3 percent) and $L_{H_o}/(\ell_b/f^{0.8}) = 18.2$--(standard deviation of ±11 percent) respectively. From Figure 41 the lateral plume growth with downwind distance can be described by $L_{H_x}/(\ell_b/f^{0.8}) = L_{H_o}/(\ell_b/f^{0.8})+3.7[x/(\ell_b/f^{0.8})]^{0.53}$--(standard deviation of ± 13 percent). Using these three equations the predicted mean and standard deviation was plotted in Figure 45.

From Figure 42 the centerline concentration decay with downwind distance can be represented by $\left(\frac{T_s}{T_a}\right)\left(\frac{\chi_\ell}{1-\chi_\ell}\right)f^{2/5} = 4.93[x/(\ell_b/f^{0.8})]^{-1.17}$--(standard deviation of ± 15 percent in $[x/(\ell_b/f^{0.8})]$).[1] Values of $\left(\frac{T_s}{T_a}\right)\left(\frac{\chi_\ell}{1-\chi_\ell}\right)f^{2/5}$ were plotted on the generalized plume coordinate system for y=0. Estimates for the off-centerline values of $\left(\frac{T_s}{T_a}\right)\left(\frac{\chi}{1-\chi}\right)f^{2/5}$ are obtained through the use of the equations $\chi/\chi_\ell = 1.0+0.105(y/\sigma_y)-0.43(y/\sigma_y)^2+0.091(y/\sigma_y)^3$ from Figure 44 and $\sigma_y = 3.02(\ell_b/f^{0.8})[x/(\ell_b/f^{0.8})]^{0.28}$ from

[1]Note that the quantity $u_H(\ell_b/f^{0.8})^2/Q$ can be reduced to $f^{2/5}$ by utilizing the definitions of the parameters $\ell_b = Qg'/u_H^3$ and $f = Q^{1/2}g'/u_H^{5/2}$.

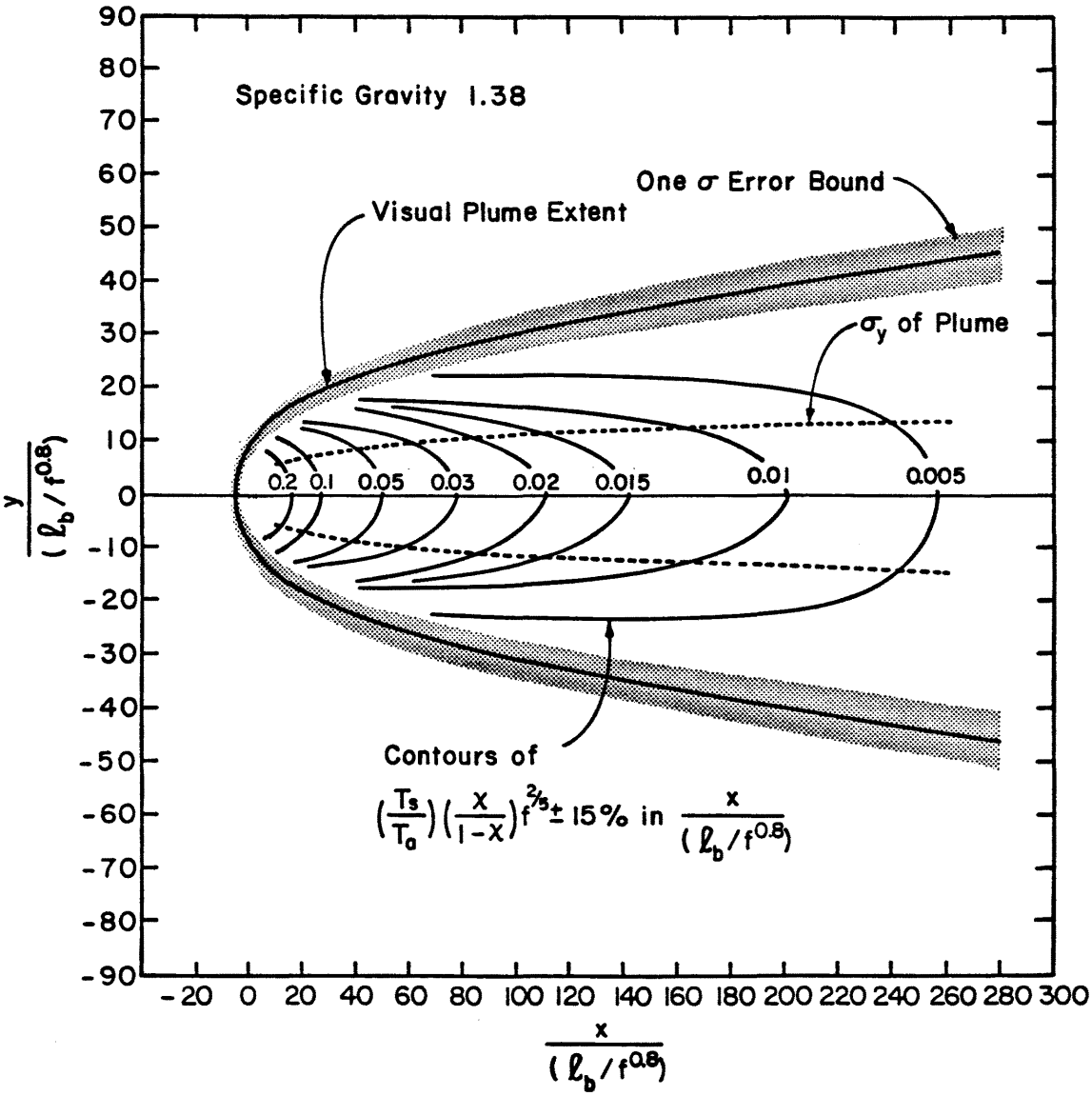

Figure 45. Generalized Plume Description for a Source Specific Gravity of 1.38

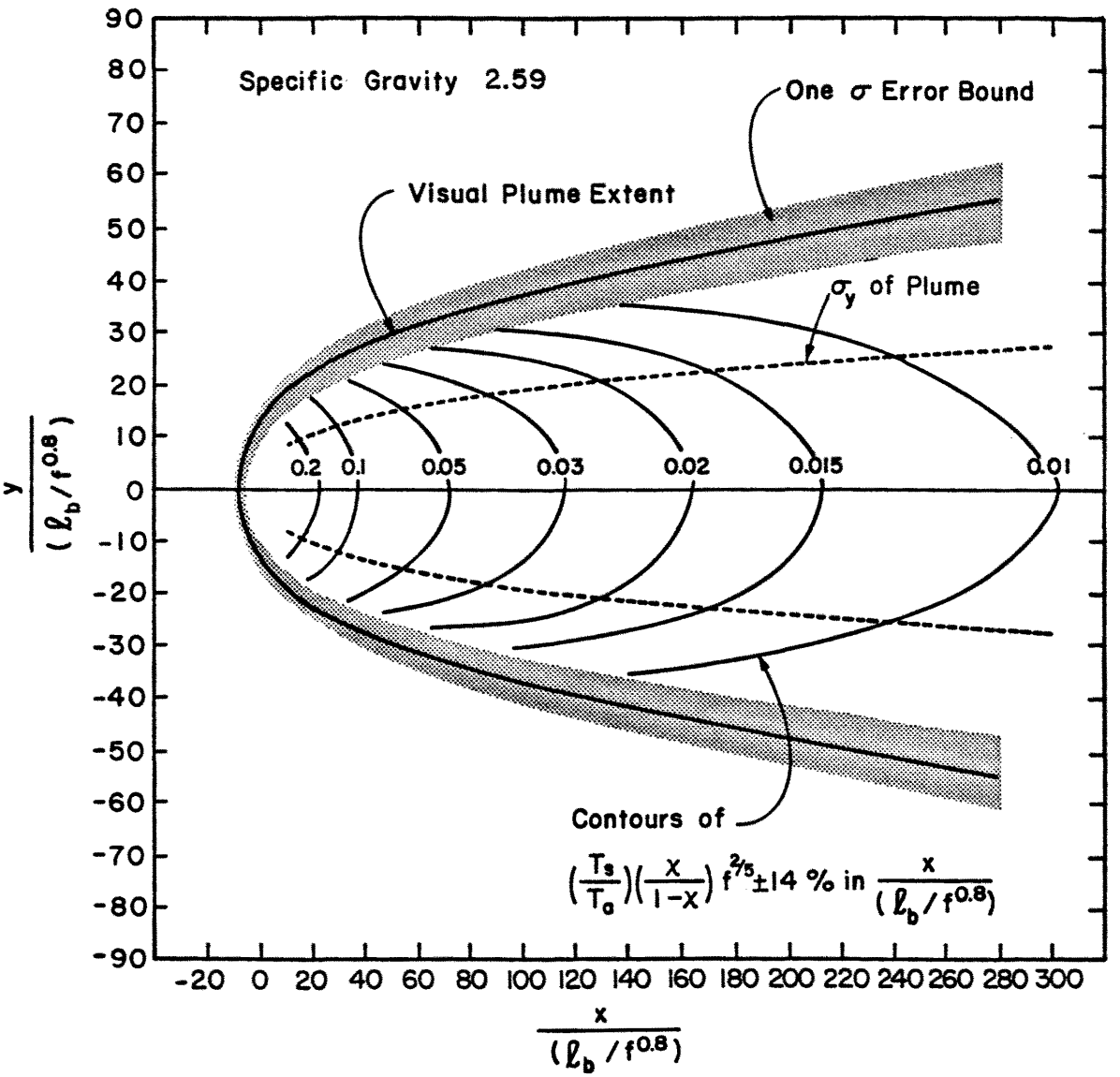

Figure 46. Generalized Plume Description for a Source Specific Gravity 2.59

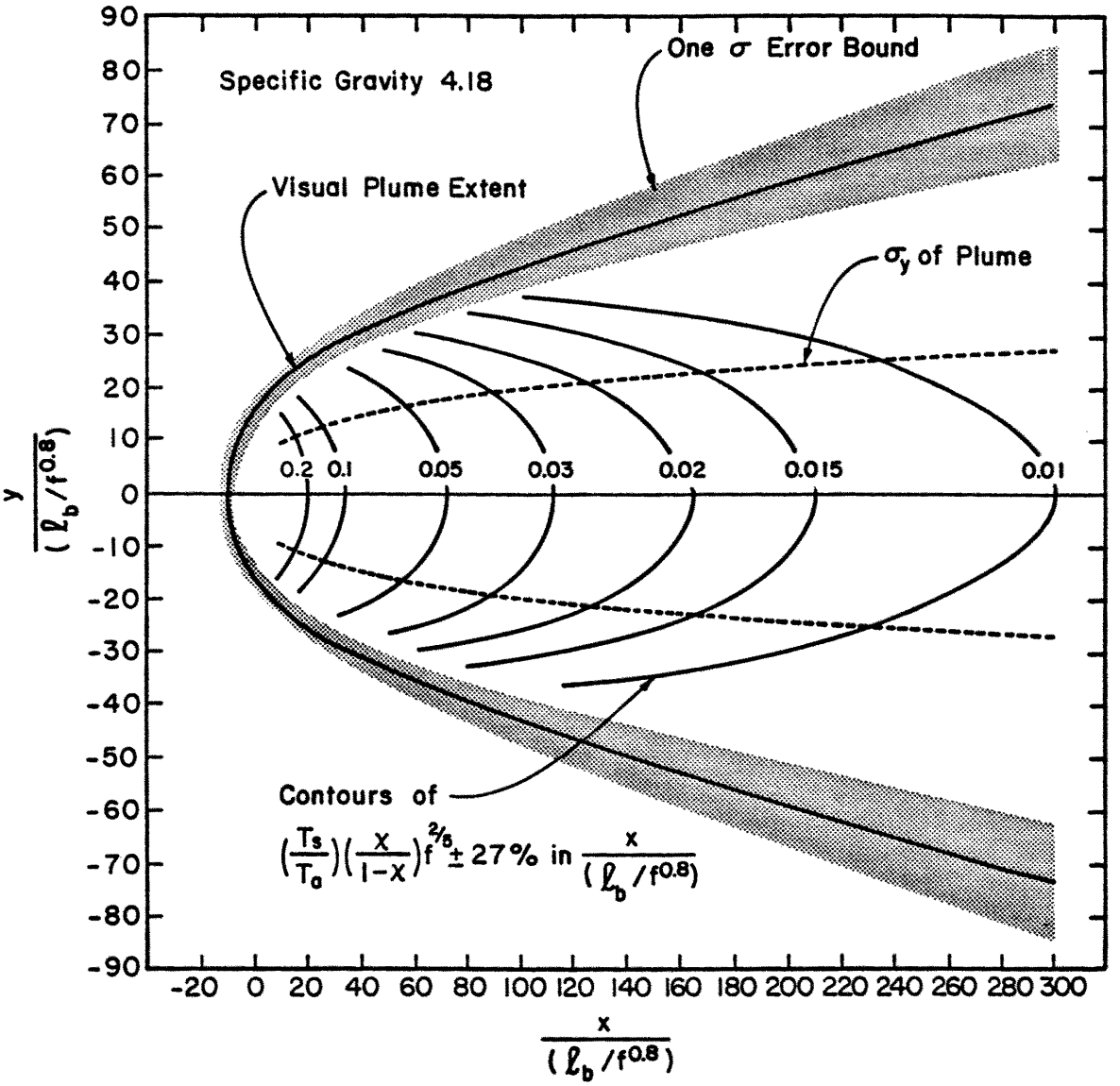

Figure 47. Generalized Plume Description for a Source Specific Gravity of 4.18

Figure 43.[1] Interpolating to find contours of $\left(\frac{T_s}{T_a}\right)\left(\frac{\chi}{1-\chi}\right)f^{2/5}$ and inclusion of the curve characteristic of the plume σ_y completes the formulation for the generalized plume model presented in Figure 45.

This simple empirical plume formulation does not predict accurately crosswind mean concentration profiles near the source. It also does not predict the concentration fluctuation intensity ($i_c = \sqrt{\chi'^2}/\chi$) variation within the different plumes studied. To help predict peak-to-mean concentration ratios for flammable plume hazards a different empirical formulation descriptive of the centerline concentration fluctuation intensity, $(i_c)_t$, variation with downwind distance, x was used. This expression is dimensionally correct but not consistent with the previous generalized plume formulations. This result is $(i_c)_t = 0.0287(x/(f\ell_b))^{0.31}$ with a standard deviation of ±6%. The probability distribution of concentration fluctuations about the mean concentration may be described by a log-normal distribution [38]. Csanady [38] demonstrated that when concentration fluctuations are log-normally distributed the peak-to-mean concentration ratio may be expressed as $\chi_p/\chi = \exp[\sqrt{2}\,\sigma_L\,\mathrm{erf}^{-1}(1-2\Omega)]\exp(-\sigma_L^2/2)$, where $\sigma_L^2 = \ln[i_c^2 + 1]$, Ω is the probability that concentrations greater than or equal to χ_p occur, and erf^{-1} is the inverse error function. From this equation the curves in Figure 48 were derived relating the peak-to-mean concentration ratio, χ_p/χ, to the concentration fluctuation intensity. This figure coupled with the above equation for $(i_c)_t$ will yield the distribution of the peak-to-mean concentration ratio for the plumes tested.

[1]The step assumes corrections laterally for the denominator term $1/(1-\chi)$ are small. Any errors introduced are of a conservative nature.

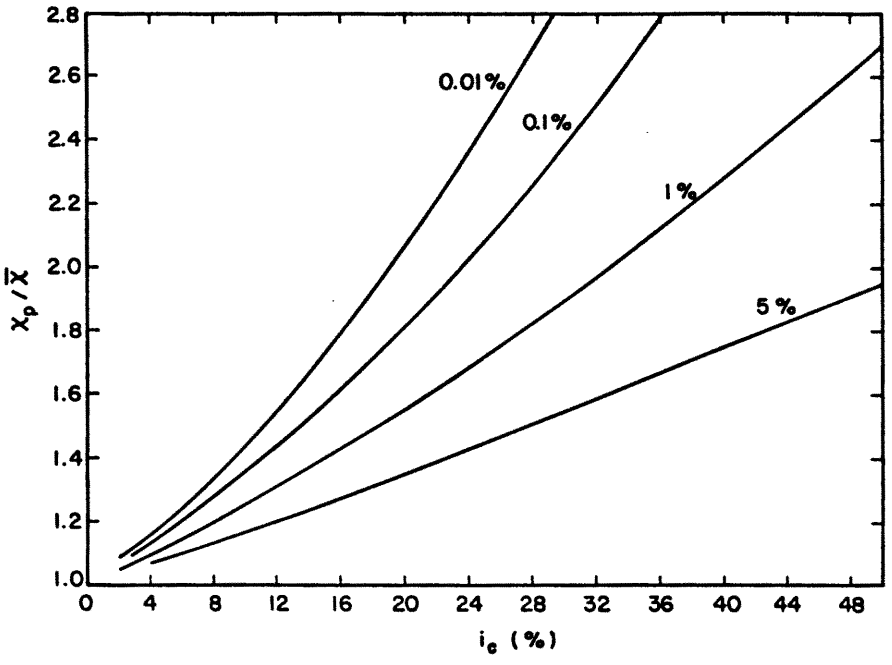

Figure 48. Peak-to-Mean Concentration Ratio versus Concentration Intensity for Several Different Probability Levels

A summary of the data regressions used to develop these models are presented in Appendix C.

These comments review aspects of these empirical models that have not been previously discussed.

- One can determine the visual plume extent from the generalized plume model for the appropriate source specific gravity from the coordinates of the visual plume extent presented in Figures 45, 46, or 47, or from the appropriate equations summarized in Appendix C.

- One can determine the concentration at a particular point of interest (x,y) most easily by using the appropriate equations summarized in Appendix C. If one desires an overview of the entire concentration field it is easiest to transform the coordinate axis of Figures 45, 46, or 47 by multiplying them by $\ell_b/f^{0.8} = Q^{0.6}g^{0.2}/u_H$ and transforming the contours of $\left(\frac{T_s}{T_a}\right)\left(\frac{\chi}{1-\chi}\right)f^{2/5}$ by the expression $\chi = \frac{K(T_a/T_s)f^{2/5}}{1+K(T_a/T_s)f^{2/5}}$ where K

is the value of the contour listed in the figure and $f = Q^{1/2}g'/U_H^{5/2}$. It is important that the variables be evaluated at the proper conditions; thus they are restated here for clarity. Q is the source gas flow rate evaluated at source temperature, T_s. T_a is the ambient air temperature. u_H is the approaching wind speed at height H = 2.1 cm. g' is equal to the local gravitational acceleration, g times the source specific gravity minus one, i.e., g' = g(S.G.-1).

- If one is interested in the distance to a specific concentration value then solving the equation presented in Figure 42 and listed in Appendix C for a source specific gravity of 1.38 yields

$$x = (\ell_b/f^{0.8})\left[\left(\frac{T_s}{T_a}\right)\left(\frac{\chi_t}{1-\chi_t}\right)f^{2/5}/4.93\right]^{-1/1.17} .$$

- It should be noted that the generalized plume formulation for a source specific gravity of 2.59 and 4.18 are nearly identical in their respective concentration fields, but the visual plume growth is slightly greater for the 4.18 case. Due to the empirical nature of these plume formulations this result must be considered fortuitous rather than physically deliberate even though it is quite consistent with the observations made in Section 5.1 on the effects of source density distortion.

- Note that the quantity $f^{0.8}$ used in the empirically derived length scaling for the generalized plume can be shown to be equal to a plume Richardson number by the following formulation:

  Using the length scale, $L \alpha Q^{2/5}g'^{-1/5}$, and velocity scale $u \alpha Q^{1/5}g'^{2/5}$ the Reynolds number for buoyancy-viscous behavior is $Re_B = uL/\nu = Q^{3/5}g'^{1/5}/\nu$ and the Reynolds number for buoyancy-turbulence behavior is $Re = u_H L/\nu = u_H(Q^{2/5}g'^{-1/5})/\nu$. Expressing the Richardson number as the square of the ratio of these two quantities we have

$$Ri = \left(\frac{Re_B}{Re}\right)^2 = \frac{Q^{2/5}g'^{4/5}}{u_H^2} = f^{0.8} .$$

6.2 EXTENSION OF LABORATORY EMPIRICAL MODELS TO ATMOSPHERIC CONDITIONS

Chapter 2 of this report discusses the scaling laws that relate laboratory wind-tunnel conditions to those of atmospheric scale

conditions. Chapter 5 of this report discusses the implications of the present ground level dense plume data set on the validity of these different scaling techniques. In Section 5.1 it is shown that the relaxation of source density ratio equality resulted in a significant distortion in plume similarity for source specific gravities less than 2.0. To demonstrate the conversion of laboratory data results to expected behavior of atmospheric scale LNG spills we will assume here that the extent of the loss of similarity between a source specific gravity of 1.38 (the laboratory argon gas data) and 1.55 (methane vapor at boiloff conditions) is small compared with the other approximations employed in modeling this phenomena[1]. In Section 5.2 it is shown that for plumes with the same characteristic length scales (ℓ_b = cons't) the Flux Froude number ($\dot{F}r$) can be used as the sole plume similarity criteria over a limited volume ratio (V) distortion range. In section 2.2.1.3 the variability in the selection of characteristic length scale relationship between the wind tunnel and the field is discussed. Section 4.4 argues that the optimal choice for this length scale relationship is 1:1000.

Two different scale transformation schemes may be derived to relate the source gas specific of 1.38 for the modeled data to the expected LNG vapor plume behavior. The more rigorous of the two requires Densimetric

[1]In section 2.2.1.4 it was shown that, (1) if equality of source gas specific gravity is maintained in an isothermal model of LNG vapor dispersion the models plume will be larger than the field plume in adiabatic mixing, (2) the entrainment of water vapor by an LNG vapor cloud will tend to decrease its spacial variation of specific gravity upon mixing, and (3) any thermal convection within an LNG vapor cloud will tend to enhance its downwind mixing. The trend of each of these effects is the same as the observed trends while modeling a plume of source specific gravity of 1.55 by a source gas specific graivty of 1.38. The different aspects of loss in plume similarity are somewhat self compensating.

Froude number (Fr) equality and Volume Ratio (V) equality. For this specification the scale relationships between field and model are (see Appendix A):

$$U_p = (g'_p/g'_m)^{1/2}(L_p/L_m)^{1/2}U_m \text{ and } Q_p = (g'_p/g'_m)^{1/2}(L_p/L_m)^{5/2}Q_m.$$

The top graph in Figure 49 shows the range of model test conditions from which the generalized empirical model for a source specific gravity of 1.38 was developed and the range of field conditions predicted from the above two equations for three different model length scale factors, 1:250, 1:500, and 1:1000. The lower half of this same figure shows the enhancement of this range of applicability if one chooses the less rigorous scaling methodology of Flux Froude number equality with Volume Flux Ratio distortions by up to 1.5.

The reference height used in the laboratory was $H_m = 2.1$ cm. The equivalent field reference height must be $H_p = H_m x(LS)$. Similarly the appropriate equivalent field surface roughness will be $(z_o)_p = (z_o)_m$ x (LS), where $(z_o)_m \cong 0.01$ cm. A field velocity specified at a more standard location, z, can be calculated from

$$U(z) = (U_H)_p \frac{\ln(z/(z_o)_p)}{\ln(2.1/.01)} = 0.187(U_H)_p \left[\ln \left(\frac{z}{LS}\right) + 9.21\right]$$

where z is in meters. Figure 17 relates $(z_o)_p$ magnitudes to typical ground cover.

A similar procedure may be employed to determine the range of predictability of the empirical models for the source gas specific gravities of 2.59 and 4.18. For these higher specific gravities (greater than 2.0) one can vary the source specific gravity ratio without significant losses in plume similarity.

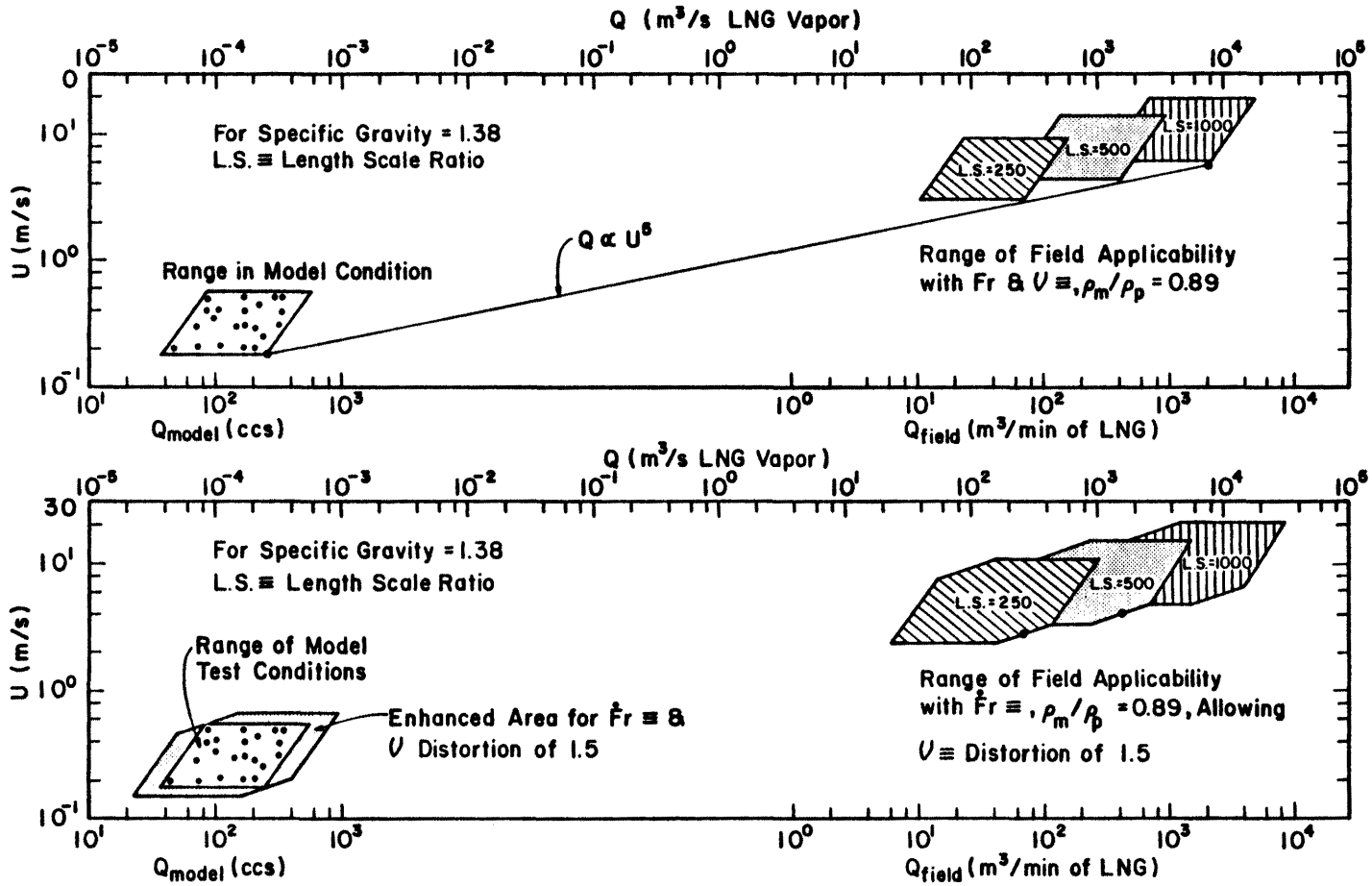

Figure 49. Range of Field Applicability for the Generalized Plume of Source Specific Gravity 1.38

These empirical models were developed for the continuous release of a ground-level heavy plume with negligible initial momentum on a level smooth surface with no wake influences of any kind.

6.3 HAZARD ZONE CALCULATIONS FOR A 400 M^3/MIN LNG SPILL

This section is designed to permit one to determine hazard zone information from the empirical correlations of wind tunnel data. Since LNG at boiloff conditions has a specific gravity of 1.55 the empirical correlations for the 1.38 specific gravity group will be the most representative of field plume behavior. For a model to field length scale ratio 1:1000 the model limitations are:[1]

1) The terrain in the vicinity of the plume source and downwind is flat.

2) Nearby building structures and pipelines are small enough not to influence plume diffusion.

3) The field roughness length $(z_o)_p$ = L.S.x$(z_o)_m$ = 1000x0.01 = 10 cm. Figure 17 demonstrates that this value is representative of farm crops or rural settings for the ground cover conditions.

4) The duration of the spill is long enough to form a fully developed plume, and 400 m^3/min of LNG is evaporating from the spill area.

5) The wind field is neutrally stable.

6) The air humidity is low (i.e., less than 10%).

7) The field height at which the reference wind speed must be evaluated for use in the empirical correlations and in Figure 49 is:

$$H_p = H_m(L.S.) = 0.021(1000) = 21 \text{ meters}$$

[1]The choice of the model to field length scale relationship is not well understood at the present time. The 1:1000 scale ratio used here correlates well with strong wind atmosphere data but actual model simulations of field plumes at a scale of 1:85 have been quite accurate. The only effect the length scale relationship has on the plume empirical correlations is on their range of applicability in field conditions.

Figure 49 displays the range of wind speeds (evaluated at a 21 meter height) for which the empirical correlations are applicable. For rigid scaling (Fr & V^{*} ≡) the wind speed may vary from 6 m/s to 9 m/s. For enhanced scaling (Fr ≡ and V^{*} distortion of 1.5) the wind speed may vary from 5 m/s to 14 m/s.

The following equation converts the wind speed, U_{H_p}, ranges cited in limitation (7) above to a height, z, other than H_p = 21 meters:

$$U(z) = 0.187\ U_{H_p}[\log_e(z/LS)+9.21] = 0.187\ U_{H_p}[\log_e(z)+2.3] \qquad (1)$$

For rigid scaling the wind speed ranges at 3, 10, and 21 meters height are:

Height (m)	3	10	21
Wind Speed Range (m/s)	3.8 to 5.8	5.2 to 7.8	6 to 9

The wind speed at 21 meters height must be used in the empirical correlations for plume structure calculations.

Interest is now focused on plume behavior for a wind speed of 4 m/s at 3 meters height. It is desired to find:

a) General plume concentration patterns,
b) Ground level 5% mean concentration contour, and
c) The maximum distance to 5% peak concentration for 0.01, 0.1, and 1.0% probability of occurrence.

The procedure is:

1) Calculate the wind speed at height $H_p = 0.021(L.S.) =$ 21 meters. This is

$$U_{H_p} = U(z)/(0.187[\log_e(z)+2.3]) = 6.3 \text{ m/s},$$

when $U(z) = 4$ m/s and $z = 3$ meters.

2) Calculate plume vapor release rate, $Q_{NG} = \left(\frac{\rho_{NG\ @\ b.o.}}{\rho_{LNG}}\right)Q_{LNG} =$ $3.8 \times 400\ m^3/min$ LNG = $1520\ m^3/s$.

3) Calculate plume scaling length parameter, $\ell_b/f^{0.8} = Q^{0.6}g'^{0.2}/U_H$. $g' = g(S.G.-1) = 9.81(1.38-1) = 3.73\ m/s^2$, $Q = 1520\ m^3/s$, and $U_{H_p} = 6.3$ m/s; thus $\ell_b/f^{0.8} = 1520^{0.6}3.73^{0.2}/6.3 = 16.75$ meters.

4) Trace all plume contours shown in Figure 45, and multiply the coordinate axis by the calculated scaling length, $\ell_b/f^{0.8}$ = 16.75 meters.

5) Calculate the concentration scaling parameter $(T_s/T_a)f^{2/5}$. LNG boils at T_s = 111°K. Assuming the ambient air temperature is T_a = 295°K, and $f = Q^{0.5}g'/U^{2.5}$ yields,

$$(T_s/T_a)f^{2/5} = 0.438.$$

6) With K equal to the contour value shown in Figure 45 the percent concentration for this contour is calculated from

$$\chi(100) = \frac{(100)K(T_a/T_s)f^{-2/5}}{1+K(T_a/T_s)f^{-2/5}} = \frac{(100)K/0.438}{1+K/0.438} \quad .$$

These values are placed on the appropriate contours traced from Figure 45. See Figure 50 for the results for this example plume.

7) The centerline distance to the 5% mean concentration contour can be estimated from a logarithmic interpolation between the 6.4 and 4.4 percent values or from the appropriate equation correlating the data for specific gravity group 1.38 in Figure 42. Solving this equation for x yields,

$$x = (\ell_b/f^{0.8})[(\frac{T_s}{T_a})(\frac{\chi}{1-\chi})f^{2/5}/4.93]^{-1/1.17}$$

$$= 16.75\ [0.438(\frac{0.05}{1-0.05})/4.93]^{-0.855} = 1643 \text{ meters}$$

The off-centerline 5% contour position is approximated from this known centerline position and the form of the 6.4 and 4.4 percent contours.

8) Finding the maximum distance, x, to a 5% peak concentration which occurs with a probability Ω requires an implicit solution to the following equation:

$$\chi_p/\bar{\chi} = \exp[\sqrt{2}\ \sigma_L\ \text{erf}^{-1}(1-2\Omega)]\exp(-\sigma_L^2/2)$$

where $\bar{\chi} = 4.93\ (\frac{x}{\ell_b/f^{0.8}})^{-1.17}(\frac{T_a}{T_s})f^{-2/5}/[1+4.93(\frac{x}{\ell_b/f^{0.8}})^{-1.17}(\frac{T_a}{T_s})f^{-2/5}]$

$= 304x^{-1.17}/[1+304x^{-1.17}]$ from Figure 42

$i_c = 0.0287(x/(f\ell_b))^{0.31} = 0.0097\ x^{0.31}$

$$\sigma_L^2 = \log_e[i_c^2+1] = \log_e[(9.41\text{x}10^{-5})x^{0.62}+1]$$

$$\chi_p = 0.05$$

For this example problem the maximum distances to 5% peak concentration are:

Probability Level	0.01%	0.1%	1.0%
$erf^{-1}(1-2\Omega)$	2.630	2.184	1.645
Distances (meters)	2,334	2,186	2,026

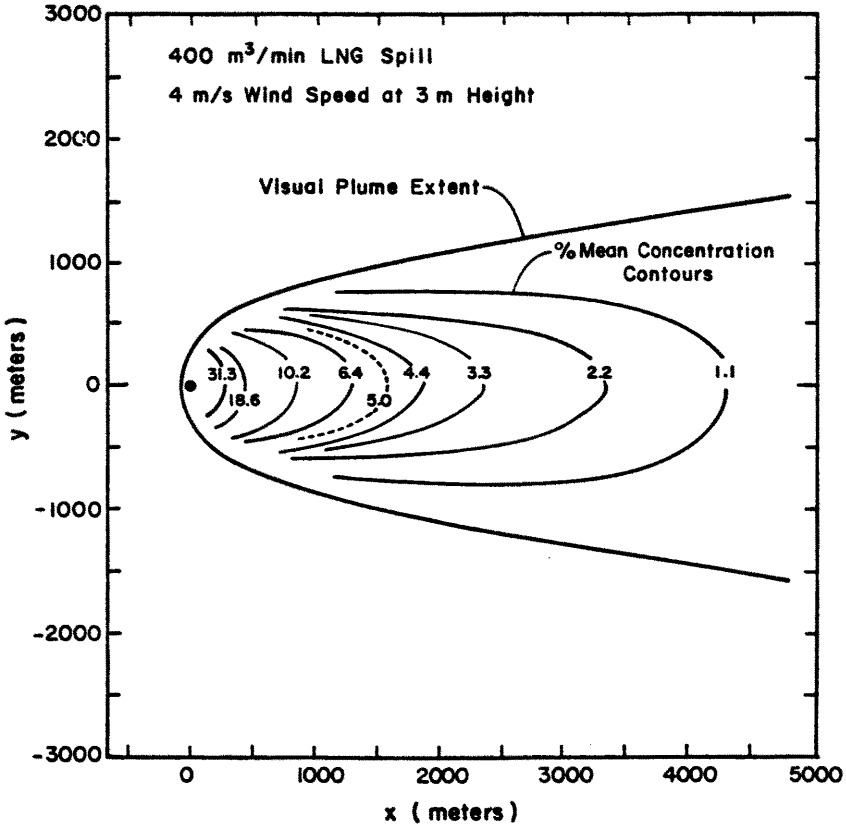

Figure 50. Plume Structure for a 400 m^3/min LNG Spill

7.0 CONCLUSIONS

Physical modeling of atmospheric plumes in wind tunnels is an important predictive technique. To use this technique properly its limitations must be well defined. Having defined these limitations, wind-tunnel models can be used to develop empirical descriptions of the behavior of a large class of atmospheric plume senerios. Wind-tunnel measurements also provide a data base to aid in the development of analytical models. In this report these three goals:

1. the acquisition of a large data base,
2. definition of physical modeling limitations, and
3. development of empirical descriptions

are addressed for the ground level release of heavy plumes with negligible initial momentum into a wind tunnel boundary layer unperturbed by topographic or wake influences. All three goals were achieved for continuous release plumes, but only the first of these goals was achieved for time transient plumes.

7.1 HEAVY PLUME DATA BASE

All plumes were released into a smooth floor boundary layer with no topographic or wake influences. This boundary layer was found to be Reynolds number invariant with respect to passive plumes at wind velocities equal to the lowest used for the heavy plume data set. The wind tunnel boundary layer was characterized by a roughness length of ~0.01 centimeters. Since the model boundary layer scaled at ~1:1000 the model data behaves like plumes dispersion over farm crops or in rural settings.

Maximum ground level visual extent measurements were obtained on forty-one continuous-release heavy plumes. These data included a large

coverage of the test variables of source gas specific gravity (ranging from 1.38 to 4.18), source gas flow rate, and approach flow wind velocity.

Concentrations downwind of thirty-eight continuous release heavy plumes were obtained. These data included a large coverage of the test variables of source gas specific gravity (ranging from 1.22 to 4.18), source gas flow rate, and approach flow wind velocity.

Concentrations downwind of sixty-one transient release plumes were obtained. Twelve different combinations of the test variables of source gas specific gravity, source gas flow rate, and approach flow velocity were used, and during each of these twelve types five or six source gas release durations were specified.

7.2 PHYSICAL MODELING LIMITATIONS

An investigation into the extent of physical similarity between the different continuous release model plumes was undertaken to determine limitations in wind-tunnel plume models. Three schemes considered were:

1. Similarity of plumes when the source gas density ratio is distorted while maintaining equality of both the Densimetric Froude number and Volume Flux ratio,

2. Similarity of plumes when the Volume Flux Ratio is distorted while maintaining equality of both the source gas density ratio and the Flux Froude number, and

3. Similarity of plumes when the velocity field length scale has been distorted.

Scheme one was found to cause significant changes in plume structure up to source gas specific gravities of 2.0. Above this value the distortion between plume structures is minimal. Scheme two was found to cause changes in plume structure dependent on the magnitude of the distortion of the Volume Flux Ratio. For Volume Flux Ratio distortions less than ~1.5 these changes in plume structure were small. The full extent of

plume similarity via scheme three was not retrievable from the data set since a coupling between the distortion in length scale and distortion of the Volume Flux Ratio exists. It appears, however, that a distortion of at least 1.5 is acceptable.

A paradox was found to exist during the determination of the appropriate length scale relationship between the wind-tunnel boundary layer and the atmospheric boundary layer. From a comparison of the mean and turbulent characteristics of the model wind field to those cited for a strong wind atmospheric wind field the length scale relationship was found to be 1:1000. At this length scale the model results would only compare to field surface roughness conditions similar to farm crops and rural areas. Yet in the recent wind tunnel simulations of the 40 m^3 LNG spill test series at China Lake, California, [5] this same boundary layer was used over a 1:85 scale model to reproduce the mean wind shear at this site (which was characteristic of very low surface roughness). At this scale (1:85) good reproduction of the field plume structure was obtained. This observation suggests that the following ill-understood factors are at play:

1. The scales of turbulent motion that are documented for strong wind atmospheric conditions are not applicable to the low wind speed conditions of interest for heavy plume dispersion, and/or

2. Large distortions in the scales of the approach flow turbulent motion have little effect on near field dense plume dispersion. This suggests correct modeling of the mean wind shear over the height of the plume may be all that is important.

A better understanding of the above two points must be obtained to clarify the range of applicability of wind tunnel plume data. Atmospheric spectral measurements at the China Lake site close to the

ground (~2 meters) and at low winds speeds would help resolve this paradox.

7.3 GENERALIZED PLUME DESCRIPTIONS

Three different generalized empirical descriptions were formulated to describe the behavior of most of the continuous release heavy plume tests performed. Each reproduces the behavior of one of the major source gas specific gravity groups tested: 1.38, 2.59, and 4.18. These descriptions are convenient to use as they were cast in a coordinate system which collapses a large number of plume conditions onto single curves. The concentration fields for the specific gravity groups 2.59 and 4.18 are very similar, but the predicted visual plume growth for the 4.18 specific gravity group is greater than for the 2.59 group. Such differences in visual plume growth between these two groups (2.59 and 4.18) is unexpected. The 1.38 source specific gravity group produces smaller transport distances and concentration magnitudes than the 2.59 and 4.18 specific gravity groups. This behavior difference was expected.

The range of applicability for the 1.38 specific gravity generalized plume in predicting LNG vapor plume behavior was determined for a variety of tunnel to field length scale relationships. The paradox mentioned in section 7.2 prevents a definite statement as to the complete range of possible field conditions which are described by this model.

8.0 RECOMMENDATIONS

This report is a reasonably complete presentation, overview, and description of the ground level continuous release of heavy plumes with small initial momentum. Nonetheless an additional sequence of tests would be helpful to determine:

1. The maximum amount of volume distortion and length scale distortion permissible before plume similarity is lost,
2. The effect of volume distortion and length scale distortion in the presence of topography and structural wake influences, and
3. The effect of the source release technique on the resultant plume extent and concentration field.

Another topic that needs clarification is the length scale relationships between the atmospheric and wind tunnel boundary layers. Acquisition of the spectral characteristics of atmospheric winds at the China Lake site would be of value in this respect. Finally a thorough investigation of the transient plume data base presented in this report should be undertaken.

REFERENCES

1. Fay, J. A. (1973) "Unusual Fire Hazard of LNG Tanker Spills," Combustion Science and Technology, Vol. 7, pp. 47-49.

2. Burgess, D. S., Biardi, J., and Murphy, J. N. (1972) "Hazards of Spillage of LNG into Water," Bureau of Mines, MIPR No. Z-70099-9-12395.

3. American Gas Association (1974) "LNG Safety Program, Interim Report on Phase II Work," Report on American Gas Association Project IS-3-1, Battelle Columbus Laboratories.

4. Neff, D. E., Meroney, R. N., and Cermak, J. E. (1976) "Wind Tunnel Study of Negatively Buoyant Plume Due to an LNG Spill," Report prepared for R & D Associates, California, Fluid Dynamics and Diffusion Laboratory Report CER76-77DEN-RNM-JEC22, Colorado State University, Fort Collins, Colorado, 241 p.

5. Neff, D. E. and Meroney, R. N. (1981) "The Behavior of LNG Vapor Clouds: Wind-Tunnel Simulations of 40 m^3 LNG Spill Tests at China Lake Naval Weapons Center, California," Colorado State University Report CER81-82DEN-RNM1 for Gas Research Institute, GRI Report No. 80/0094.

6. Kothari, K. M., Meroney, R. N., and Neff, D. E. (1981) "LNG Plume Interaction with Surface Obstacles," Colorado State University Report CER81-82KMK-RNM-DEN22 for Gas Research Institute, Contract No. 5014-352-0203.

7. Hinze, J. O. (1975) Turbulence, McGraw-Hill, 790 p.

8. Pasquill, F. (1974) Atmospheric Diffusion, D. von Nostrand Co., 429 p.

9. Ermak, D. L., Chan, S. T., Morgan, D. L., and Morris, L. K. (1981) "A Comparison of Dense Gas Dispersion Model Simulations with Burro Series LNG Spill Test Results," Lawrence Livermore National Laboratory, University of California, Livermore, California, 46 pp.

10. Havens, J. A. (1977) "Predictability of LNG Vapor Dispersion from Catastrophic Spills onto Water: An Assessment," Department of Transportation Report, 140 p.

11. Cermak, J. E. (1971) "Laboratory Simulation of the Atmospheric Boundary Layer," AIAA Jl., Vol. 9, No. 9, pp. 1746-1754, September.

12. Kline, S. J. (1965) Similitude and Approximation Theory, McGraw-Hill, 229 p.

13. Cermak, J. E. (1975) "Applications of Fluid Mechanics to Wind Engineering, A Freeman Scholar Lecture," J. of Fluid Engineering, Vol. 97, Ser. 1, No. 1, pp. 9-38.

14. Kaimal, J. C., Wyngaard, J. C., Izumi, Y., and Cote, O. R. (1972) "Spectral Characteristics of Surface-Layer Turbulence," Quart. J. R. Met. Soc., 98, pp. 563-589.

15. Schlichting, H. (1968) Boundary Layer Theory, McGraw-Hill, New York.

16. Halitsky, J. (1969) "Validation of Scaling Procedures for Wind Tunnel Model Testing of Diffusion Near Buildings," Geophysical Sciences Laboratory, Report No. TR-69-8, New York University, New York.

17. Hall, D. J. (1977) "Further Experiments on a Model of an Escape of Heavy Gas," Warren Springs Laboratory Report CR 1341 (AP), Department of Industry, United Kingdom.

18. Hoot, T. G., Meroney, R. N., and Peterka, J. A. (1974) "Wind Tunnel Tests of Negatively Buoyant Plumes," Fluid Dynamics and Diffusion Laboratory Report CER73-74TGH-RNM-JAP-13, Colorado State University, Fort Collins, Colorado, October.

19. Skinner, G. T. and Ludwig, G. R. (1978) "Physical Modeling of Dispersion in the Atmospheric Boundary Layer," Calspan Advanced Technology Center, Calspan Report No. 201, May.

20. Snyder, W. H. (1981) "Guideline for Fluid Modeling of Atmospheric Diffusion," United States Environment Protection Agency Report EPA-600/8-81-009, 185 p.

21. Simpson, J. E. and Britter, R. E. (1979) "The Dynamics of the Head of a Gravity Current Advancing over a Horizontal Surface," J. Fluid Mech., Vol. 94, Part 3, pp. 477-495.

22. Isyumov, N. and Tanaka, H. (1979) "Wind Tunnel Modeling of Stack Gas Dispersion-Difficulties and Approximations," 5th Int. Wind Eng. Conf., Colorado State University, Fort Collins, Colorado.

23. Meroney, R. N., Cermak, J. E., Garrison, J. A., Yang, B. T., and Nayak, S. K. (1974) "Wind Tunnel Study of Stack Gas Dispersal at the Avon Lake Power Plant," Fluid Dynamics and Diffusion Laboratory Report CER73-74RNM-JEC-BTY-SKN35, Colorado State University, Fort Collins, Colorado, April.

24. Isyumov, N., Jandali, T., and Davenport, A. G. (1976) "Model Studies and the Prediction of Full Scale Levels of Stack Gas Concentration," presented at 67th Annual Meeting of APCA, Denver, Colorado and published in APCA Journal, Vol. 26, No. 10, October 1976.

25. Janssen, L. A. M. (1981) "Wind Tunnel Modelling of the Dispersion of LNG Vapor Clouds in the Atmospheric Boundary Layers," TNO Ref. nr.:81-07020, File nr.:8710-13770, Apeldoorn, Netherlands, June.

26. Peterka, J. A. and Cermak, J. E. (1974) "Simulation of Atmospheric Flows in Short Wind Tunnel Test Sections," Colorado State University, Fluid Mechanics Program Technical Report CER73-74JAP-JEC32.

27. Sandborn, V. A. (1972) Resistance Temperature Transducers, Metrology Press, 545 p.

28. Blackshear, P. L., Jr., and Fingerson, L. (1962) "Rapid Response Heat Flux Probe for High Temperature Gases," ARS Journal, November 1962, pp. 1709-1715.

29. Netterville, D. D. J. (1979) "Concentration Fluctuations in Plumes," Syncrude Environmental Research Monograph 1979-4, 288 p.

30. Kuretsky, W. H. (1967) "On the Use of an Aspirating Hot-Film Anemometer for the Instantaneous Measurement of Temperature," Thesis, Master of Mechanical Engineering, University of Minnesota, Minneapolis, Minnesota.

31. Counihan, J. (1975) "Adiabatic Atmospheric Boundary Layers: A Review and Analysis of Data from the Period 1880-1972," Atmospheric Environment, Vol. 9, pp. 871-905.

32. "Characteristic of Atmospheric Turbulence near the Ground," Engineering Science Data Item Number 74030 and 74031, October 1974.

33. Bendat, J. S. and Piersol, A. G. (1971) Random Data: Analysis and Measurement Procedures, John Wiley and Son, New York, 407 p.

34. Raine, J. K. (1974) "Modeling the Natural Wind: Wind Protection by Fences," Ph.D. Dissertation, Department of Mechanical Engineering, University of Canterbury, Christchurch, New Zealand, Vol. 1 and 2, 558 pp.

35. Neff, D. E. and Meroney, R. N. (1979) "Dispersion of Vapor from LNG Spills--Simulation in a Meteorological Wind Tunnel of Spills at China Lake Naval Weapons Center, California," Fluid Dynamics and Diffusion Laboratory Report CER78-79DEN-RNM41, Colorado State University, Fort Collins, Colorado, March.

36. Meroney, R. N., Neff, D. E., and Kothari, K. M. (1980) "Behavior of LNG Vapor CLouds: Tests to Define the Size, Shape, and Structure of LNG Vapor Clouds," Annual Report prepared by Colorado State University for Gas Research Institute, GRI Report No. 79/0073.

37. Britter, R. E. (1980) "The Ground Level Extent of a Negatively Buoyant Plume in a Turbulent Boundary Layer," Atmospheric Environment, Vol. 9, pp. 779-785.

38. Csanady, G. T. (1973) Turbulent Diffusion in the Environment, D. Reidel Publishing Company, 248 p.

APPENDIX A

THE CALCULATION OF MODEL SCALE FACTORS

The following is a list of parameters commonly used in the physical scaling of plume dispersion.

Plume Specific Gravity	$S.G. = \rho_s/\rho_a$
Volume Flux Ratio	$V = Q/U_a L^2$
Mass Flux Ratio	$M = \rho_s Q/\rho_a U_a L^2$
Momentum Flux Ratio	$F = \rho_s Q/\rho_a U_a^2 L^4$
Flux Froude Number	$\dot{F}r = U_a^3 L/g'Q$
Densimetric Froude Number (relative to air inertia)	$Fr = U_a^2/g'L$
Densimetric Froude Number (relative to plume inertia)	$Fr_s = Q^2/g(\frac{\rho_s-\rho_a}{\rho_s})L^5$

where $g' = (\frac{\rho_s-\rho_a}{\rho_a})g$ and Q is the volume flow rate at source conditions.

The following is a list of the plume source flow rate and approach flow velocities scales which are obtained from several different scaling procedures.

	Equality of	$\frac{U_m}{U_p}$	$\frac{Q_m}{Q_p}$
1.	all parameter listed above	$(LS)^{1/2}$	$(LS)^{5/2}$
2.	V, Fr_a or $V, \dot{F}r$	$(g'_m/g'_p)^{1/2}(LS)^{1/2}$	$(g'_m/g'_p)^{1/2}(LS)^{5/2}$
3.	F, Fr_a, Fr_s	$(g'_m/g'_p)^{1/2}(LS)^{1/2}$	$(SG_p/SG_m)^{1/2}(g'_m/g'_p)^{1/2}(LS)^{5/2}$
4.	$F, \dot{F}r$	$(SG_p/SG_m)^{1/4}(g'_m/g'_p)^{1/2}(LS)^{1/2}$	$(SG_p/SG_m)^{3/4}(g'_m/g'_p)^{1/2}(LS)^{5/2}$
5.	$M, \dot{F}r$	$(SG_p/SG_m)^{1/2}(g'_m/g'_p)^{1/2}(LS)^{1/2}$	$(SG_p/SG_m)^{3/2}(g'_m/g'_p)^{1/2}(LS)^{5/2}$
6.	$\dot{F}r$, SG	$(Q_m/Q_p)^{1/3}(LS)^{-1/3}$	$(U_m/U_p)^3(LS)$

where $LS = L_m/L_p$ and $g'_m/g'_p = (SG_m-1)/(SG_p-1)$

For all scaling approaches in which equality of V is not maintained and/or one or both of the plumes are thermal then the concentration fields must be corrected by the following equation

$$\chi_p = \frac{\chi_m}{\chi_m + (1-\chi_m)[(\frac{T_a}{T_s})V]_m / [(\frac{T_a}{T_s}V]_p}$$

APPENDIX B

CALCULATION OF THERMAL CAPACITANCE EFFECTS DURING ISOTHERMAL MODELING OF AN LNG VAPOR CLOUD

For the calculation of the plume specific gravity ratio in the isothermal model we have

$$\left(\frac{\rho}{\rho_a}\right)_m = \frac{\frac{P\bar{M}}{\bar{R}T}}{\left(\frac{P\bar{M}}{\bar{R}T}\right)_a} = \chi_{iso}\left(\frac{M_s}{M_a}-1\right) + 1 = \frac{\chi_{th}\left(\frac{M_s}{M_a}-1\right) + 1}{\chi_{th}+(1-\chi_{th})\left(\frac{T_m}{T_p}\right)} \qquad (1)$$

where the relationship between concentrations measured in the isothermal model, χ_{iso} and the concentrations measured in the thermal prototype, χ_{th} is given by

$$\chi_{iso} = \frac{\chi_{th}}{\chi_{th}+(1-\chi_{th})\left(\frac{T_m}{T_p}\right)} \text{ (see section 2.2.2 for further details).}$$

For the calculation of the plume specific gravity ratio in the thermal LNG vapor plume we have from the consideration of adiabatic mixing of the two ideal gases with constant properties that

$$\rho = \frac{P\bar{M}}{\bar{R}T_{mix}} \text{ where } T_{mix} = \frac{\chi_{th}\gamma T_s+(1-\chi_{th})T_a}{\chi_{th}(\gamma-1) + 1}\ ,\ \bar{M} = \chi_{th}M_s+(1-\chi_{th})M_a,\ \gamma = \frac{(C_p^*)_s}{(C_p^*)_a}$$

$$\text{thus } \left(\frac{\rho}{\rho_a}\right)_p = \frac{[\chi_{th}(\gamma-1)+1][\chi_{th}\left(\frac{M_s}{M_a}-1\right)+1]}{[\chi_{th}\left(\gamma\left(\frac{T_s}{T_a}\right)-1\right)+1]}\ . \qquad (2)$$

Equations 1 and 2 with the information that $\left(\frac{M_s}{M_a}\right)_p = \frac{16}{29}$, $\left(\frac{T_s}{T_a}\right) = \left(\frac{T_p}{T_m}\right) = \frac{111}{295}$, $\left(\frac{\rho_s}{\rho_a}\right)_p = 1.466$, $\gamma = 1.2$, $\left(\frac{M_s}{M_a}\right)_m = 1.466$ were used to generate Figure 7.

For the generation of Figure 8 consider the unconfined mixing of two gas flows. Writing the conservation of mass for this system we obtain

$\dot{n}_a + \dot{n}_s = \frac{PQ_a}{\bar{R}T_a} + \frac{PQ_s}{\bar{R}T_s} = \frac{PQ_{mix}}{\bar{R}T_{mix}}$ rewriting this result and dividing through by $Q_a + Q_s$ yields

$$\frac{Q_{mix}}{Q_a + Q_s} = \frac{T_{mix}}{T_a}\left(\frac{Q_a}{Q_a+Q_s}\right) + \frac{T_{mix}}{T_s}\left(\frac{Q_s}{Q_a+Q_s}\right) = \frac{U_{mix}A_{mix}}{U_sA_s+U_aA_a}$$

Now then using the facts that

$$\frac{Q_a}{Q_a+Q_s} = 1 - \chi_{iso} = \frac{(1-\chi_{th})}{\chi_{th}\left(\left(\frac{T_s}{T_a}_p\right) -1\right)+1}, \quad \frac{Q_s}{Q_a+Q_s} = \chi_{iso} = \frac{\chi_{th}}{\chi_{th}\left(1-\left(\frac{T_a}{T_s}_p\right)\right)+\left(\frac{T_a}{T_s}_p\right)},$$

and $$T_{mix} = \frac{\chi_{th}\gamma T_s+(1-\chi_{th})T_a}{\chi_{th}(\gamma-1)+1},$$

coupled with the conclusion that downwind of the source of the plume $u_{mix} = u_s = u_a$ yields

$$\frac{A_{th}}{A_{iso}} = \left(\frac{\chi_{th}(\frac{\gamma}{\alpha}-1) + 1}{\chi_{th}(\gamma-1) + 1}\right)\left(\frac{1-\chi_{th}}{\chi_{th}(\frac{1}{\alpha}-1) + 1}\right) + \left(\frac{\chi_{th}(\gamma-\alpha) + \alpha}{\chi_{th}(\gamma-1) + 1}\right)\left(\frac{\chi_{th}}{\chi_{th}(1-\alpha) + \alpha}\right)$$

where $\gamma = \frac{(C_p^*)_s}{(C_p^*)_a} = 1.2$ and $\alpha = \frac{T_a}{T_s} = \frac{295}{111} = 2.66$

This analysis will provide an upper bound on the cross-sectional distortion between the two plumes since there will actually be a profile variation in χ at the downwind cross-section rather than χ = constant as assumed here.

APPENDIX C

STATISTICAL REGRESSIONS ON CONTINUOUS PLUME DATA

S.G. ≡ source specific gravity and $\ell_e = \ell_b / f^{0.8}$

Plume Upwind Extent

S.G. = 1.38	$L_u = 5.3\ (\ell_e)$	σ in $L_u/\ell_e = 0.44$
S.G. = 2.59	$L_u = 8.1\ (\ell_e)$	σ in $L_u/\ell_e = 1.015$
S.G. = 4.18	$L_u = 9.6\ (\ell_e)$	σ in $L_u/\ell_e = 1.4$

Plume Lateral Extent at the Source

S.G. = 1.38	$L_{H_o} = 18.2\ (\ell_e)$	σ in $L_{H_o}/\ell_e = 2.02$
S.G. = 2.59	$L_{H_o} = 25.4\ (\ell_e)$	σ in $L_{H_o}/\ell_e = 4.05$
S.G. = 4.18	$L_{H_o} = 31.1\ (\ell_e)$	σ in $L_{H_o}/\ell_e = 3.63$

Plume Lateral Extent at Downwind Distances

S.G. = 1.38	$(L_{H_x} - L_{H_o})/\ell_e = 3.7(x/\ell_e)^{0.53}$	σ in $(L_{H_x} - L_{H_o})/\ell_e = 13\%$
S.G. = 2.59	$(L_{H_x} - L_{H_o})/\ell_e = 3.8(x/\ell_e)^{0.55}$	σ in $(L_{H_x} - L_{H_o})/\ell_e = 14.6\%$
S.G. = 4.18	$(L_{H_x} - L_{H_o})/\ell_e = 2.58(x/\ell_e)^{0.67}$	σ in $(L_{H_x} - L_{H_o})/\ell_e = 15\%$

Plume Centerline Concentration Decay

S.G. = 1.38	$\left(\frac{T_s}{T_a}\right)\left(\frac{\chi_{\ell}}{1-\chi_{\ell}}\right)\left(\frac{U_H \ell_e^2}{Q}\right) = 4.93(x/\ell_e)^{-1.17}$	σ in $(x/\ell_e) = 15\%$
S.G. = 2.59	$\left(\frac{T_s}{T_a}\right)\left(\frac{\chi_{\ell}}{1-\chi_{\ell}}\right)\left(\frac{U_H \ell_e^2}{Q}\right) = 6.11(x/\ell_e)^{-1.12}$	σ in $(x/\ell_e) = 14\%$
S.G. = 4.18	$\left(\frac{T_s}{T_a}\right)\left(\frac{\chi_{\ell}}{1-\chi_{\ell}}\right)\left(\frac{U_H \ell_e^2}{Q}\right) = 5.75(x/\ell_e)^{-1.11}$	σ in $(x/\ell_e) = 27\%$

Plume Centerline Concentration Fluctuation Intensity

All S.G.	$(i_c)_{\ell} = 0.0287(x/(f\ell_b))^{0.31}$	σ in $(i_c)_{\ell} = 6\%$